NATIONAL ENERGY TECHNOLOGY LABORATORY

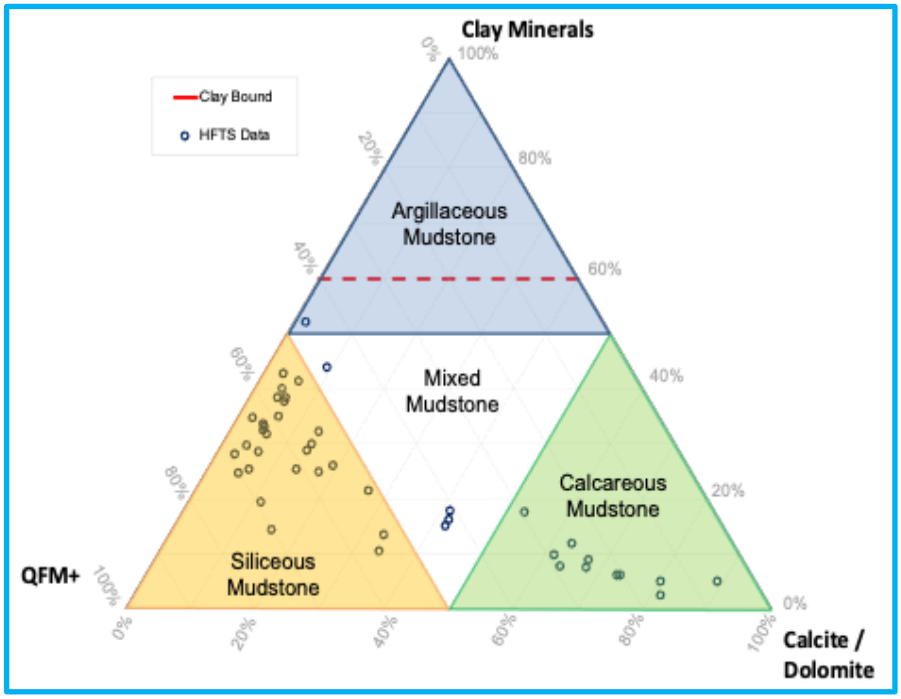

HFTS-1 Natural Joint Data and Engineering Summary

28 January 2022

U.S. DEPARTMENT OF ENERGY | NATIONAL ENERGY TECHNOLOGY LABORATORY

Office of Fossil Energy

DOE/NETL-2022/3724

Disclaimer

This project was funded by the Department of Energy, National Energy Technology Laboratory an agency of the United States Government, through a support contract.

Cover Illustration: A ternary diagram for classification of rock samples from HFTS-1 site.

Suggested Citation: Lindner, E. *HFTS-1 Natural Joint Data and Engineering Summary;* DOE.NETL-2022.3724; NETL Technical Report Series; U.S. Department of Energy, National Energy Technology Laboratory: Morgantown, WV, 2022; p 120. DOI: 10.2172/1842829.

An electronic version of this report can be found at:
https://netl.doe.gov/energy-analysis/search

The data in this report can be accessed from NETL's Energy Data eXchange (EDX) online system (https://edx.netl.doe.gov) using the following link:
https://edx.netl.doe.gov/group/hfts-1-phase-1-group

HFTS-1 Natural Joint Data and Engineering Summary

Ernest N. Lindner[1,2]

[1] U.S. Department of Energy, National Energy Technology Laboratory, 3610 Collins Ferry Road, Morgantown, WV 26507

[2] NETL Support Contractor, 3610 Collins Ferry Road, Morgantown, WV 26507

DOE/NETL-2022/3724

28 January 2022

This page intentionally left blank.

Table of Contents

Table of Contents (cont.)

List of Figures

List of Figures (cont.)

List of Tables

Acronyms, Abbreviations, and Symbols

Term	Description
Acronyms/Abbreviations	
CaO_3	Calcium oxide
COI	Compact Oil-Base Mud Microimager
COP	ConocoPhillips
.csv	Comma-separated values file
CT	Computed tomography
DOE	U.S. Department of Energy
EDX	NETL's Energy Data eXchange
GR	Gamma ray reading
HFTS-1	Hydraulic Fracture Test Site #1
.las	Log ASCII standard file for well data
MR	Magnetic resonance
NETL	National Energy Technology Laboratory
QFM+	Quartz, feldspar, and mica content
RQD	Rock quality designation
TOC	Total organic carbon
XRF	X-ray fluorescence
Units / Symbols	
API	American Petroleum Institute’s unit for gamma ray emissions
°	degrees, orientation from north or horizontal
bpm	barrels per minute
cv	coefficient of variation
ft	feet
g/cm^3, g/cc	grams per cubic centimeter
lb/gal	pounds per gallon
m	meters
mm	millimeters (10^{-3} m)
Mpsi	Megapound per square inch (10^6 psi)
psi	pounds per square inch

Acknowledgments

This work was completed as part of the Science-informed Machine learning to Accelerate Real Time decision making for Oil & Gas (SMART-OG) Initiative (edx.netl.doe.gov/SMART). Support for this initiative was provided by the U.S. Department of Energy's (DOE) Office of Fossil Energy's Oil and Natural Gas program through the National Energy Technology Laboratory (NETL). The authors wish to acknowledge Jared Ciferno (NETL, Acting Onshore Oil and Gas Technology Manager), Sailendra Mahapatra (DOE Office of Fossil Energy, Program Manager for Oil and Gas Upstream Research and Machine Learning/Deep Learning/Artificial Intelligence Programs, and Elena Melchert (DOE Office of Fossil Energy, Director, Upstream Oil & Gas Research Division) for programmatic guidance, direction and support.

ABSTRACT

This report provides an analysis of engineering and geologic data collected from the Hydraulic Fracturing Test Site #1 (HTSF-1) project in the southern Midland Basin, Reagan County, Texas. The site is being studied as part of the Science-informed Machine Learning for Accelerating Real-Time Decisions in Subsurface Applications (SMART) Initiative at the National Energy Technology Laboratory (NETL). The data collected is intended to provide a basis of understanding of the site and to construct simulation models. This report provides a summary analysis of the engineering and geologic data collected from the project to provide a basis of understanding of the site and to construct simulation models.

The report examines various possible correlations in engineering properties based on natural fracture data from the program, which consisted of 11 horizontal wells, one vertical well, and one slant well. The horizontal wells are in two horizons: 1) Upper and 2) Middle Wolfcamp formations. Program data include: fracture frequency and fracture orientation data from four core runs in a slant well; fracture spacing and orientation from a vertical pilot well; laboratory triaxial testing and mineralogical determinations; and porosity results from magnetic resonance analyses from various wells, together with observations based on the data collection. In addition, available references were reviewed on the site for additional insights. As the focus of the report is on the natural system, hydraulic fracture data from the site were not examined in detail in this report.

Data variability is the chief observation in examination of the database. Fracture frequency in the slant well can range from sections with values as high as five fractures per ft to sections up to 100+ ft in length with no natural observed fractures. Fracture spacing across is typically less than 10 ft, but can range up to hundreds of feet. Apparent fracturing shows the trends in two predominate orientations, E-SW and WNW-ESE, but minor variations exist. The rock units vary across the site from siliceous mudstones to calcareous mudstones, showing a general layering with depth. The laboratory properties such as strength and modulus show no apparent trend with depth, but appear to correlate with rock mineralogy with high strength and modulus values where calcium content is high.

In addition, an attempt to examine variability and mineralogy on a larger scale was made using a color-coded system based on gamma ray measurements. A staged colored approach was adopted, presuming that lower gamma ray values indicate higher value of calcium content (blue scale) and that higher gamma ray values indicate higher clay mineral content (orange scale). As provided in report appendices, the system correlated well with visual examination of the slant core and the petrofabric analyses of the vertical pilot well. The results showed large variability in mineral content along the horizontal plane across the site. The change in mineral content was also rapid, on a scale less than that of the average hydraulic fracture stage length of about 180 ft.

The data used in this report is available on NETL's Energy Data eXchange (EDX) website: https://edx.netl.doe.gov/group/hfts-1-phase-1-group

1. BACKGROUND

1.1 PURPOSE

This report provides an analysis of engineering and geologic data from Hydraulic Fracturing Test Site #1 (HFTS-1) as a basis for developing an understanding of the site and to construct simulation modeling for machine learning. With effective simulation modeling, engineers will be able to design and execute effective hydraulic fracture stages that significantly contribute to production of petroleum in the United States.

This summary report was created from the database obtained during the Phase 1 work on HFTS-1, a collaborative, field-based research project funded by the U.S. Department of Energy (DOE) through the National Energy Technology Laboratory (NETL). The work was a public-private partnership involving a number of exploration and production firms, together with support from academia. The overall field work utilized a range of testing including micro diagnostic formation injection tests, advanced petrographic imaging, tracer testing, microseismic surveys, tilt-meter surveys, bottom-hole pressure data, side-wall coring, as well as multiple pre- and post-treatment cross-well seismic surveys (Ciezobka et al., 2018).

This report is focused on the natural system component of HFTS-1, to examine and evaluate the data on natural fractures at the site, to evaluate the related engineering properties to identify possible parameter correlations, and to examine data aspects that could indicate the uniformity of the rock mass. The effort reviewed available core logs and well surveys, examined reports on approximately 595 ft of rock coring, evaluated laboratory testing on rock strength, modulus, porosity, saturation, bulk density, and mineralogy, as well as examined basic results from gamma radiation results across the site.

The database used in this report is maintained on the NETL's Energy Data eXchange (EDX) website: https://edx.netl.doe.gov/group/hfts-1-phase-1-group.

1.2 TEST SITE

As described by Ciezobka et al. (2020), the HFTS-1 site is in the southern Midland Basin, located in the northern portion of Reagan County, Texas. The overall Phase 1 test program consisted of 11 horizontal wells, one vertical well, and one slant well across the site. The horizontal wells are in two horizons: 1) Upper Wolfcamp Formation and 2) Middle Wolfcamp Formation. Horizontal well spacing in the same formation is approximately 660 ft.

To provide a context for this effort, a site location map and other relevant cross-sections are provided in Appendix A. Additional data from the literature are included in Appendix B. Appendix C provides plots of various logs from the vertical pilot well. Appendix D provides gamma ray (GR) logs for the set of horizontal logs at the site.

1.3 PRIOR LOG ANALYSIS

Reports by Gale et al. (2017, 2018) describe coring operations at HFTS-1, including core acquisition, handling, and preparation. These topics are not described further in this report. Of importance, Gale et al. also reviewed core and core logs from the site, identifying both natural and hydraulic fractures, and provided reports on their observations. As a general conclusion, natural fractures were seen to be either sealed, partly sealed (original fracture porosity), or parted. In the latter case, cement was observed on the fracture wall(s). For intact fractures in

segment of cored borehole in the slant core, core apertures were typically less than 1-mm wide, and the dominant filling mineral is calcite with some minor pyrite.

2. NATURAL FRACTURES - SLANT WELL

2.1 GENERAL – SLANT WELL FRACTURE DATA – WELL SUGG-A #171 6TW

Data for slant core well fractures is taken from:

- File: Master fracture data sheet_All Cores.xls.
- Directory: First Round Data/beg-hfts-phase-1/BEG HFTS Phase 1/BEG fracture descriptions.
- EDX: https://edx.netl.doe.gov/workspace/resources/smart_task_6_development?folder_id=de6f2d43-7188-4079-8dbb-04d91983a9ce
- Each line of data is considered a fracture.

2.2 CORE #1 – SLANT WELL FRACTURE DATA – WELL SUGG-A #171 6TW

Core #1 extends from 9,276 ft to 9,365 ft (*inclusive*) (approximately 90 ft) in the Upper Wolfcamp Formation (Figure 1). The natural fractures in the core show variable spacing with zones where no fractures were detected. It appears that the rock quality designation (RQD) index[1] of the core is generally high except near 9,312 ft and 9,339 ft. Two faults are indicated at depths of 9,278.7 ft and 9,332.0 ft, which correlate with more-intense fracturing of the core.

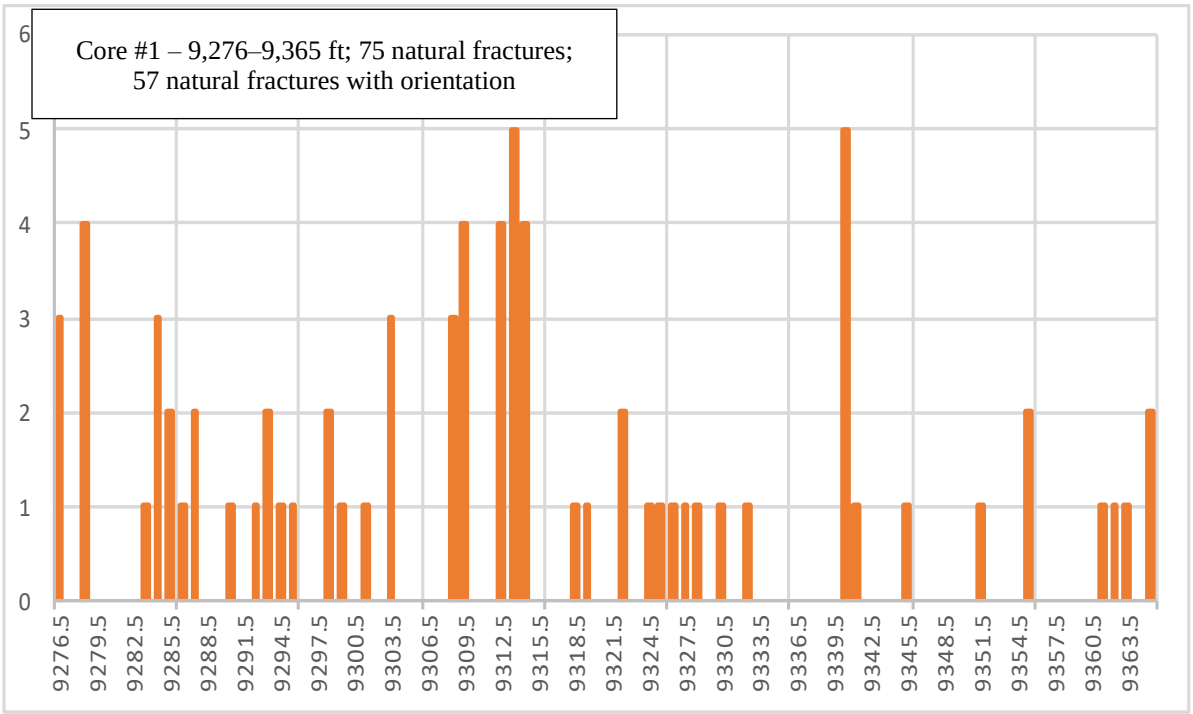

Figure 1: Core #1 natural fracture count per foot in the Upper Wolfcamp Formation.[2]

[1] RQD is a rough measure of the degree of jointing or fracture in a rock mass, measured as a percentage of the drill core in lengths of 10 cm or more (Wikipedia). RQD in this context is an only rough estimate.

[2] The "number of natural fractures with orientation" excludes faults. The number of natural fractures reported, however, includes both faults and joints.

2.3 CORE #1 – NATURAL FRACTURE ORIENTATION

Natural fractures were divided into two sets in logging. Plotting the dip direction of each set separately, two groupings with depth for each set can be observed. For Core #1 fractures, set #1 has two trends, oriented approximately as 150°/330° (see Figure 2a) and set #2 shows two trends at 40° and 220° (see Figure 2b); however, some outliers exist. The dip data of both fracture sets are highly similar, ranging from 71° to 89°.

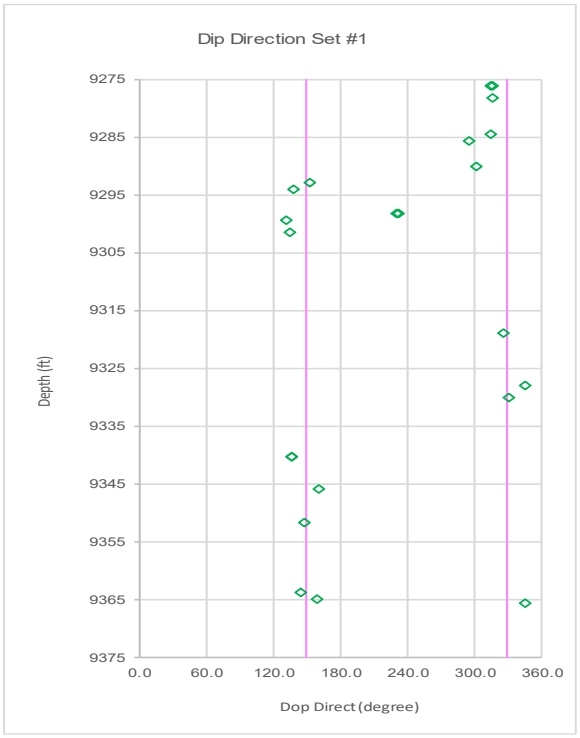

(a) 150°/330°

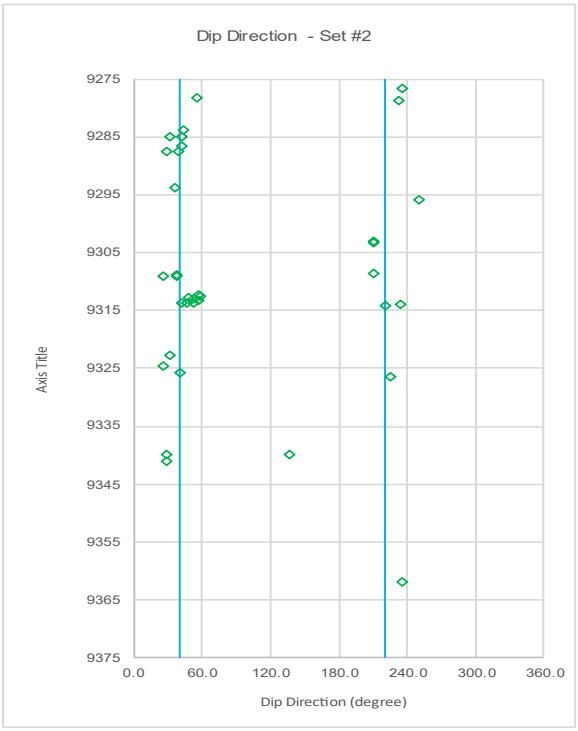

(b) 40° and 220°

Figure 2: Dip direction of natural fracture joint sets in Core #1.

2.4 CORE #2 – SLANT WELL FRACTURE DATA – WELL SUGG-A #171 6TW

Core #2 extends from 9,366 ft to 9,481 ft (approximately 115 ft) in the Upper Wolfcamp Formation (Figure 3). The natural fractures in the core show variable spacing with a large zone where no fractures were detected at approximately 9,431 ft to 9,458 ft. It appears that the RQD index of the core is generally high except near 9,397 ft. No faults are indicated for the drill interval.

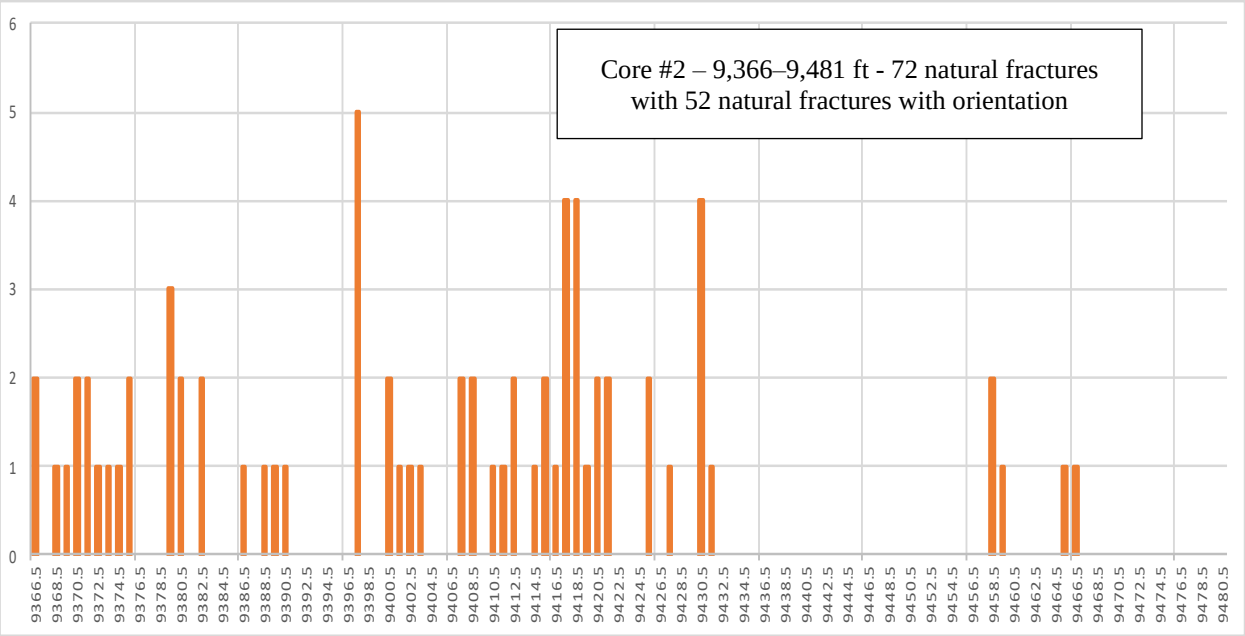

Figure 3: Core #2 natural fracture count per foot in the Upper Wolfcamp Formation.

Note: Each line of data is considered a fracture.

2.5 CORE #2 – NATURAL FRACTURE ORIENTATION

Natural fractures were divided into two sets in logging for Core #2. Plotting the dip direction of each set separately, two groupings with depth for each set can be observed. For Core #2 fractures, set #1 has two trends, oriented approximately as 130° and 310° (see Figure 4a) and set #2 shows two trends at 35° and 215° (see Figure 4b); however, one outlier exists. The dip data of both fracture sets are highly similar, ranging from 70° to 89°.

(a) 130° and 310°

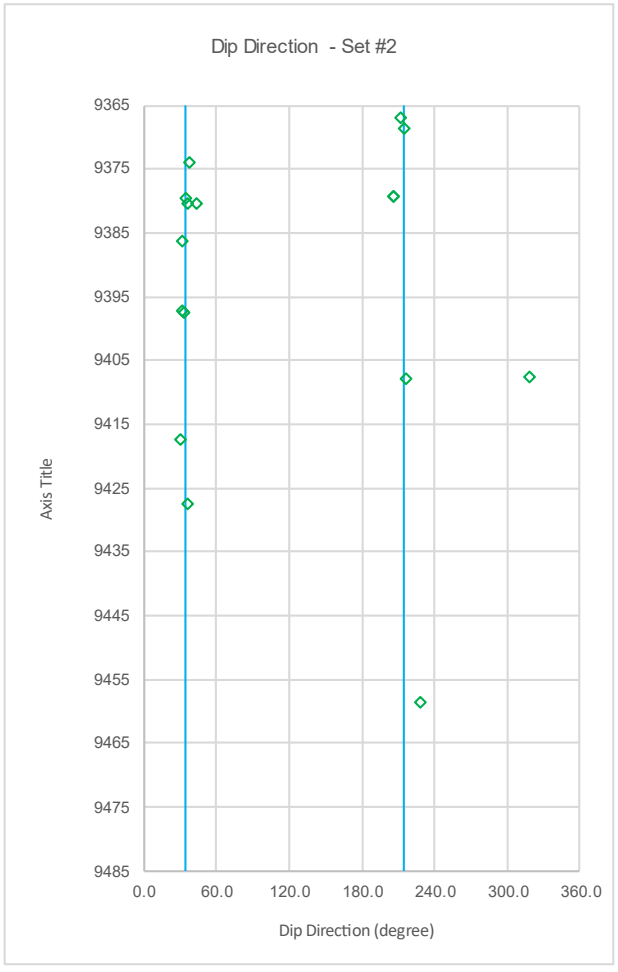

(b) 35° and 215°

Figure 4: Dip direction of natural fracture joint sets in Core #2.

2.6 CORE #3 – SLANT WELL FRACTURE DATA – WELL SUGG-A #171 6TW

Core #3 extends from 9,482 ft to 9,589 ft (approximately 108 ft) in the Upper Wolfcamp Formation (Figure 5). The natural fractures in the core show sparse spacing with a large zone where no fractures were detected at approximately 9,551 ft to 9,574 ft. It appears that the RQD index of the entire core is very high. A set of three faults is indicated at a depth of 9,580 ft.

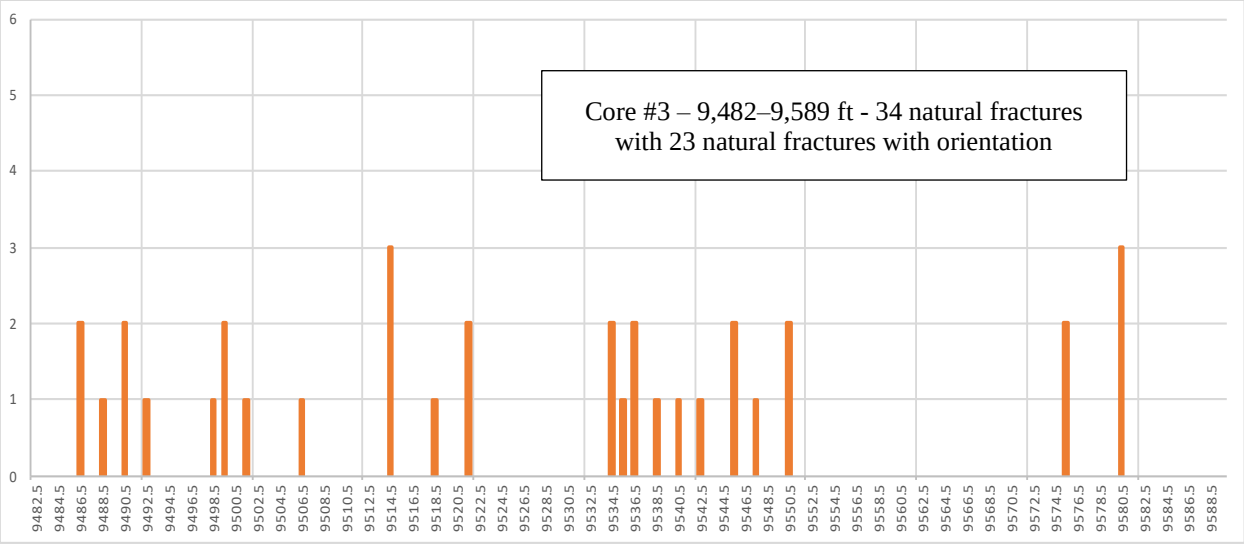

Figure 5: Core #3 natural fracture count per foot in the Upper Wolfcamp Formation.

Note: Each line of data is considered a fracture.

2.7 CORE #3 – FRACTURE ORIENTATION

Natural fractures were divided into two sets in logging for Core #3. Plotting the dip direction of each set separately, two groupings with depth for each set can be observed. As for Core #1, Core #3, set #1 fractures show two trends, oriented approximately as 135º and 315º (see Figure 6a) and set #2 shows two trends at 30º and 210º (see Figure 6b). The dip data of both fracture sets are highly similar, ranging from 81º to 88º.

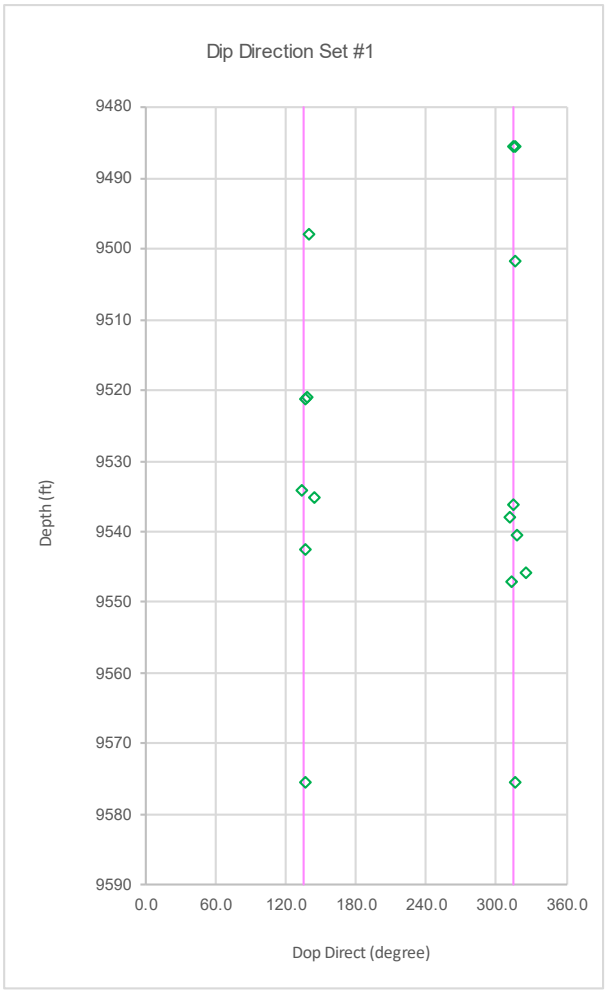

a) 135° and 315°

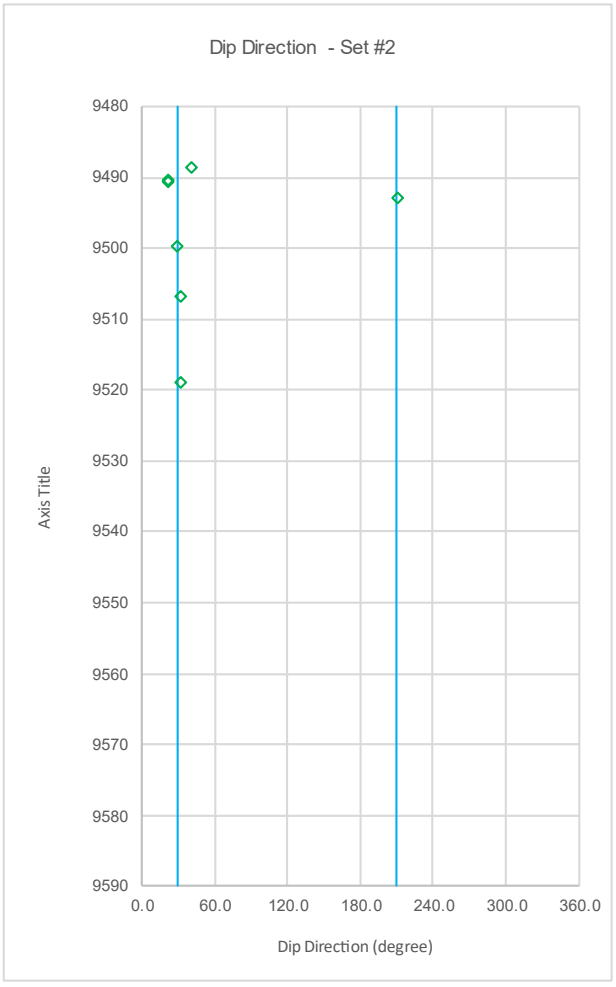

(b) 30° and 210°

Figure 6: Dip direction of natural fracture joint sets in Core #3.

2.8 CORE #4 – SLANT WELL FRACTURE DATA – WELL SUGG-A #171 6TW

Core #4 extends from 9,590 ft to 9,717.5 ft (approximately 128 ft) in the Upper Wolfcamp Formation (Figure 7). The natural fractures in the core show generally uniform spacing, with higher fracturing at: 9,611; 9,667; 9,690; 9,698; and 9,706 ft. It appears that the RQD index of the core is generally high but with zones of more fracturing. Faulting is indicated at depths of approximately of 9,675, 9,678, and 9,680 ft (7 faults).

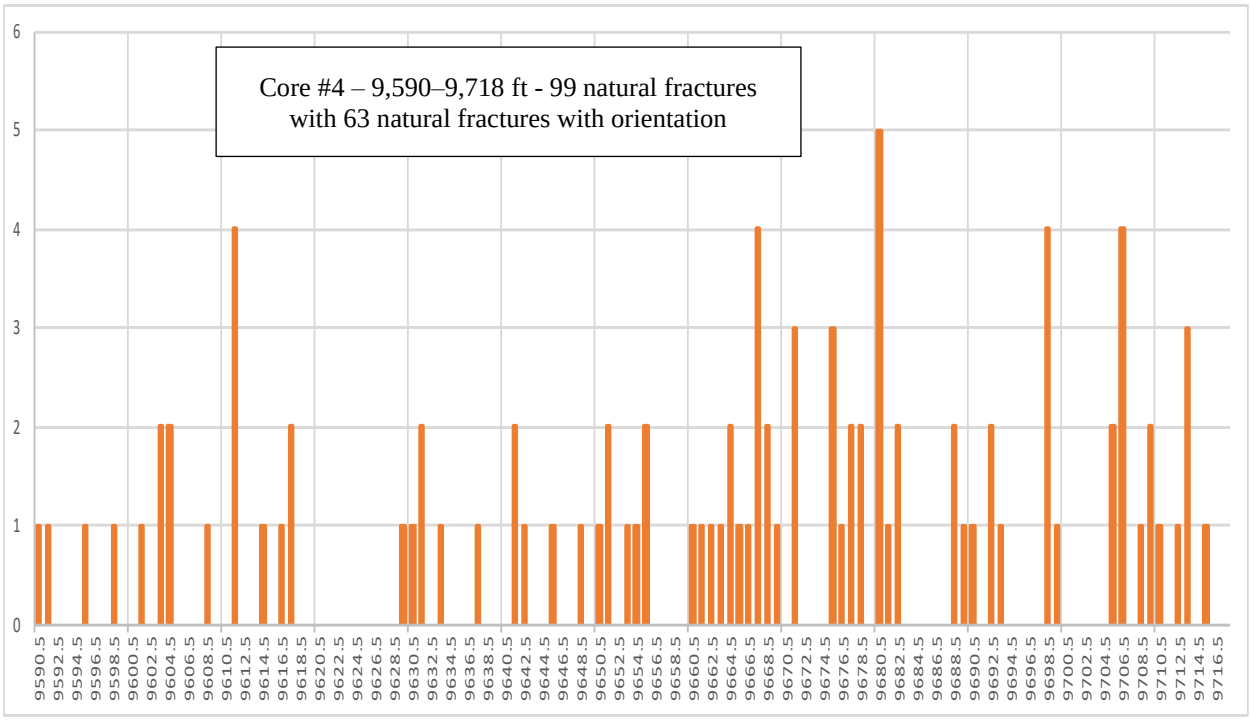

Figure 7: Core #4 natural fracture count per foot in the Upper Wolfcamp Formation.

Note: Each line of data is considered a fracture.

2.9 CORE #4 – NATURAL FRACTURE ORIENTATION

Natural fractures were divided into more than two sets in logging, but only two sets report orientation data (as in the prior runs). Plotting the dip direction of these two sets separately, two groupings with depth for each set can be observed. Similar to Core #1, set #1 fractures have two trends, oriented approximately as 135° and 315° (see Figure 8a) and set #2 shows two trends at 30° and 210° (see Figure 8b). The trends do show some scatter[3] at three locations.[4] The dip data of both fracture sets are highly similar, ranging from 77° to 89°.

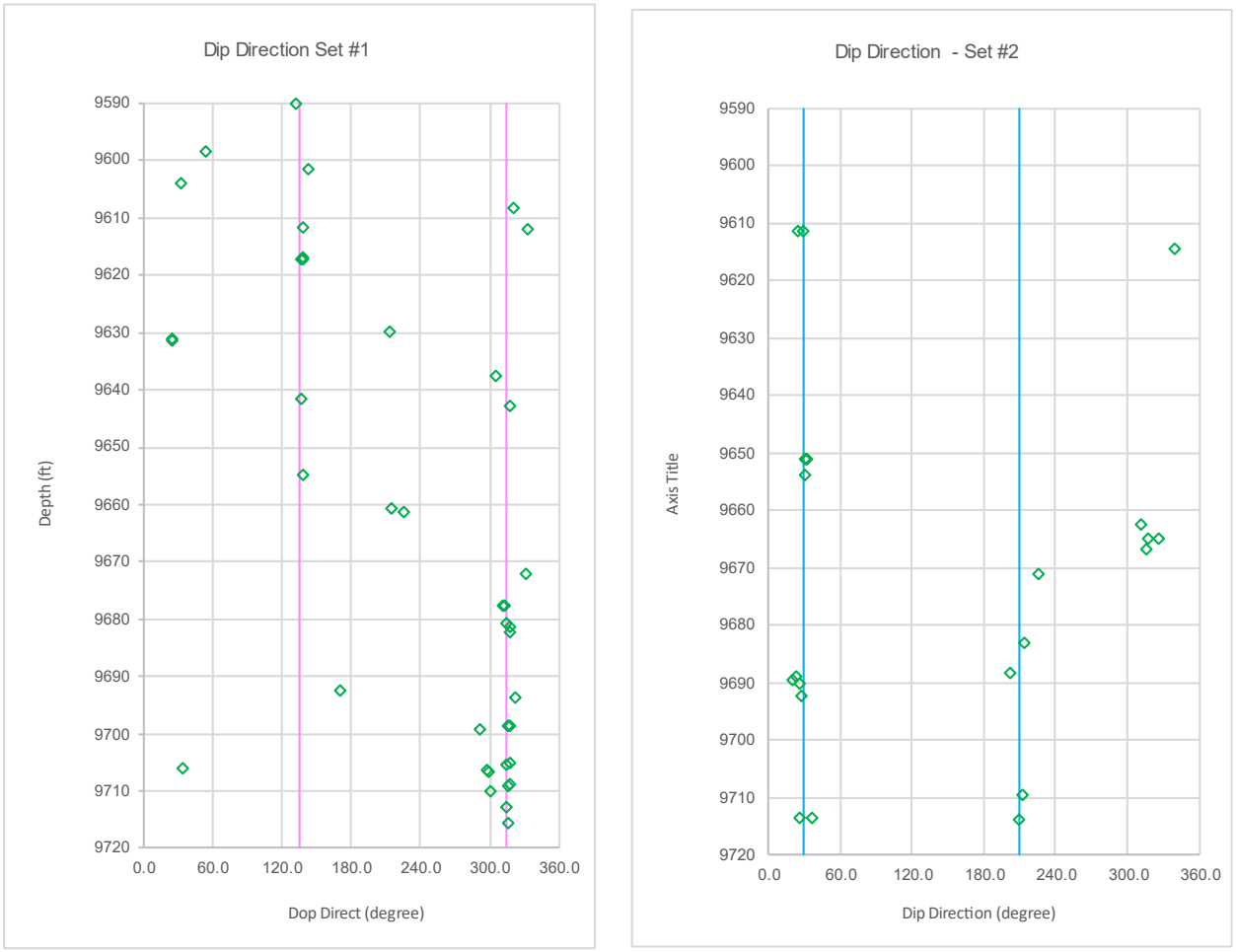

(a) 135° and 315°

(b) 30° and 210°

Figure 8: Dip direction of natural fracture joint sets in Core #4.

[3] A better fit can be obtained if two groups were incorrectly identified, and some problems were noted in the data report in this interval by Gale et al. (2017).

[4] Gale et al. (2017) also describes some minor discrepancies in the original core logs provided by ConocoPhillips (COP) in sections in slant well (9,628–9,634 ft and 9,655–9,667 ft).

2.10 CORES #5 AND #6 – SLANT WELL FRACTURE DATA – WELL SUGG-A #171 6TW

Core #5 extends from 11,525 ft to 11,559.6 ft (approximately 35 ft) and Core #6 extends from 11,564 ft to 11,685 ft (approximately 120 ft) for a total of 155 ft (Figure 9) in the Middle Wolfcamp Formation. The two cores were combined as little natural fracture data exists for Core #5. The natural fractures in the cores show generally uniform spacing, with higher fracturing at 11,604 ft together with zones of no fractures at various intervals. It appears that the RQD index of the core is generally high. No faulting is indicated in this interval.

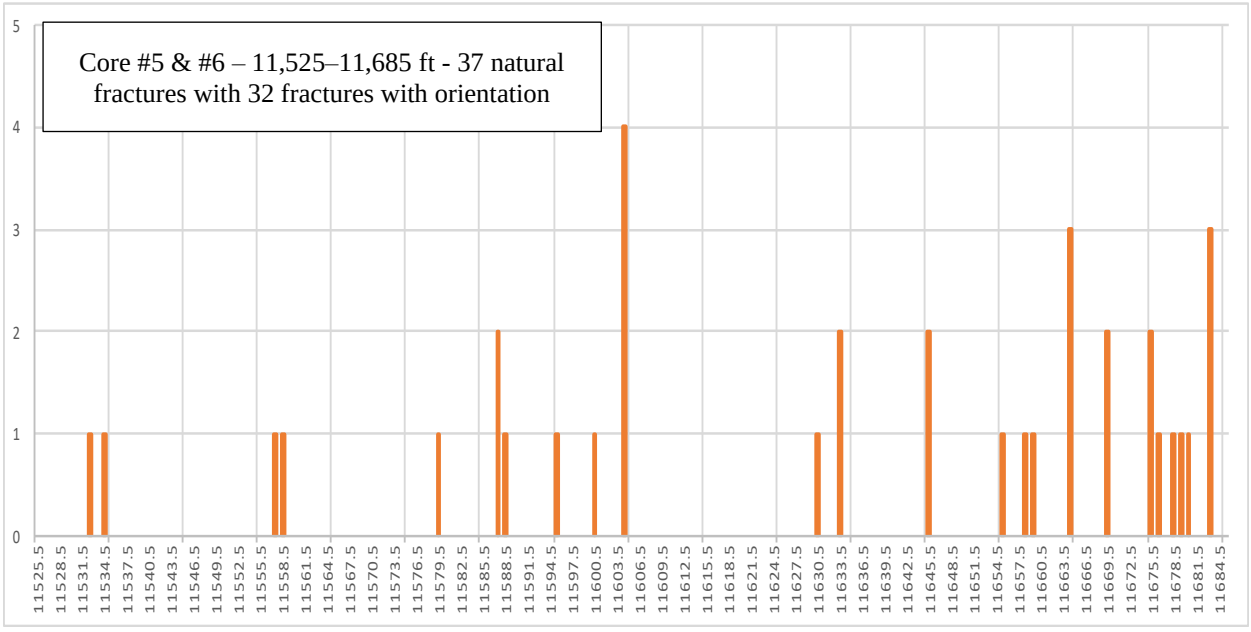

Figure 9: Core #5 and #6 natural fracture count per foot in the Middle Wolfcamp Formation.

Note: Each line of data is considered a fracture.

2.11 CORES #5 AND #6 – NATURAL FRACTURE ORIENTATION

Natural fractures were divided into two sets in logging. Plotting the dip direction of these two sets separately, two groupings with depth for each set can be observed. Similar to Core #1, fractures in set #1 show two trends, oriented approximately as 135° and 315° (see Figure 10a), and fractures in set #2 show two trends at 40° and 220° (see Figure 10b). The trends do show scatter, however. The dip data of both fracture sets are highly similar, ranging from 75° to 90°.

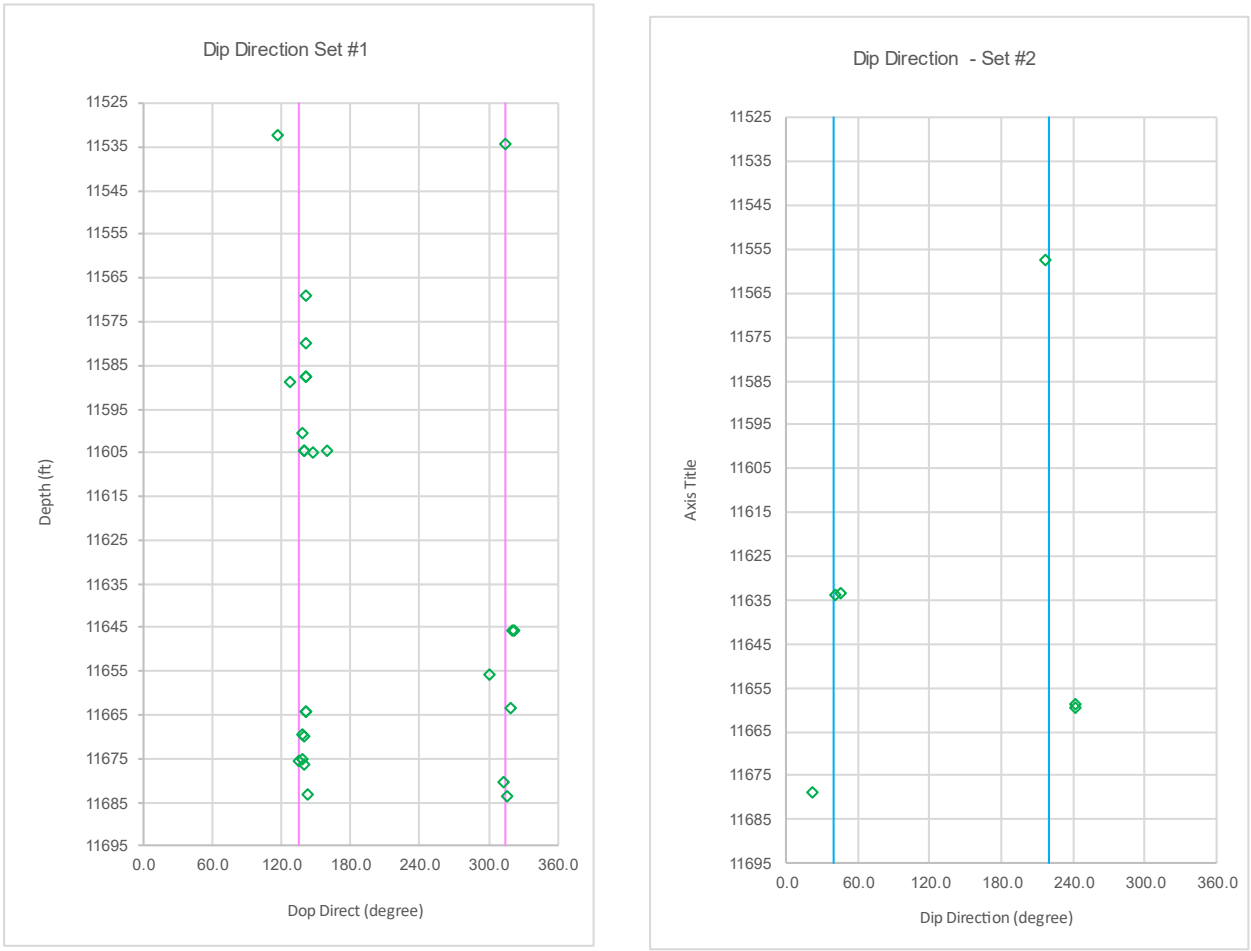

(a) 135° and 315°

(b) 40° and 220°

Figure 10: Dip direction of natural fracture joint sets in Core #5 and #6.

3. NATURAL FRACTURES – HORIZONTAL WELL– WELL SUGG-A #171 6SM

3.1 GENERAL

Data taken from:

- File: 8201-129725767_Laredo_Sugg A 171_6SM_COI_Fractures_DIP_CSV.csv
- Directory: /hfts-1-phase-1-individual-well-files/SUGG A 171 6SM Horizontal /2_Processed Image Log
- EDX: https://edx.netl.doe.gov/dataset/hfts-1-phase-1-individual-well-files

3.2 NATURAL FRACTURE DATA – WELL SUGG-A #171 6SM

The fracture record for horizontal well SUGG-A #171 6SM in the Middle Wolfcamp Formation extends from 7,771 ft to 18,283.66 ft (reference distance) or approximately 10,512 ft in length (Figure 11). The natural fractures in the record show variable spacing with most spacings less than 10 ft, and some at distances up to 165 ft. Most of the fractures are labeled as “partial” with five listed as “resistive.” A total of 1,013 fractures are recorded, for a frequency of about one fracture every 10 ft.

The fractures show a strong trend to the NNW to NW with a smaller trend to the NNE, as shown in Figure 12.

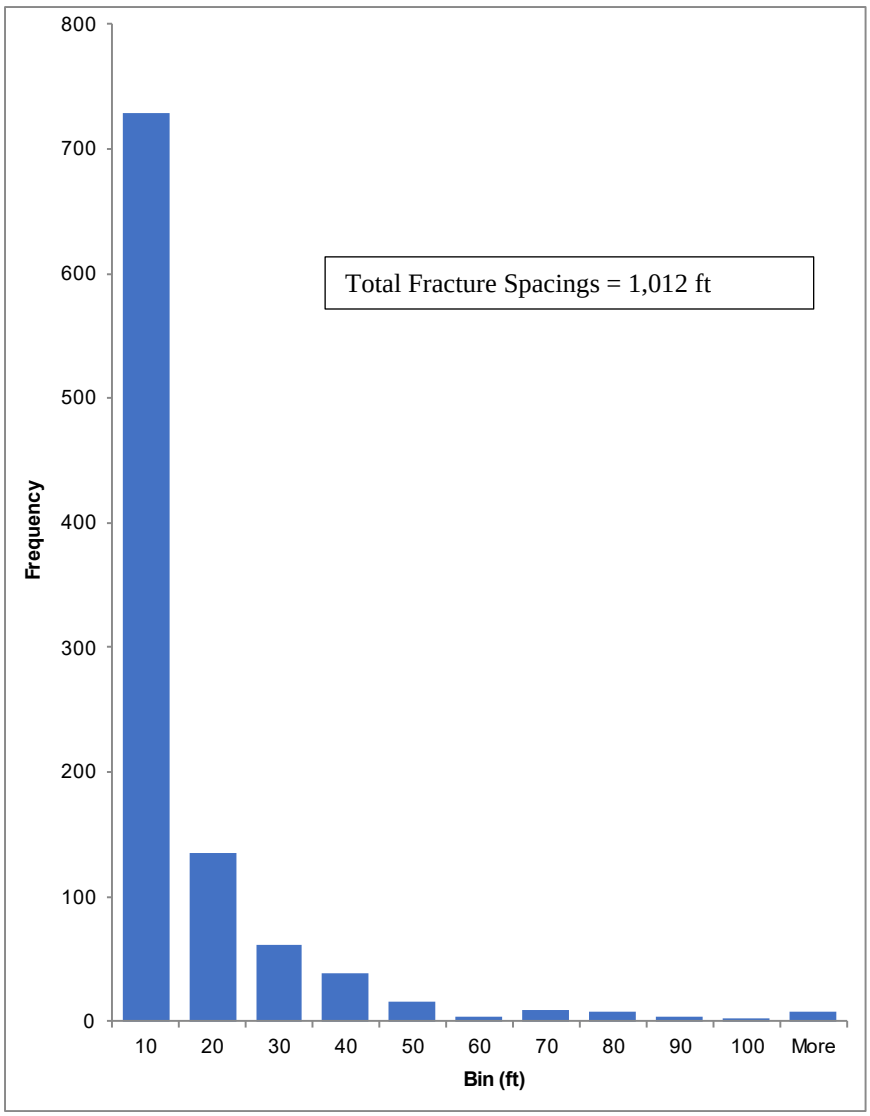

Figure 11: Fracture spacing in horizontal well in Middle Wolfcamp Formation, Well SUGG-A #171 6SM.

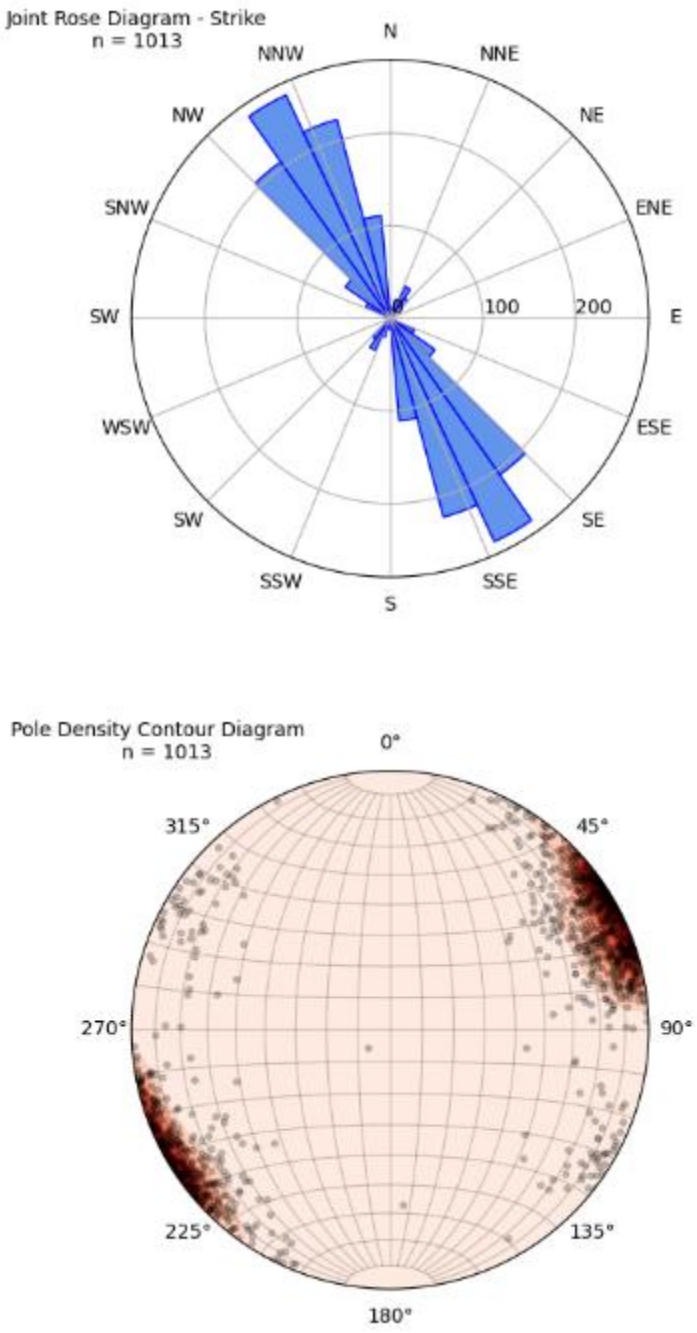

Figure 12: Strike rose diagram and pole diagram of natural (partial) fractures from horizontal well SUGG-A #171 6SM.

Notes:

1. Data from file: 8201-129725767_Laredo_Sugg A 171_6SM_COI_Fractures_DIP_CSV.csv
2. Directory: hfts-1-phase-1-individual-well-files//SUGG A 171 6SM Horizontal.

4. NATURAL FRACTURES – VERTICAL PILOT WELL SUGG-A #171 7SU

4.1 GENERAL

Data taken from:

- Files: Laredo_SUGG_A_171_7SU_dip_frac_7850_8100_Corrected.ascii, Laredo_SUGG_A_171_7SU_dip_frac.ascii
- Directory: /hfts-1-phase-1-individual-well-files/SUGG A 171 7SU Pilot Hole/2_Processed Image Log
- EDX: https://edx.netl.doe.gov/dataset/hfts-1-phase-1-individual-well-files

4.2 NATURAL FRACTURE ORIENTATION – VERTICAL PILOT WELL

In the analyses by Laredo Petroleum (2016), natural fractures in the vertical pilot well are divided into three groups: (1) resistive, (2) conductive, and (3) marginal. Resistive fractures are healed, generally calcite-filled, and strongly strike along a trend of NNW (approximately 330–360°) with a minor trend at ENE (about 80°) (Figure 13). The conductive fractures primarily strike NNE (approximately 10–30°), with smaller peaks at 75°, 105°, and 135° as shown in Figure 14. The two marginal fractures trend ENE (at about 75°). The dip of these near-horizontal fractures is 0–20°.

Looking at fracturing in each unit separately, the dip direction in the Dean Formation appears more consistent, while the fractures in the Middle and Lower Wolfcamp formations are more variable (see Figure 15). Natural fractures also appear to be somewhat clustered with depth into several (weak) groupings. Some examples of this clustering are at depths:

- 7,242 to 7,280 ft (Dean)
- 7,484 to7,542 ft (Upper Wolfcamp)
- 7,670 to 7,674 ft (Upper Wolfcamp)
- 7,902 to 7,920 ft (Middle Wolfcamp)
- 8,073 to 8,088 ft (Middle Wolfcamp 2) (fracturing at 8,073 to 8,088 being the most evident)
- 8,162 to 8,168 ft (Middle Wolfcamp 2)
- 8,346 to 8,349 ft (Lower Wolfcamp)
- 8,422 to 8,425 ft (Lower Wolfcamp)

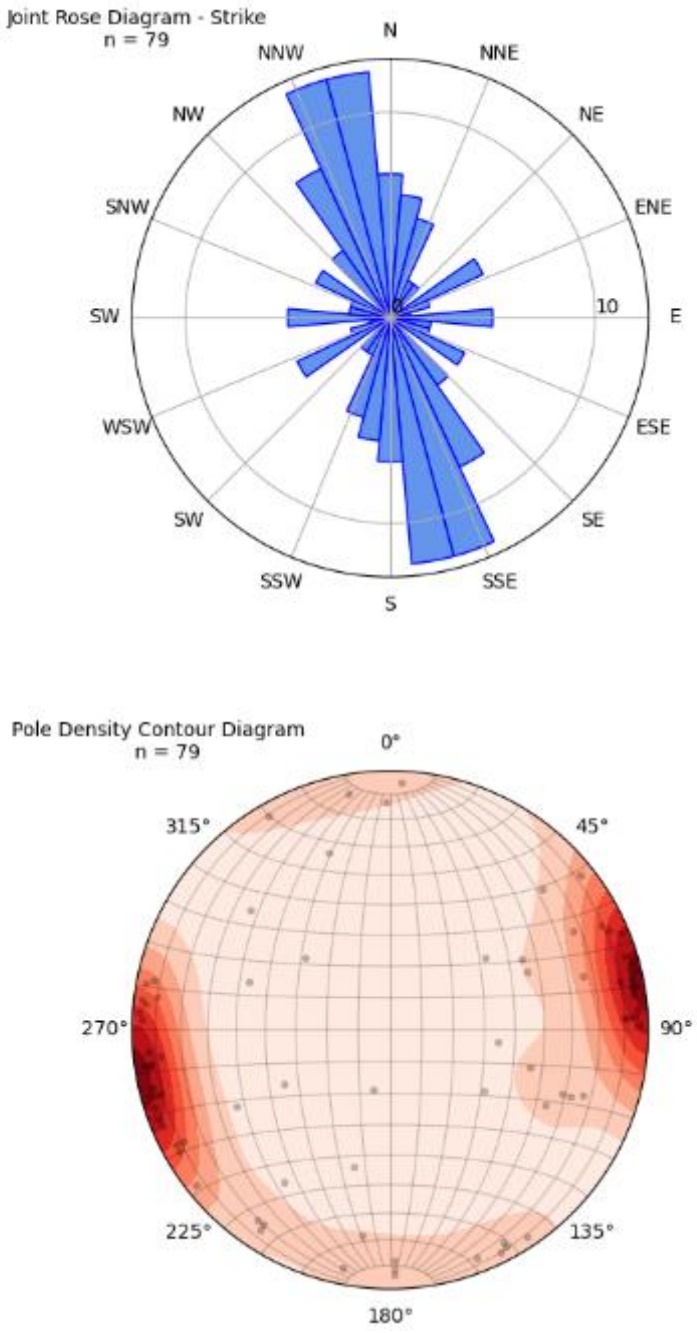

Figure 13: Strike rose diagram and pole diagram of resistive natural fractures from pilot well, SUGG-A #171 7SU.

Notes:

1. Data from file: 8201-129725767_Laredo_Sugg A 171_6SM_COI_Bedding_DIP_CSV.csv.
2. Directory: SUGG-A 171 7SU Pilot Hole/ 2_Processed Image Log. (2015).
3. Resistive fractures are sealed/filled fractures.

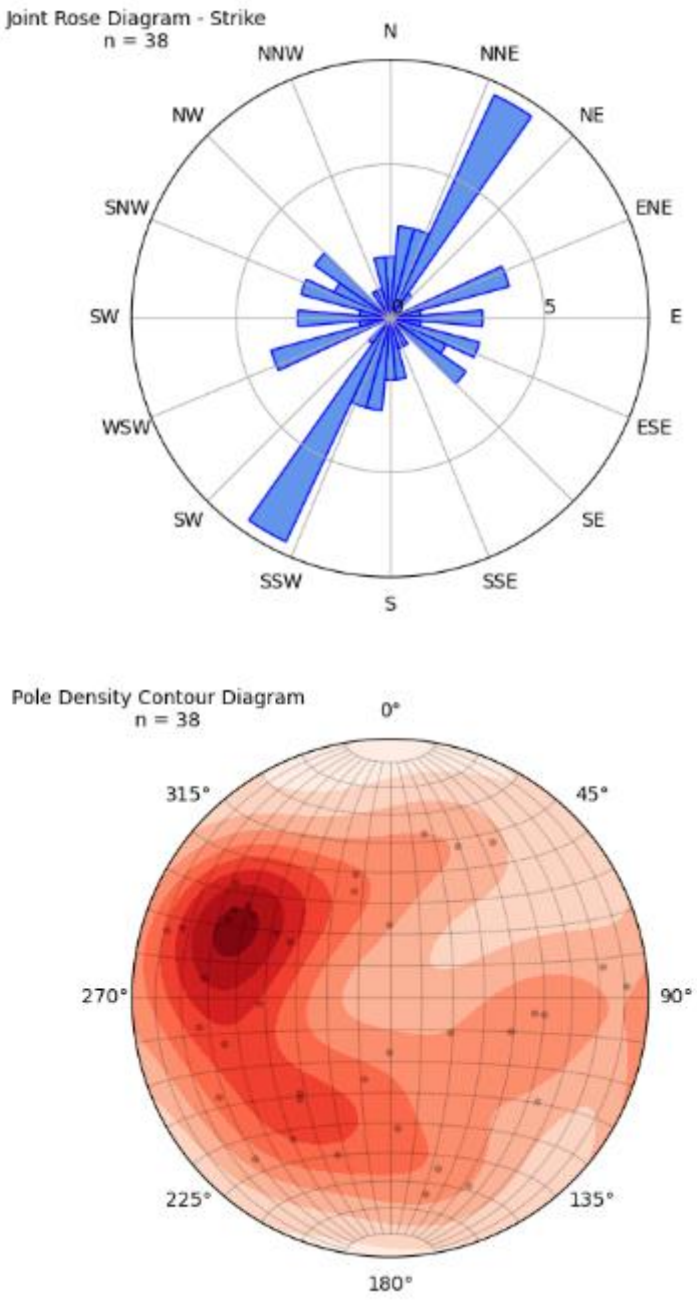

Figure 14: Strike rose diagram and pole diagram of conductive natural fractures from pilot well, SUGG-A #171 7SU.

Notes:

1. Data from file: 8201-129725767_Laredo_Sugg A 171_6SM_COI_Bedding_DIP_CSV.csv.
2. Directory: SUGG-A 171 7SU Pilot Hole/ 2_Processed Image Log. (2015).
3. Resistive fractures are open/unfilled fractures.

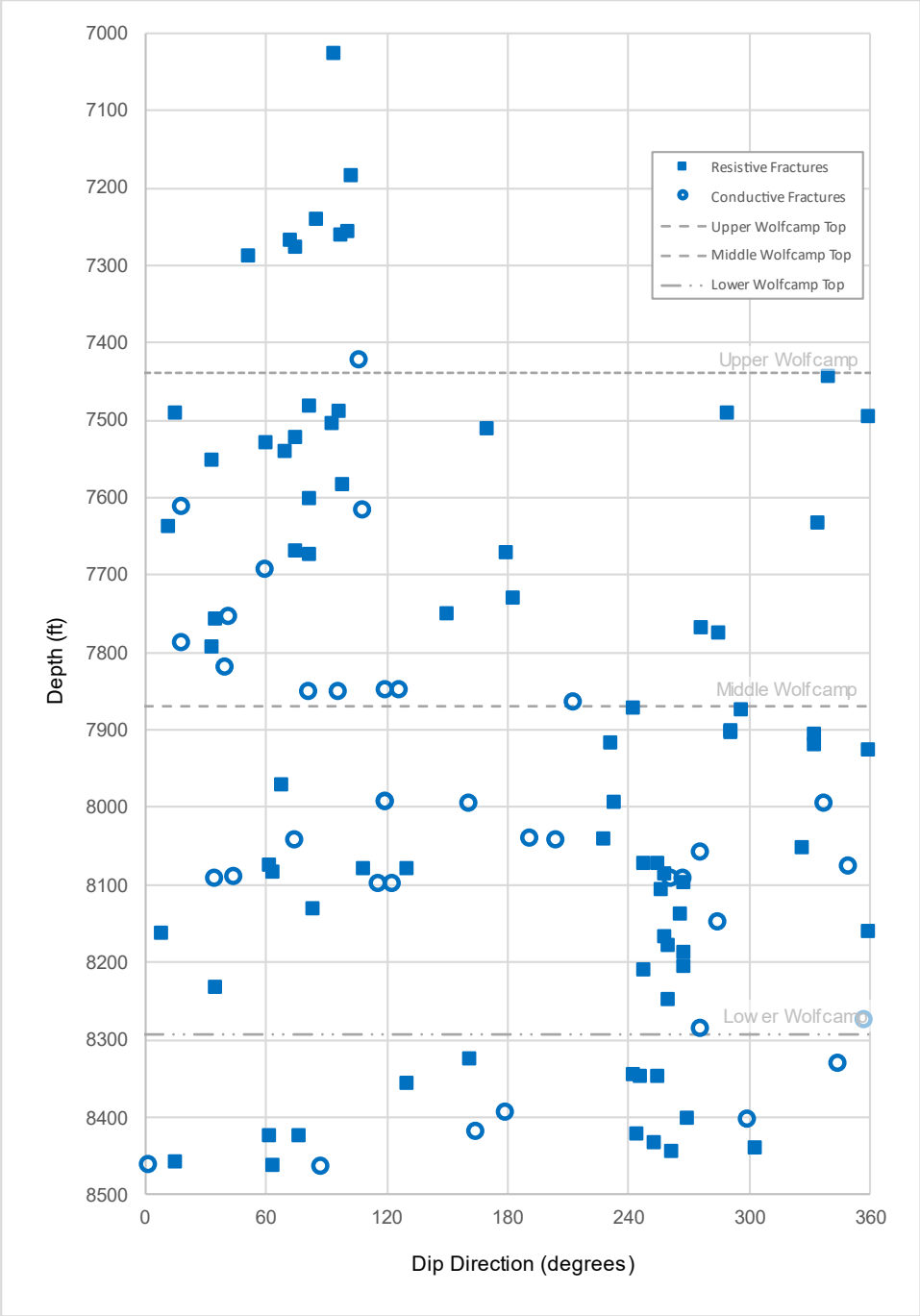

Figure 15: Dip direction of natural fractures in vertical pilot well.

Notes:

1. Data from files: Laredo_SUGG_A_171_7SU_dip_frac.ascii and Laredo_SUGG_A_171_7SU_dip_frac_7850_8100_Corrected.ascii.
2. Directory: SUGG-A 171 7SU Pilot Hole/ 2_Processed Image Log. (2015-2016).

4.3 FRACTURE SPACING – VERTICAL PILOT WELL

The fracture record for vertical pilot well SUGG-A #171 7SU extends from 6,939.67 ft to 8,464.59 ft (vertical depth) or approximately for a total of 1,525 ft (Figure 16). The natural fractures in the core show variable spacing with most spacings less than 10 ft, but some spacings are at distances up to 157 ft. The fractures are labeled as either "conductive" (38) or "resistive" (79). A total of 117 fractures are recorded, for a frequency of approximately 0.08 fractures/ft (eight fractures per 100 ft). A microfault was recorded at about 8,400 ft and two "marginal" fractures at 7,897 ft, both of which were not included in the total number of fractures.[5]

[5] A "significant feature" in the database was also excluded (a bedding plane) at approximately 7,293.3 ft.

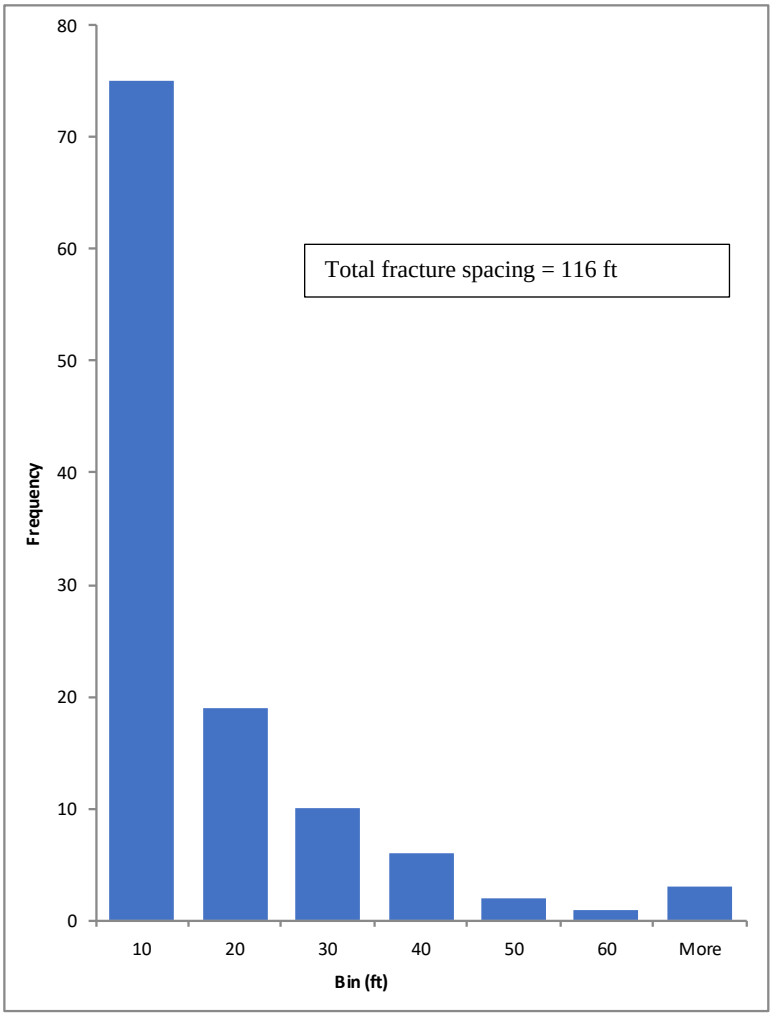

Figure 16: Fracture spacing in vertical pilot well - Well SUGG-A #171 7SU.

Notes:

1. Data from files: Laredo_SUGG_A_171_7SU_dip_frac.ascii and Laredo_SUGG_A_171_7SU_dip_frac_7850_8100_Corrected.ascii.
2. See Directory: SUGG-A 171 7SU Pilot Hole/ 2_Processed Image Log. 2015-2016.

5. LABORATORY DATA – TRIAXIAL COMPRESSIVE TESTING – PILOT WELL SUGG-A #171 7SU

5.1 GENERAL

Data taken from

- Files:
  - 150712 Multi-Stage Triaxial-Summary-LWC 1-28-16.xls
  - 150712 Multi-Stage Triaxial-Summary-MWC 1-28-16.xls
  - 150712 Multi-Stage Triaxial-Summary-Spraberry 1-28-16.xls
  - 150712 Multi-Stage Triaxial-Summary-UWC 1-28-16.xls
- Directory: *Final Inventory/Side-wall_Core_Data/7SU_Pilot/ 11_Triaxial Compressive Tests*
- EDX: https://edx.netl.doe.gov/workspace/resources/smart_task_6_development?folder_id=705e29a0-1686-425f-b324-ec035f357e4d

5.2 STRENGTH DATA

Uniaxial strength results (i.e., strength at a confining stress = 0) from the vertical pilot well SUGG-A #171 7SU are shown in Figure 17. A general average of uniaxial strength is approximately 6,000 psi. The results also show more variability and higher strengths below 7,800 ft in the Middle and Lower Wolfcamp formations.

5.3 MODULUS DATA

Young's modulus data from various laboratory tests on sidewall core from the vertical pilot well SUGG-A #171 7SU are shown in Figure 18. The data for each formation exhibits wide variation (especially below 7,800 ft), and no definitive trend is apparent in the data. A weak trend of increasing modulus can be suggested together with an increase in variability with depth, but this is tentative.

The average modulus of all values is 4.23 Mpsi and range from 1.2 to 8.3 Mpsi. With a uniaxial strength of about 6,000 psi, the rock can be considered to have an average to high modulus ratio that is not typical of shales[6] (Deere and Miller, 1966).

[6] Given the clay mineral content reported elsewhere, the Wolfcamp units are better classified (in most cases) as mixed mudstone/siltstone units rather than a typical shale.

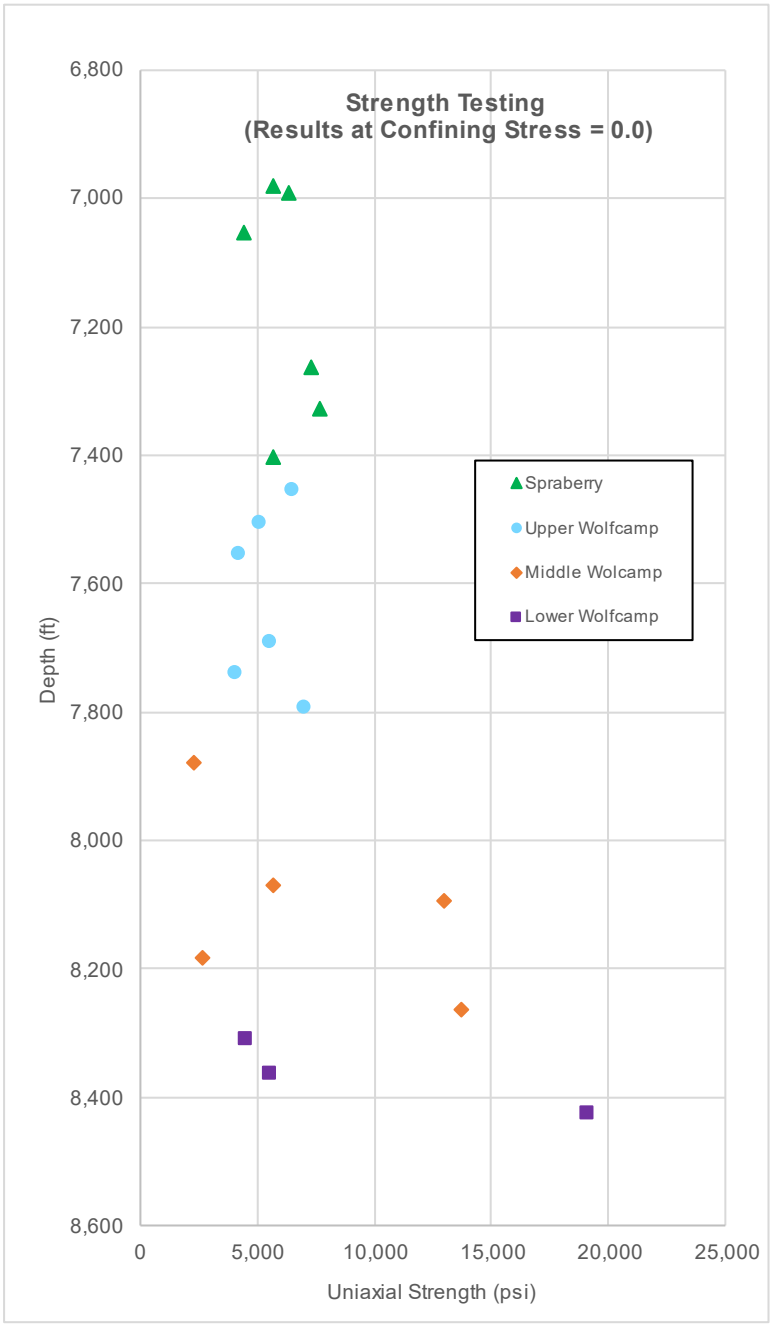

Figure 17: Uniaxial test results from vertical pilot well SUGG-A #171 7SU.

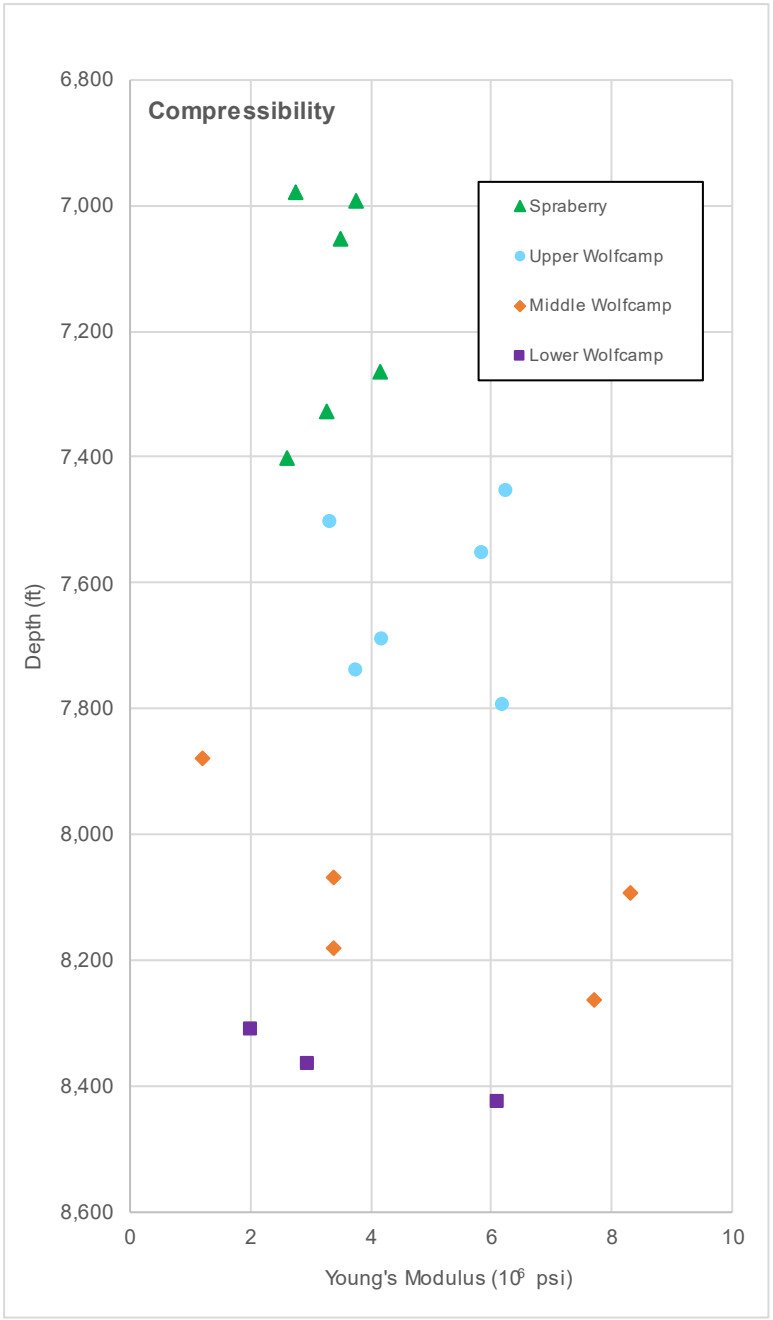

Figure 18: Young's modulus tests with depth in vertical pilot well SUGG-A #171 7SU.

Note:

1. Values based on testing at highest confining pressure measured showing results, depending on test sequence.
2. Average Young's modulus of Wolfcamp units is 4.32 Mpsi; average Young's modulus of Spraberry is 3.68 Mpsi.

6. MAGNETIC RESONANCE AND OTHER TESTING – PILOT WELL SUGG-A #171 7SU

6.1 POROSITY

Overall, porosity measurements of examined units are between 2% to 11.6% in the pilot well. Porosity was measured on core samples manually as well as using magnetic resonance. The manual samples (Figure 19) are variable, averaging approximately 6.5% and show no obvious trend in the Wolfcamp formations, while the samples from the Spraberry are lower in value. The porosity values from magnetic resonance average somewhat lower (averaging about 5.5%). However, the Middle Wolfcamp values in this group appear higher than this trend, and as a group average approximately 7.4% (Figure 20). The Spraberry measurements average about 5.5%.

6.2 WATER SATURATION AND BULK DENSITY

Water/oil saturation and bulk density were also measured on core from the pilot well SUGG-A #171 7SU using magnetic resonance, and results are shown in Figure 21 and Figure 22. Water saturation varies over a wide span from 3% to 79% with somewhat higher values in the Spraberry Formation.

Bulk density results from magnetic resonance (MR) range from 2.4 to 2.8 g/cm^3 as shown in Figure 22. The results show wide variability around an average of 2.59 g/cm^3 with somewhat more variability in the Middle Wolfcamp Formation.

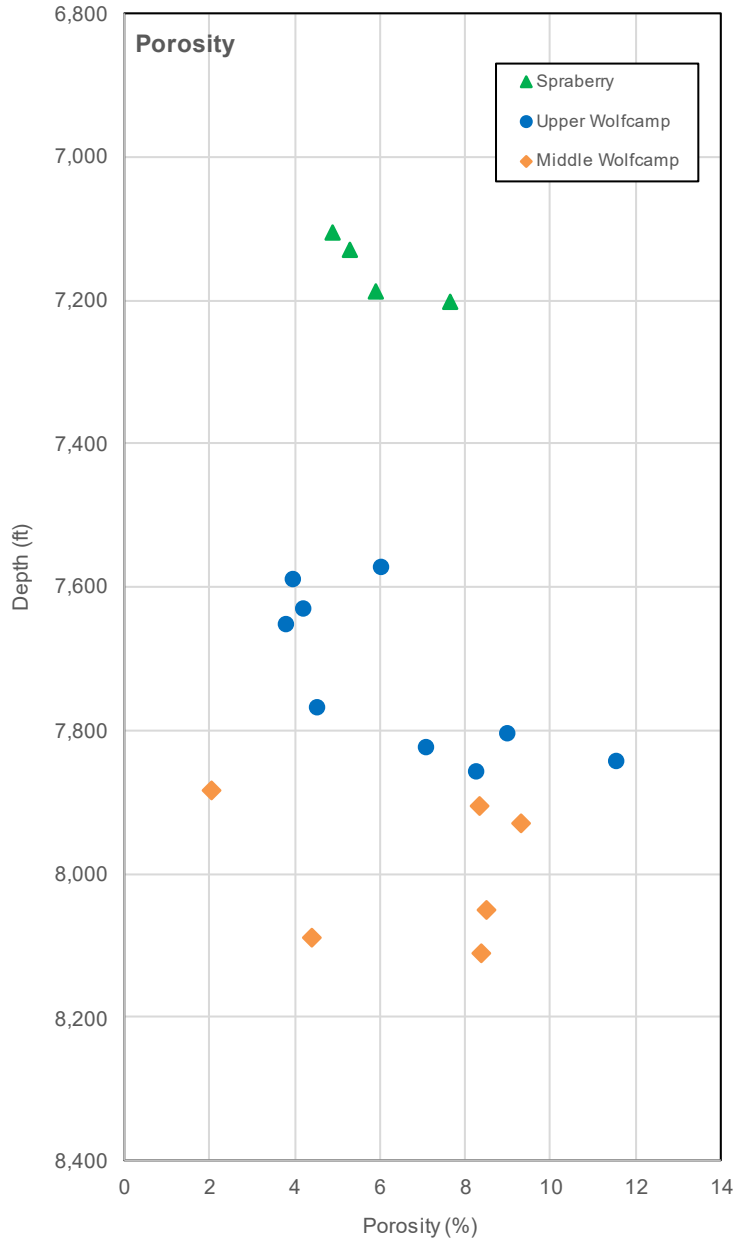

Figure 19: Porosity from manual testing in vertical pilot well SUGG-A #171 7SU.

Notes:

1. Data from file: Sugg_A_#171_7SU_Core_Vault_GRI_Jan_22_2016.xlsx.
2. Directory: SUGG A 171 7SU Pilot Hole/Corevault GRI.
3. Average porosity of Upper Wolfcamp = 6.5%; average of Middle Wolfcamp = 6.8%.

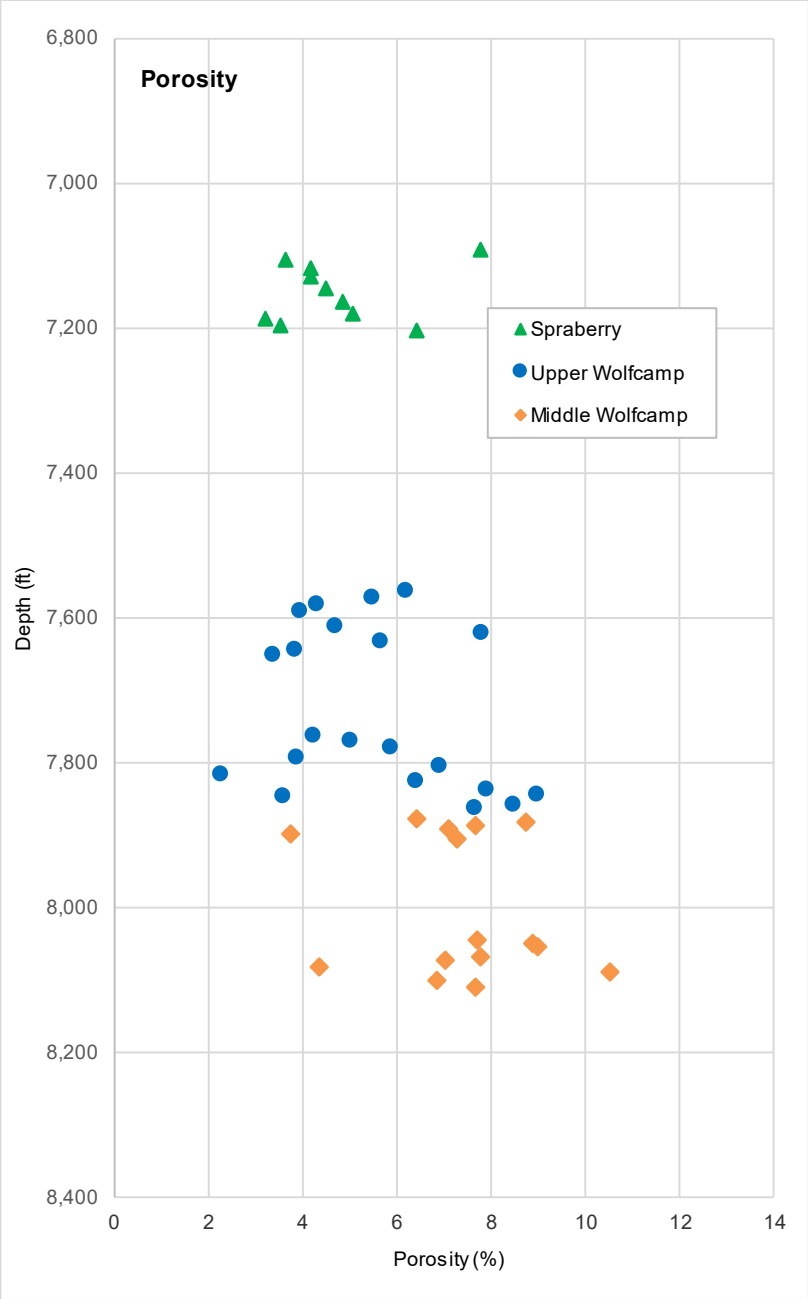

Figure 20: Porosity from MR testing in vertical pilot well SUGG-A #171 7SU.

Notes:

1. Data from file: 150712 MR Shale-Sats Report 11-3-15 (1).xlsx.
2. Directory: SUGG A 171 7SU Pilot Hole/Magnetic Resonance.
3. Average porosity of Upper Wolfcamp = 5.5%; average of Middle Wolfcamp = 7.4%.

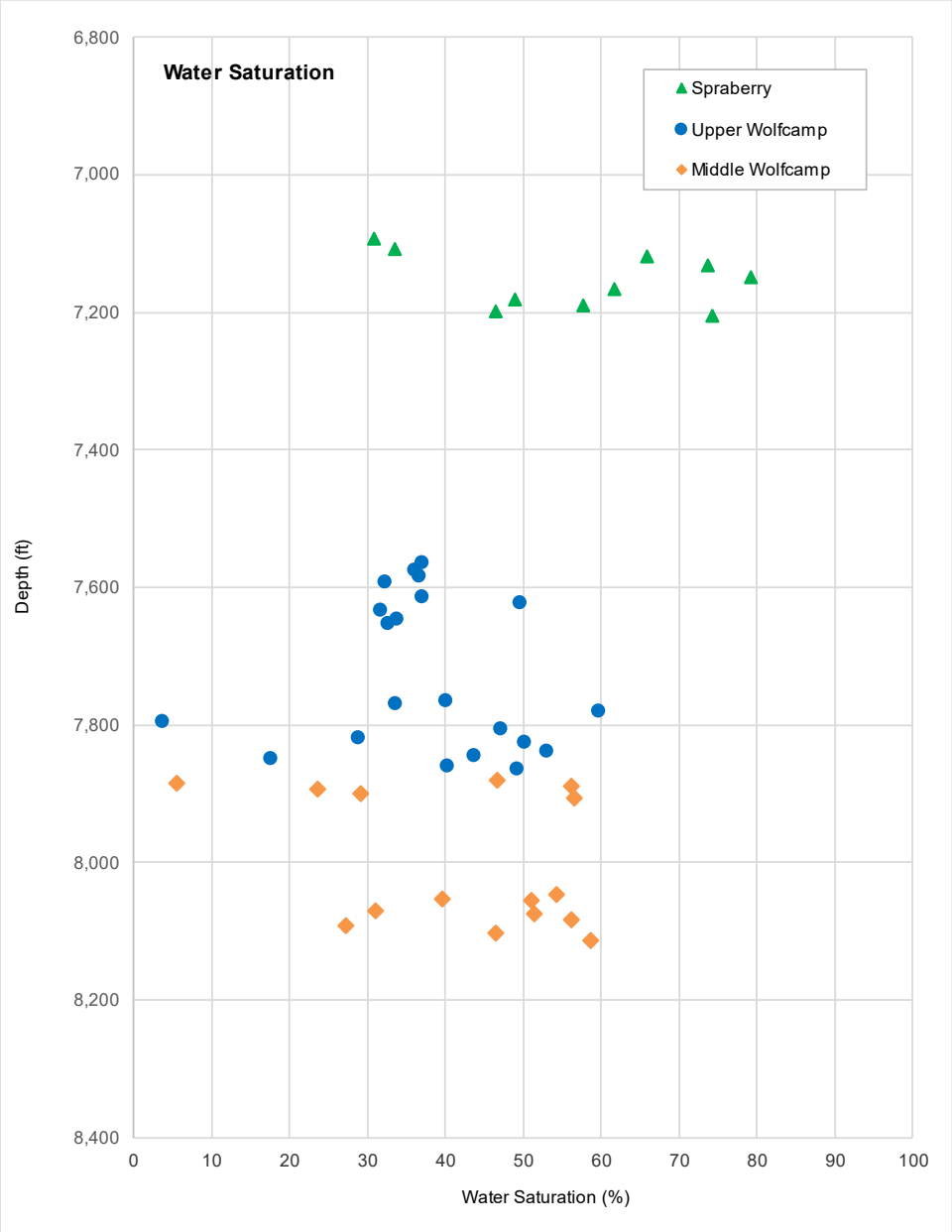

Figure 21: Water saturation from MR testing in vertical pilot well SUGG-A #171 7SU.

Notes:

1. Data from file: 150712 MR Shale-Sats Report 11-3-15 (1).xlsx.
2. Directory: SUGG A 171 7SU Pilot Hole/Magnetic Resonance.
3. Average porosity of Upper Wolfcamp = 5.5%; average of Middle Wolfcamp = 7.4%.

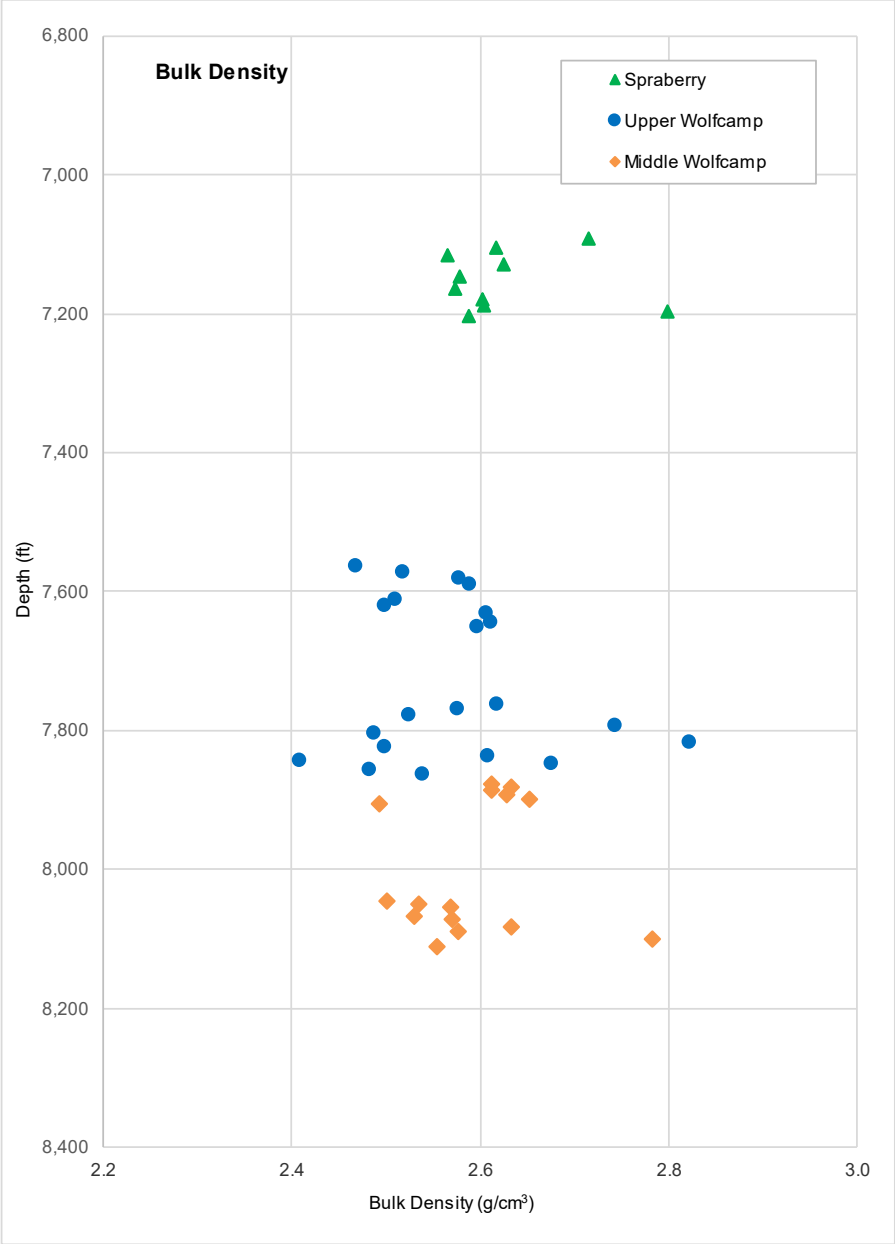

Figure 22: Bulk density from MR testing from well SUGG-A #171 7SU.

Notes:

1. Data from file: 150712 MR Shale-Sats Report 11-3-15 (1).xlsx.
2. Directory: SUGG A 171 7SU Pilot Hole/Magnetic Resonance.
3. Average bulk density = 2.59 g/cm^3.
4. Results similar to Smye et al. (2019).

7. OBSERVATIONS

7.1 NATURAL FRACTURES IN SLANT WELL – SUGG-A #171 6TW

Core logging of natural fractures in the slant core well involved approximately 594 ft of 4-in. core with Cores #1 to #4 involving about 441 ft and Cores #5 and #6 involving approximately 153 ft of core. From fracture frequency plots of the slant core well by COP, it is evident that the core in runs #1 to #4 show moderate to few natural fractures per foot, averaging less than 1 fracture per foot, and with larger gaps in fracturing (approximately 25 ft) existing at two points. Some locations of greater fracturing (showing five fractures per foot) exist, which could indicate zones of lower RQD. Fracture logs for core runs #5 and #6 show only sporadic fracturing with less than 0.5 fracture per foot together with larger zones of no-fracturing.

A total of 302 natural fractures[7] and 15 faults are reported in the data, with 227 fractures having orientation data (dip direction). Two defined sets[8] are designated in the frequency data and show little variation in orientation, with a few exceptions (which may be an issue in grouping in the appropriate fracture set). From the available data files, set #1 has 141 observed fractures, and set #2 has 86 observed members. Set #1 is trending approximately 130°–310° (WNW-ESE) and set #2 is about 35°–215° (NE-SW).

As observed by Gale et al. (2019), the aperture-size distribution for NE-SW fractures follow a negative-exponential function, whereas WNW-ESE fractures follow a weak power-law (see Figure 26). They also state that fracture cluster widths are 100–200 m, and cluster spacings range from 350 to 600 m. Fractures in compact oil-base mud microimager (COI) image logs in two other wells have lower cv (1.59 to 2.32).

The orientation of total observed natural fractures from the source data were compared to calcite-filled-only natural fractures from Gale et al. (2017, 2018, 2020) for the two defined joint sets (Figure 23) and show a similar trend in dip direction. Gale et al. (2019) also note that the observed fracture apertures are all below a few millimeters, and most are below a 1 millimeter, as shown in Figure 26.

7.2 VARIABILY AND FAULTING – SLANT WELL – SUGG-A #171 6TW

The parent rock of siliceous mudstone shows distinct layers of calcareous mudstone in the Wolfcamp Formation and other formations. In examining core from the slant core well, the carbonate content in instances corelates with lighter color core sections where rock mineralogy approaches 40% calcium oxide (CaO_3), as shown in Figure 24. Clay mineral content in these zones also appear lower.

Some faulting is also apparent in the core, however the extent of these features appears minor, and they can be termed microfaults in this context (Figure 25). The surfaces do show slickensides, however. Gale et al. (2017) characterized two types of faults in slant well core: (1) early, soft-sediment deformation faults and (2) moderately dipping structures with oblique slip indicated by slickensides on the fault walls (Figure 25). In one case, the slickensides suggest normal and dextral components of oblique slip. Some faults have a small amount of calcite

[7] Each line on the data table is assumed to represent one fracture.

[8] Some additional fracture sets are identified but with no dip direction data.

cement. There are a total of 11 faults in the Upper Wolfcamp, with 7 of them in Core #4, but none was observed in the Middle Wolfcamp.

7.3 FACIES CLASSIFICATION IN PILOT WELL SUGG-A #171 7SU

Mineralogical testing of samples from the Spraberry, Dean, and Wolfcamp formations were conducted in the pilot well at various depths (see Table 1). Based on a ternary classification approach, most observed results are either a siliceous mudstone or a calcareous mudstone; however, one result is classified as an argillaceous mudstone from the Upper Spraberry (Figure 27). This ternary evaluation is comparable to other measurements in the Wolfcamp Formation of the Midland Basin (see Appendix B).

The ternary evaluation also suggest that the data are in two separate groups, one in the siliceous mudstone and the other in the calcareous mudstone categories. Overall, it can also be inferred that the clay mineral content of these formations is below 60%[9], and therefore, the units are not typical shales. The petrographic log supports this assessment of lower clay mineral content. These observations are consistent with mechanical testing discussed earlier, which indicate that the results are outside the typical "shale" category, based on modulus ratio (Deere and Miller, 1966).

[9] The upper bound is consistent with many formations designated as "oil shales". A higher clay mineral content, more than 60% can be seen as an impediment to hydraulic fracturing.

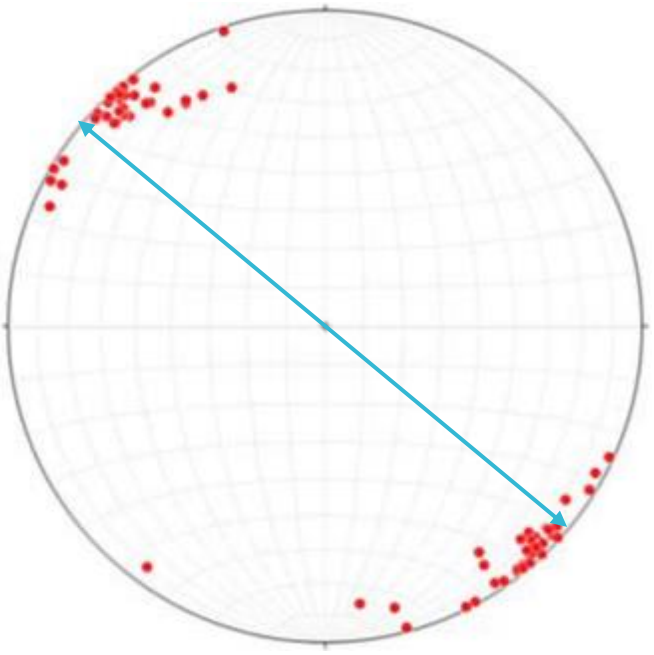

(a) Set #1

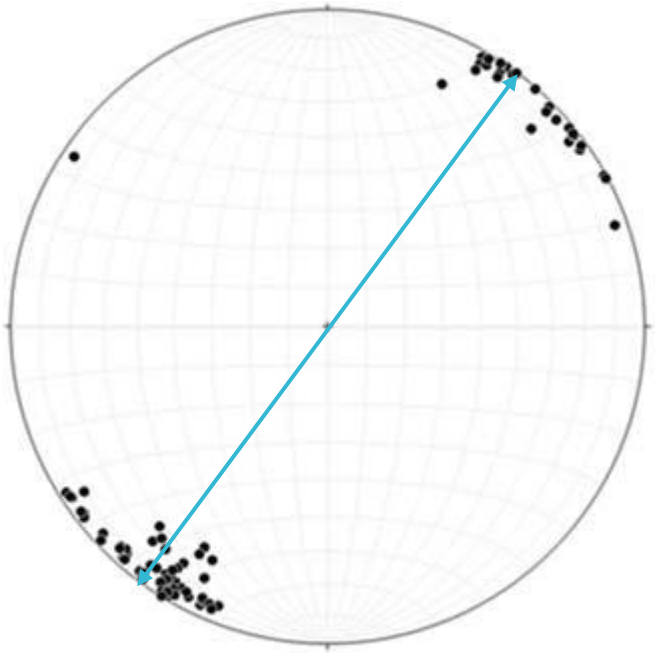

(b) Set #2

Figure 23: Lower-hemisphere stereograms of poles of natural fractures in slant core well.

Notes:

1. Modified from Gale et al. (2017) and data from COP analysis. Set numbers are reversed in Gale et al. (2017).
2. Orientation trends from present analyses of filled and unfilled natural fractures were added to figures.

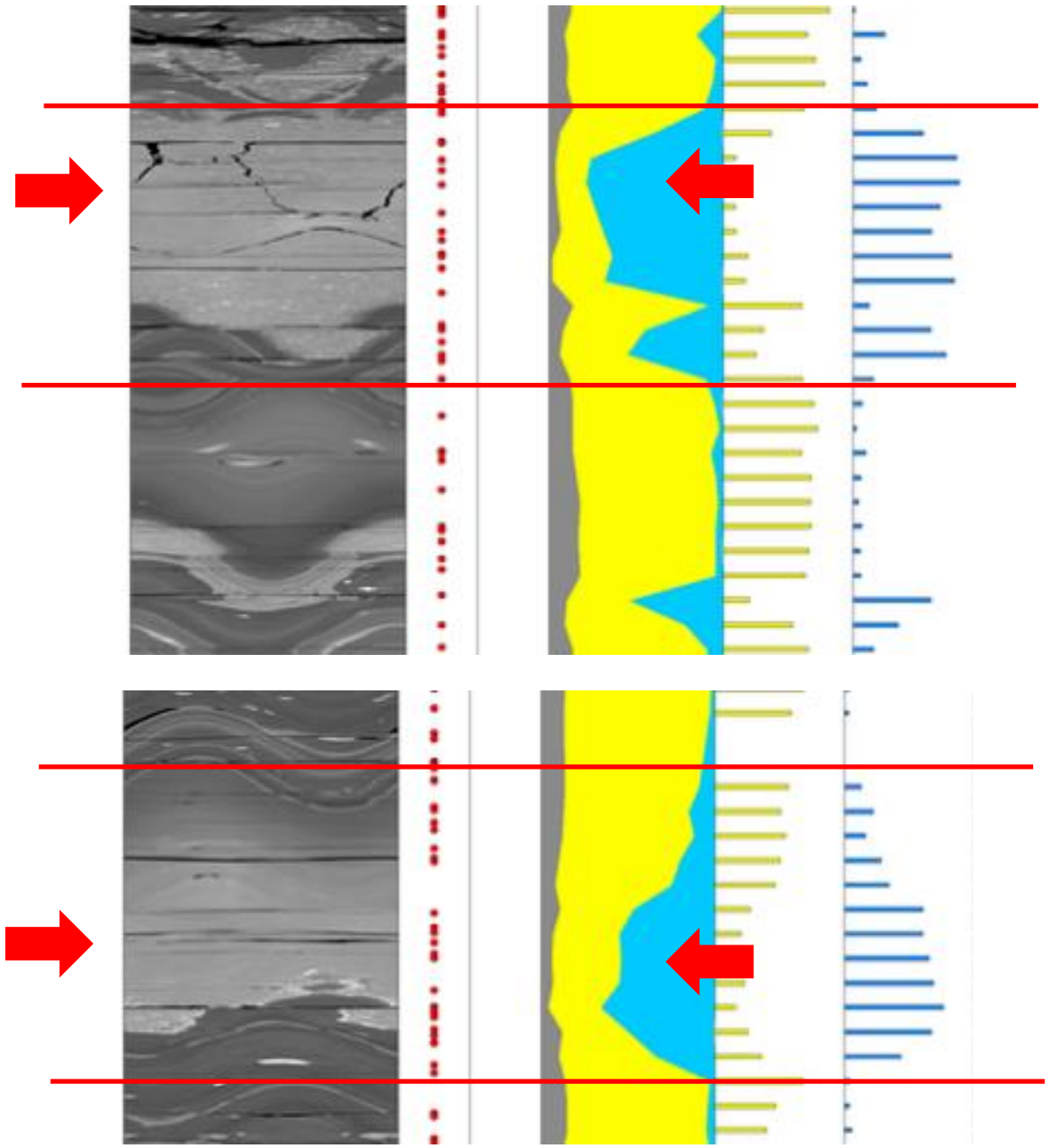

Figure 24: Coloration changes with increased carbonate content shown in HFTS-1 slant core well SUGG-A#171 6TW at 9,425 ft and 9,526 ft.

Note:

1. Modified from HFTS-1 data.
2. File: GTI Core 1-4 CT Scans-XRF-Frac - Scale 1-50.pdf.
3. Directory: Data - HFTS-1/Fracture_log (Slant Core well).
4. The zones at 9,425 ft and 9,526 ft correspond to minimum Spectral Gamma values.

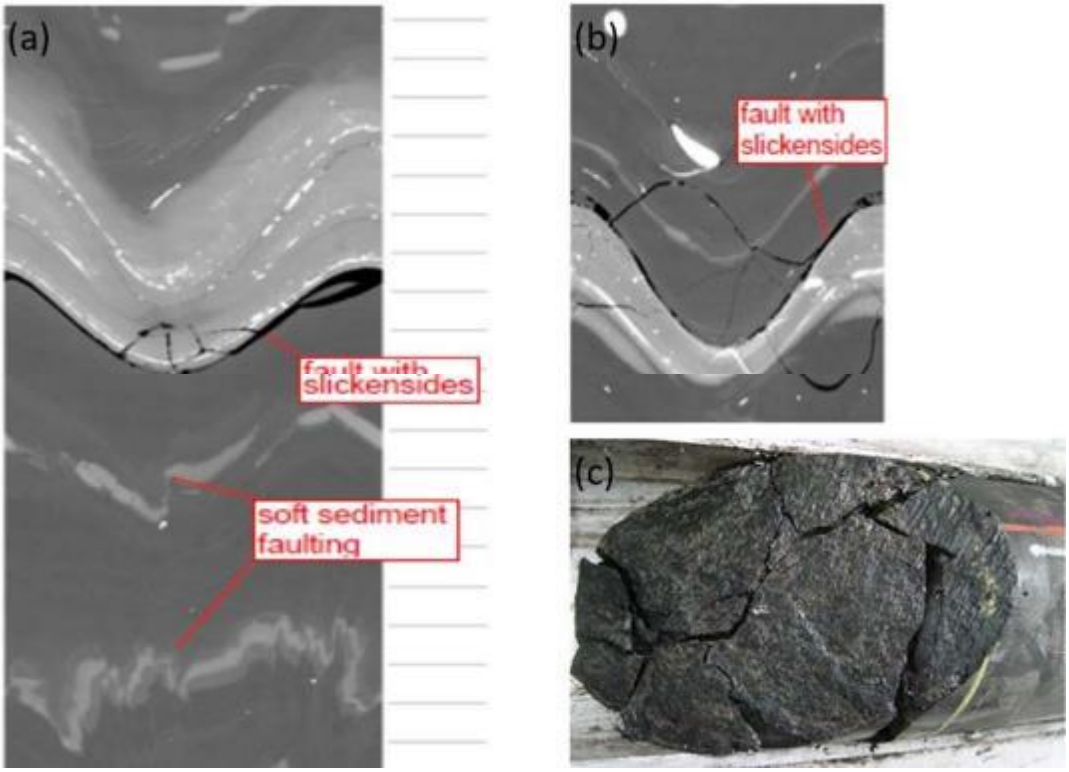

Figure 25: Faults in Core #4 at 9,675–9,681 ft in slant core well SUGG-A #171 6TW as noted by Gale et al. (2017).

Notes:

1. From Gale et al. (2017).
2. From slant core logging, faults show only limited effects on core run.

(a) Set #2

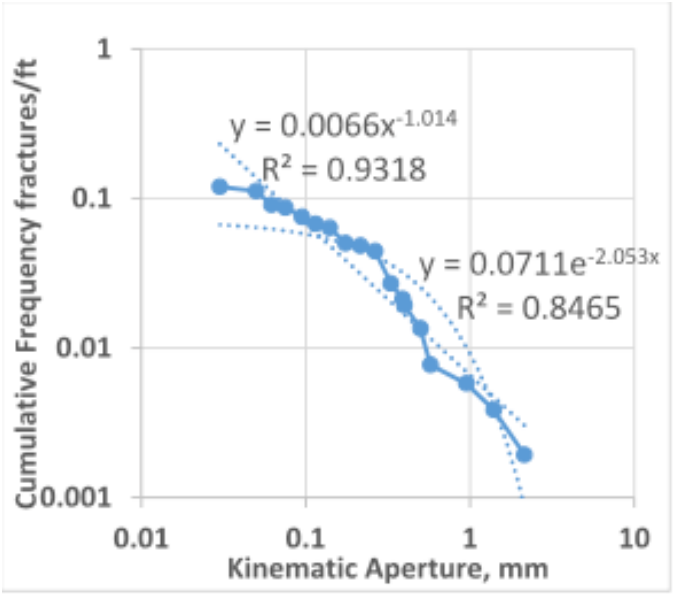

(b) Set #1

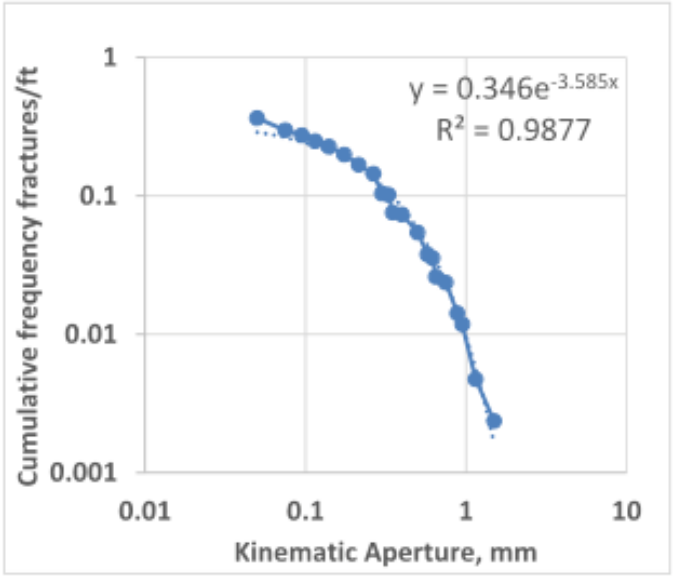

Figure 26: Natural fracture apertures from slant core well for the two joint sets.

Note:

1. From Gale et al. (2019). Set numbers are reversed in this report.
2. Fractures are described as filled.

Table 1: Approximate Formation Tops and Thicknesses Shown in the Vertical Pilot Well Log

Formation	Depth to Top (ft)	Thickness (ft)
Spraberry	6,917	376
Spraberry 2L	6,993	
Spraberry 3L	7,133	
Dean	7,293	146
Upper Wolfcamp (Wolfcamp A)	7,439	430
Upper Wolfcamp - 1	7,561	
Upper Wolfcamp - 2	7,758	
Middle Wolfcamp (Wolfcamp B)	7,869	426
Middle Wolfcamp - 2	8,058	
Lower Wolfcamp (Wolfcamp C, D)	8,295	

Notes:

1. From file: SUGG A 171 7SU PETROPHYSICS – GTI.tif.
2. Directory: /SUGG A 171 7SU Pilot Hole/7_Petrophysics; 2016.

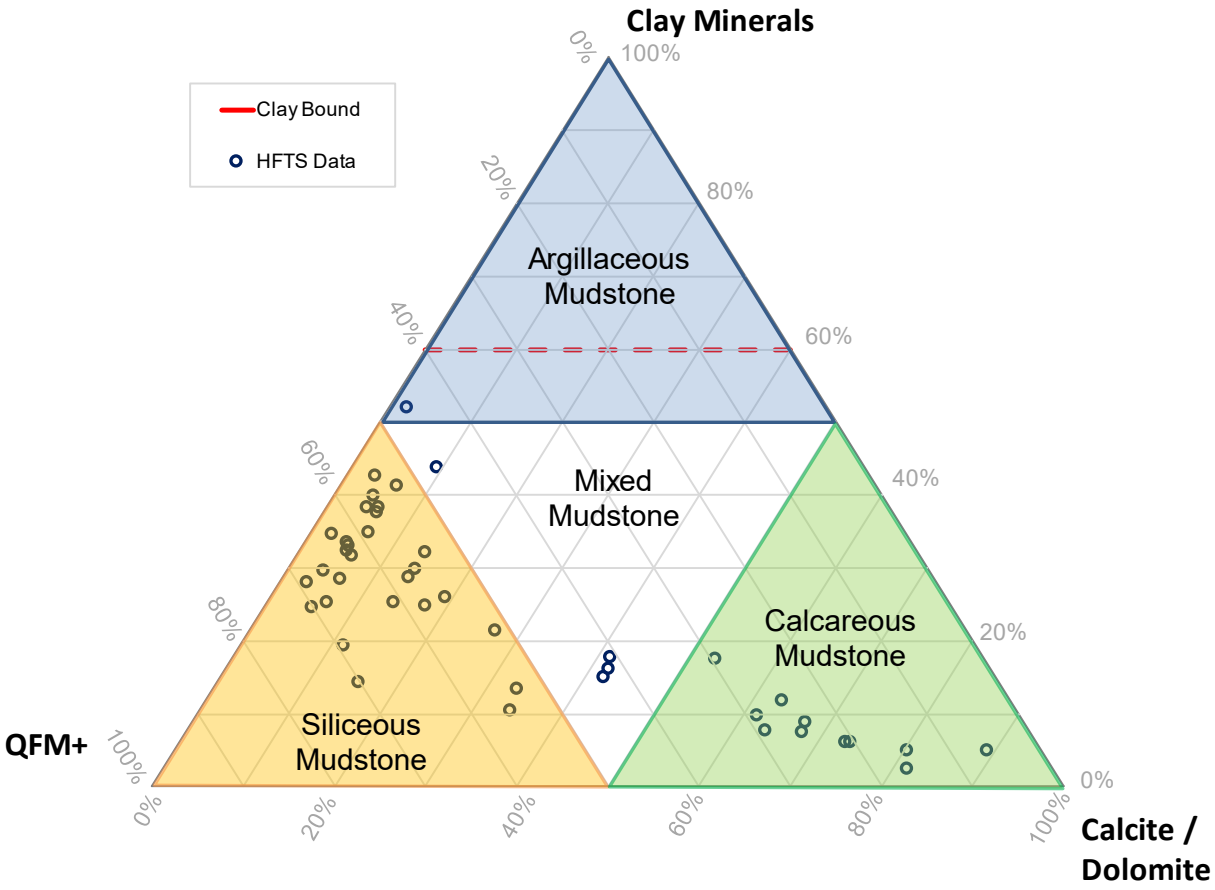

Figure 27: Mineralogy testing and classification of pilot well SUGG-A #171 7SU core samples.

Notes:

1. Based on data from Strasen (2016); however, this figure is replotted and rotated.
2. Quartz, feldspar, and mica content (QFM+) and other minerals, as plotted, includes pyrite and kerogen content as well.
3. Results are from the Spraberry, Dean, and Wolfcamp formations, but calcareous readings are from the Wolfcamp Formation only.
4. The clay bound (i.e., at 60% clay mineral content) is based on various authors who have suggested that most "oil shales" have less than 60% of clay mineral content, and therefore the units are not shales, and indicating that the rock response is not dominated by clay mineral content.

Further, the petrology log shows that the formations at the site have a general structure of repeating layers of calcareous mudstone occurring periodically within the siliceous mudstone background (see Figure 28). These calcareous units become more frequent with depth. This is consistent with the identification of two differing mineralogical groups, one for the calcareous layers and the other for the siliceous background. However, this classification does diverge (to some degree) from reports by others for the region.[10]

7.4 ENGINEERING PROPERTIES FROM PILOT WELL SUGG-A #171 7SU

As reported in Sections 5 and 6, engineering test results from side wall core testing of SUGG-#171 7SU vertical well core show variable results with no definitive trends in data. However, some weak (possible) trends in the data exist. Strength data appear to be more variable and trending higher in strength in the Middle and Lower Wolfcamp formations (below 7,800 ft). The general trend in uniaxial strength is approximately 6,000 psi, but values tend to increase at depth. Compressibility (i.e., Young's modulus) appears to increase with depth across the entire sampling sequence and with more variability in results at depth. General trends in Young's modulus data show an increase from 3.0 Mpsi to 6.0 Mpsi with depth. These compressibility values are consistent with results by Patterson (2017).[11]

Looking at possible correlations, there appears to be a general relation of gross bulk density with static Young's modulus. As shown in Figure 29, bulk density results of less than 2.55 g/cm^3 correlate with lower modulus results on the order of 2 to 4.5 Mpsi, while bulk modulus results greater than 2.65 g/cm^3 correlate with higher modulus results on the order of 5.5 to 8.5 Mpsi.

As discussed earlier, porosity, water saturation, and bulk density data from MR tests on sidewall core from SUGG-A #171 7SU also show large variability. The water saturation exhibit very wide variability with depth ranging from 3% to 79% with no apparent trends, although the Spraberry Formation results seem to be higher. The porosity results vary from 2% to 11% (mostly in the range of 3% to 10%) and show a weak trend of porosity to increase with depth below 7,800 ft in the Middle and Lower Wolfcamp formations.[12]

The average bulk density result appears roughly constant with depth, averaging about 2.59 g/cm^3, but varies widely from 2.4 to 2.8. The average is consistent with results reported by Syme et al. (2019) of 2.56 g/cm^3.

[10] For example, Green and others indicate that the Wolfcamp A to C units are silicate-rich calcareous shales (Green et al., 2020). Syme et al. (2019) report the Wolfcamp units in the Midland Basin as a "siliceous mudrock, calcareous mudrock, muddy bioclast-lithoclast floatstone, skeletal wackestone/packstone." Patterson (2017) states that the formation includes "fossiliferous limestone, organic-rich limestone, silty mudstone, calcareous silty mudstone, siliceous silty mudstone, cemented limestone, and dolomitic micrite." Baumgardner et al. (2014) identified four facies: "(1) siliceous mudrock, (2) calcareous mudrock, (3) carbonate-clast conglomerate, and (4) skeletal wackestone/packstone."

[11] Modulus results from Patterson (2017) range from 2.5 to 3.5 Mpsi in Wolfcamp A, and 2.8 to 3.5 Mpsi in Wolfcamp B.

[12] The porosity results from Patterson (2017) range from 5.59-9.30 for Wolfcamp A and Wolfcamp B, with Wolfcamp B having higher values.

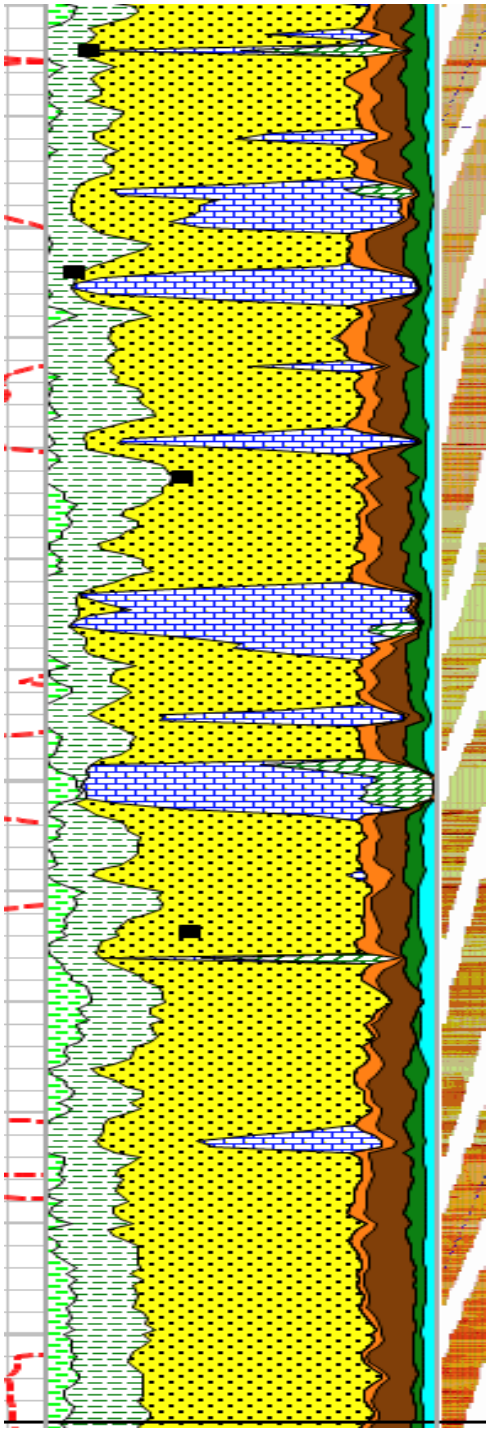

Figure 28: Example of repeating calcite/dolomite layers in the Upper Wolfcamp Formation at 7,630 to 7,760 ft in pilot well.

Notes:

1. From file: SUGG A 171 7SU PETROPHYSICS – GTI.tif.
2. Directory: /SUGG A 171 7SU Pilot Hole/7_Petrophysics. 2016.

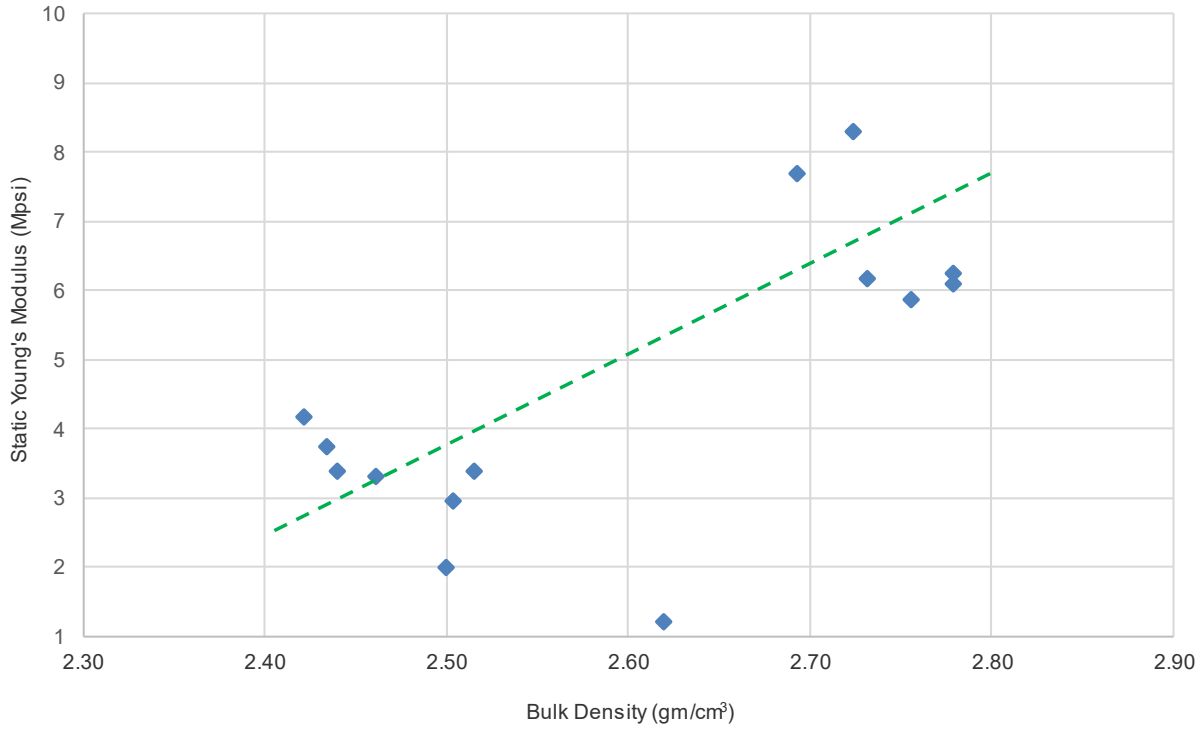

Figure 29: Bulk density versus static Young's modulus for Wolfcamp Formation in pilot well.

Notes:

1. Data from files: 150712 Multi-Stage Triaxial-Summary-LWC 1-28-16.xls, 150712 Multi-Stage Triaxial-Summary-MWC 1-28-16.xls, 150712 Multi-Stage Triaxial-Summary-UWC 1-28-16.xls.
2. Directory: SUGG A 171 7SU Pilot Hole/11_Triaxial Compressive Tests.
3. Modulus results taken at highest confining stress for each triaxial test, at confining pressures of 1,510 to 2,670 psi.

8. REFERENCES

AAPG Wiki. *Quick-look Lithology from Logs*. American Association of Petroleum Geologists, 2019. https://wiki.aapg.org/Quick-look_lithology_from_logs (accessed Sept 7, 2021).

Bai, M. Why are Brittleness and Fracability not Equivalent in Designing Hydraulic Fracturing in Tight Shale Gas Reservoirs. *Petroleum* **2016,** *2*, 1–19.

Baumgardner, R. W. Jr.; Hamlin, H. S.; Rowe, H. D. High-Resolution Core Studies of Wolfcamp/Leonard Basinal Facies, Southern Midland Basin, Texas. Proceedings of 2014 Southwest Section Annual Convention, Midland, TX, 2014; Search and Discovery Article #10607.

Campbell, W.; Wicker, J.; Courtier, J. Natural and Hydraulic Fracture Density Prediction and Identification of Controllers. Proceedings of Unconventional Resources Technology Conference, Houston, TX, 2018; URTeC:2934611.

Ciezobka, J.; Eisenlord, S.; Covatch, G. Hydraulic Fracturing Test Site (HFTS) A Field Site Dedicated to Environmental Safety and Stimulation Efficiency Research in the Permian Basin. Proceedings of Penn State Extension Webinar, April 19, 2018. https://psu.mediaspace.kaltura.com/media/1_tvjteuz6 (accessed June 15 2021).

Ciezobka, J.; Reeves, S. Overview of Hydraulic Fracturing Test Sites (HFTS) in the Permian Basin and Summary of Selected Results (HFTS-I in Midland and HFTS-II in Delaware). Proceedings of Latin America Unconventional Resources Technology Conference, 2020; URTeC: 1544.

Deere, D. U.; Miller, R. P. *Engineering Classification and Index Properties for Intact Rock*; Technical Report AFWL-TR-65-116; Air Force Weapons Laboratory, Air Force Systems Command. University of Illinois, Urbana, IL, 1966; p 327.

EIA. U.S. Energy Information Administration. Independent Statistics & Analysis. Permian Basin, Part 2: Wolfcamp Shale Play of the Midland Basin, Geology Review; U.S. Department of Energy: Washington, DC, 2020. https://www.eia.gov/maps/pdf/Permian_Wolfcamp_Midland_EIA_reportII.pdf (accessed June 15 2021).

Gale, J. F. W.; Elliott, S. J.; Laubach, S. E. Hydraulic Fractures in Core from Stimulated Reservoirs: Core Fracture Description of HFTS Slant Core, Midland Basin, West Texas. Proceedings of Unconventional Resources Technology Conference (URTeC), Houston, Texas, 2018; URTeC: 2902624.

Gale, J. F. W.; Elliott, S. J.; Li, J. Z. Forstner S. *HFTS Project, Final Report*; Bureau of Economic Geology, University of Texas at Austin: Austin, Texas, 2017; p 25. https://edx.netl.doe.gov/dataset/db558c13-5b74-4ec6-bbdd-873f07e77336/resource/51190907-90fd-49cf-8ef8-1d9c75c9daa4 (accessed Sept 22, 2021).

Gale, J. F. W.; Elliott, S. J.; Li, J. Z. Laubach, S. E. Natural Fracture Characterization in the Wolfcamp Formation at the Hydraulic Fracture Test Site (HFTS-1), Midland Basin, Texas. Proceedings of SPE/AAPG/SEG Unconventional Resources Technology Conference, Denver, CO, July 2019; URTEC: 2019-644-MS.; p 16.

Gale, J. F. W.; Elliott, S. J.; Rysak, B. G.; Laubach, S. E. Characterization of Hydraulic Fractures in Slant Core from the Hydraulic Fracture Test Site Project. Proceedings of Bureau of Economic Geology Seminar Series, December 4, 2020. https://www.youtube.com/watch?v=NlA1NlRWf7w (accessed May 12, 2021).

Green, H.; Šegvic', B.; Zanoni, Omodeo-Salé, S.; Adatte, T. Evaluation of Shale Source Rocks and Clay Mineral Diagenesis in the Permian Basin, USA: Inferences on Basin Thermal Maturity and Source Rock Potential. *Geosciences MDPI* **2020,** *10*, 32.

Laredo Petroleum, Inc. Extended Range Micro Imager with Dip Results (Corrected). File: *60in_Annotated_Log_Laredo_SUGG_A_171_7SU_Corrected.pdf*. 2016. https://edx.netl.doe.gov/dataset/hfts-1-phase-1-individual-well-files (accessed Sept 22, 2021).

Patterson, R. A. Characterizing Complex Fracture Geometry Through Data Integration in the Permian Basin. Master's Thesis, Petroleum Engineering, Texas A&M University, College Station, TX, 2017.

Perry, K. F. The Hydraulic Fracturing Test Site—Midland Basin, West Texas - A Resource Recovery Field Research Experiment in the Wolfcamp Formation, 2018. https://www.gti.energy/wp-content/uploads/2018/10/Hydraulic-Fracturing-Test-Site-Midland-Basin-Resource-Recovery-Field-Research-Experiment-Presentation_Perry-Jun2018.pdf (accessed May 11, 2021).

Petrowiki. *Gamma Ray Logs;* Society of Petroleum Engineers, 2017. https://petrowiki.spe.org/Gamma_ray_logs (accessed Sept 7, 2021).

Phan, T. N. CO_2 Huff-N-Puff in Unconventional Resources Plays – An Integrated Modeling Approach Focusing on Permian Basin. Master's Thesis, Graduate College, University of Oklahoma, Norman, OK, 2019.

Pioneer Natural Resources. The Wolfcamp Shale, Technical Learnings to Date and Challenges Going Forward. Proceedings of Ryder Scott Company 2014 Reserves Conference. https://www.ryderscott.com/wp-content/uploads/RSC-2014-Reserves-Conference_01Flumerfelt.pdf?r=false (accessed May 11, 2021).

Rickman, R.; Mullen, M.; Petre, E.; Grieser, B.; Kundert, D. A Practical Use of Shale Petrophysics for Stimulation Design Optimization: All Shale Plays are not Clones of the Barnett Shale. Proceedings of 2008 SPE Annual Technical Conference and Exhibition, Denver, CO, Sept. 21–24, 2008; SPE 115258.

Sadeghvishkaei, M. Modelling of Geomechanics for Informed Hydraulic Fracturing Operations. PhD Thesis, Schulich School of Engineering, University of Calgary, Calgary, Alberta, 2017. https://prism.ucalgary.ca/handle/11023/4109 (accessed Sept 2, 2021).

Salahshoor, S.; Maity, D.; Ciezobka, J. Stage-Level Data Integration to Evaluate the Fracturing Behavior of Horizontal Wells at the Hydraulic Fracturing Test Site (HFTS): An Insight into the Production Performance. Proceedings of Unconventional Resources Technology Conference (URTeC), Houston, TX, 2020. URTeC: 3058.

Sayers, C. M.; Dasgupta, S.; Koesoemadinata, A.; Shoemaker, M. Rock Physics of the Wolfcamp Formation, Delaware Basin. *Geophysics* **2019,** *84*.

Schwartz, B. A. The Role of Pore Structure in Permeability Evolution Observed in Laboratory Studies of Marcellus and Wolfcamp Shale. PhD Thesis, Department of Energy and Mineral Engineering, Pennsylvania State University, 2018.

Smye, K. M.; Hamlin, H. S.; Eastwood, R.; McDaid, G. Variability of Geologic Properties in Shale Gas and Tight Oil Plays. *Journal of the Gulf Coast Association of Geological Societies (GCAGS Journal)* **2019,** *8*, 191–209.

Strasen, J. L. (Core Laboratories, Inc.). *Thin Section Petrology of Conventional Core Samples, SUGG–A #171 7SU Well, Reagan County, Texas;* No.: 150712G; Core Laboratories Reservoir Geology File: Big Lake, TX, January 2016. https://edx.netl.doe.gov/dataset/hfts-1-phase-1-individual-well-files (accessed Sept 22, 2021).

Waite, L. Stratigraphic Framework of the Wolfcamp – Spraberry of the Midland Basin. Presentation to the Roswell Geologic Society; Department of Geosciences, Permian Basin Research Lab University of Texas at Dallas, 2019. https://labs.utdallas.edu/app/uploads/sites/39/2019/10/Strat-Framwork_WFMP-SPBY_Midland-Basin.pdf (accessed May 11, 2021).

Zoback, M.; Kohli, A. Chapter 2. Composition, Fabric, Elastic Properties and Anisotropy. In *Unconventional Reservoir Geomechanics: Shale Gas, Tight Oil, and Induced Seismicity*; Cambridge University Press, Cambridge, United Kingdom, 2019; pp 31–64.

APPENDIX A: SITE MAPS AND GEOLOGIC CONTEXT OF HFTS-1

A.1 LOCATION AND GEOLOGIC CONTEXT

Hydraulic Fracturing Test Site Number #1 (HFTS-1) is in the southern Midland Basin, in the northern portion of Reagan County, Texas (Figure A1). The program consisted of 11 horizontal wells, one vertical well, and one slant well. The horizontal wells are in two horizons: 1) Upper and 2) Middle Wolfcamp formations (see Figure A2 to Figure A4).

Geologically, the program investigated five formations in the Lower Permian System (Figure A5):

1. Spraberry
2. Dean
3. Upper Wolfcamp (Wolfcamp A)
4. Middle Wolfcamp (Wolfcamp B)
5. Lower Wolfcamp (Wolfcamp C)

The location of the site in Midland Basin is shown in Figure A6 with nearby stratigraphic structures.

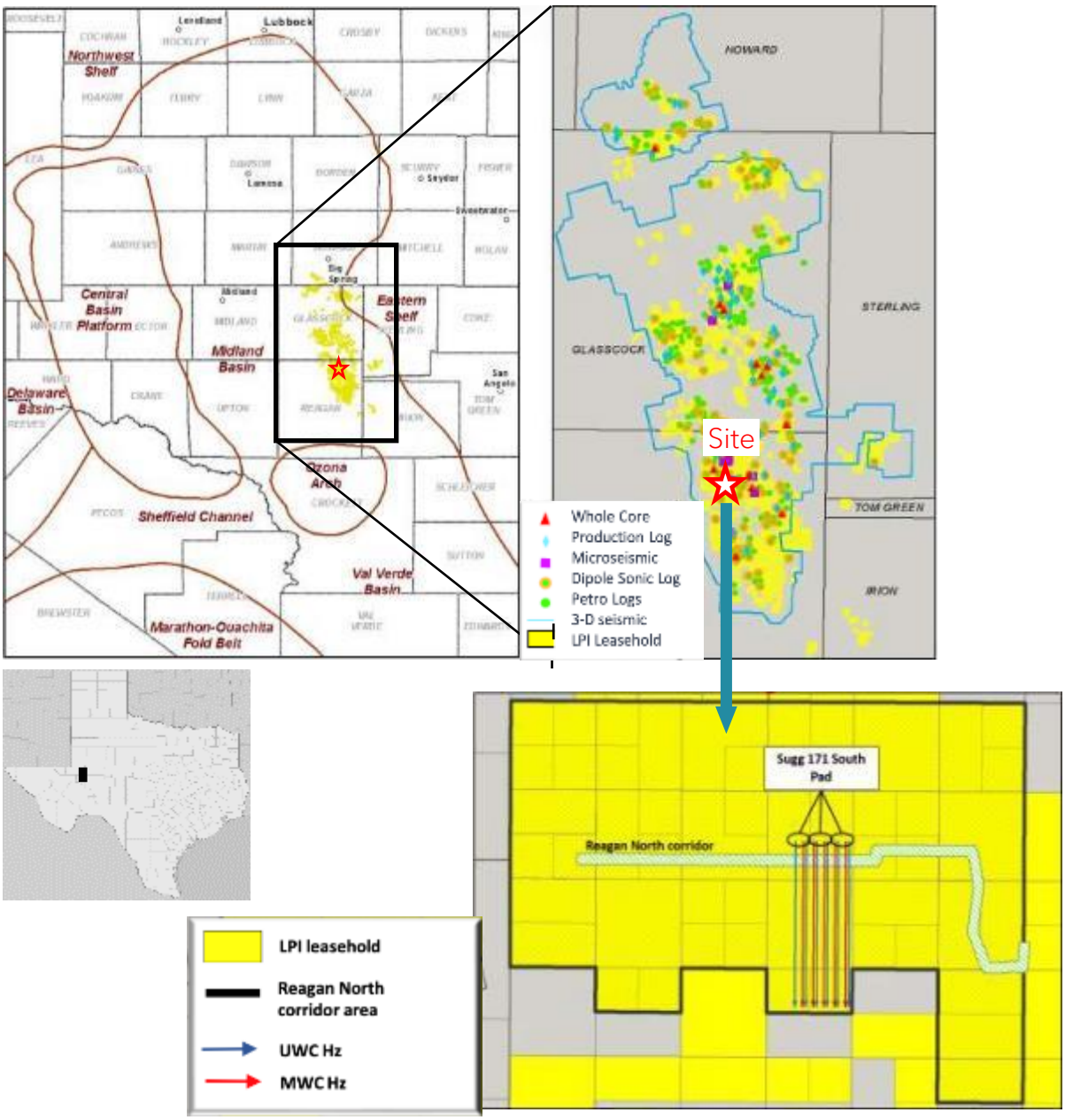

Figure A1: General site location of HFTS-1 in Midland Basin, Reagan County, Texas.

Note: Modified from Perry (2018).

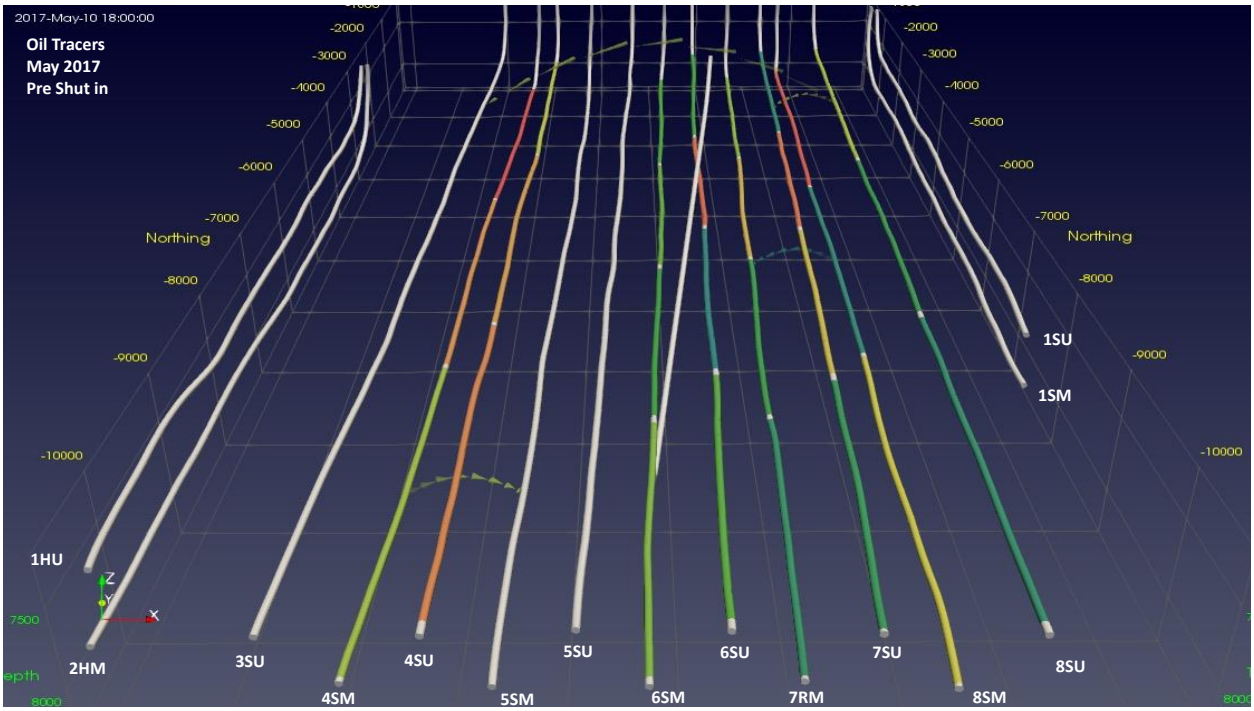

Figure A1: Rotated section showing horizontal HFTS-1 wells and other nearby wells.

Note:

1. From file: GTI Presentation 12-04-2017.pptx. (Presentation by Wood, T. and Leonard, D. (Protechnics) Hydraulic Fracturing Test Site: Tracer Update, 2017).
2. Wells in the immediate site area (not all in HFTS-1 program): 1HU, 2HM, 3SU, 4SM, 4SU, 5SM, 5SU, 6SM, 6SM, 7RM 7SU, 8SM, 8SU, 1SM, 1SU, and 6TW (slant core well – center, unlabeled).
3. Well numbers are generally prefixed with “SUGG-A #171” for lease name.

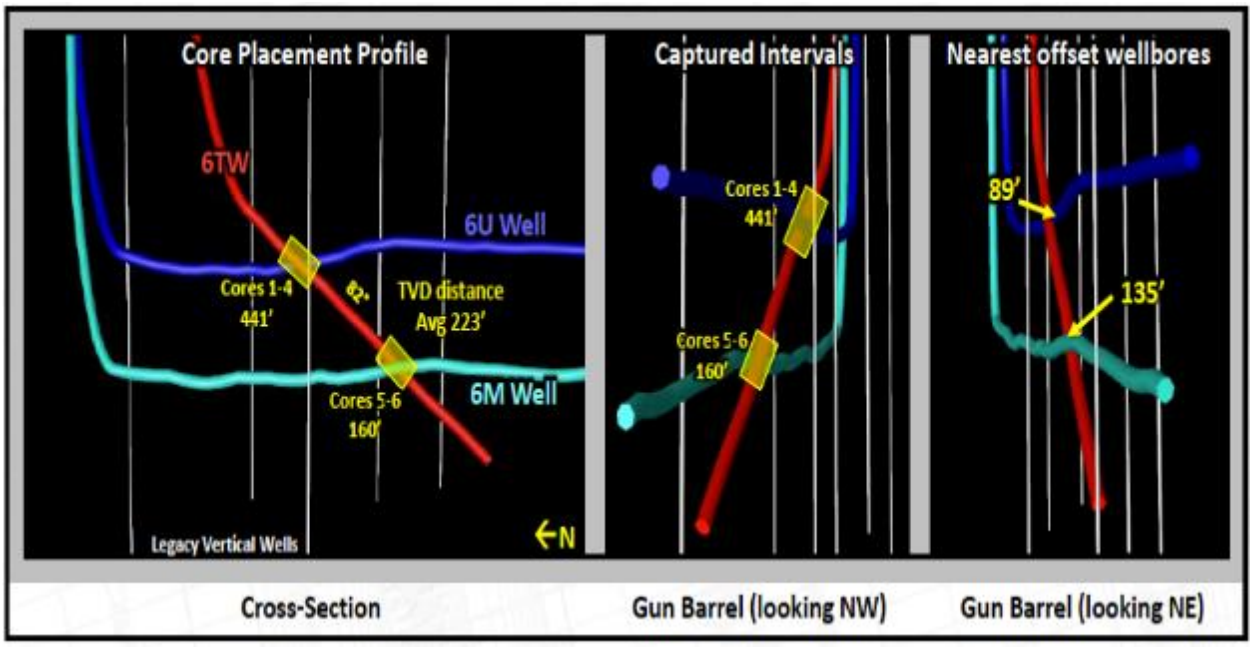

Figure A3: Slant core well 6TW location near other horizontal wells.

Note:

1. From file: smart_data-inventory.pptx. (Presentation by Kumar, A. Task6: Multi-Level Data Driven Fracture Network Imaging for Rapid Decision Making. 2020).
2. Slant core well is inclined approximately 81°–82° and was drilled after horizontal wells.

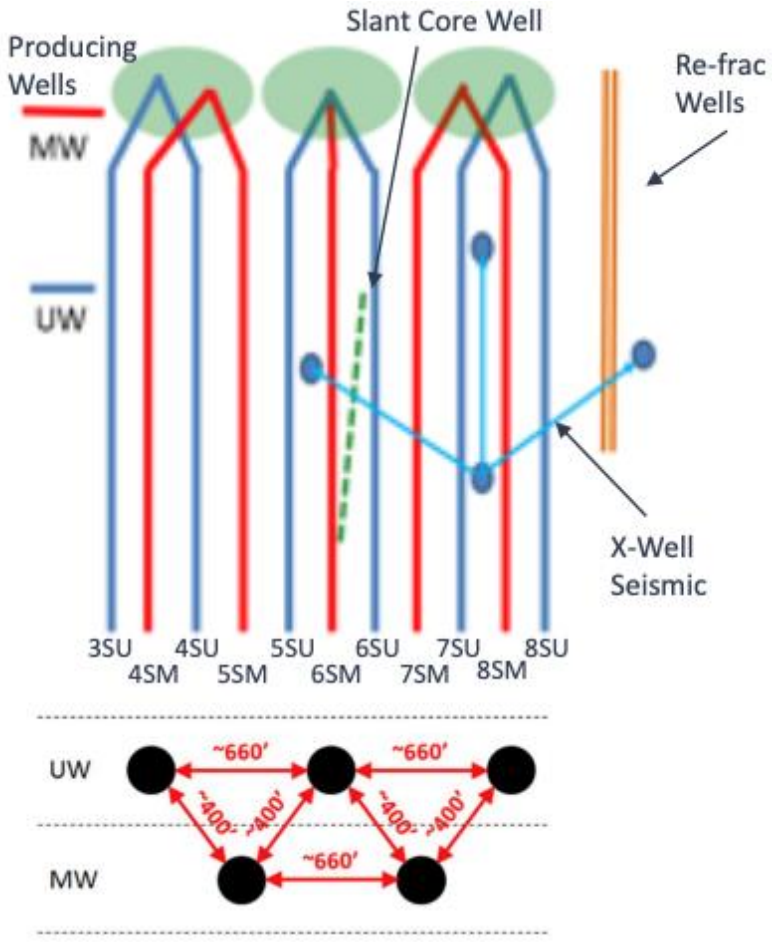

Figure A4: Plan view of HFTS-1 well program together with partial cross-section.

Note:

1. From Ciezobka et al. (2018).
2. Blue wells are in Upper Wolfcamp (UW) Formation; red wells are in Middle Wolfcamp (MW) Formation.
3. Well #7SM should be relabeled as #7RM.
4. Slant core well (dashed line) is SUGG-A #171 6TW.
5. Well numbers are generally prefixed with "SUGG-A #171" for lease name.
6. Distances are in feet.
7. The wells were drilled using a "zipper frac" completion sequence approach (with crew and number of stages in parentheses) as follows:
    - Zipper Frac Completion 1 (frac crew 1): Wells 7SU (43 stages) and 8SU (37 stages)
    - Zipper Frac Completion 1 (frac crew 2): Wells 5SU (37 stages), 6SU (37), and 6SM (37 stages)
    - Zipper Frac Completion 2 (frac crew 1): Wells 7SM (49 stages) and 8SM (37 stages)
    - Zipper Frac Completion 2 (frac crew 2): Wells 3SU (37 stages) and 4SU (45 stages)
    - Zipper Frac Completion 3 (frac crew 2): Wells 4SM (37 stages) and 5SM (37 stages)

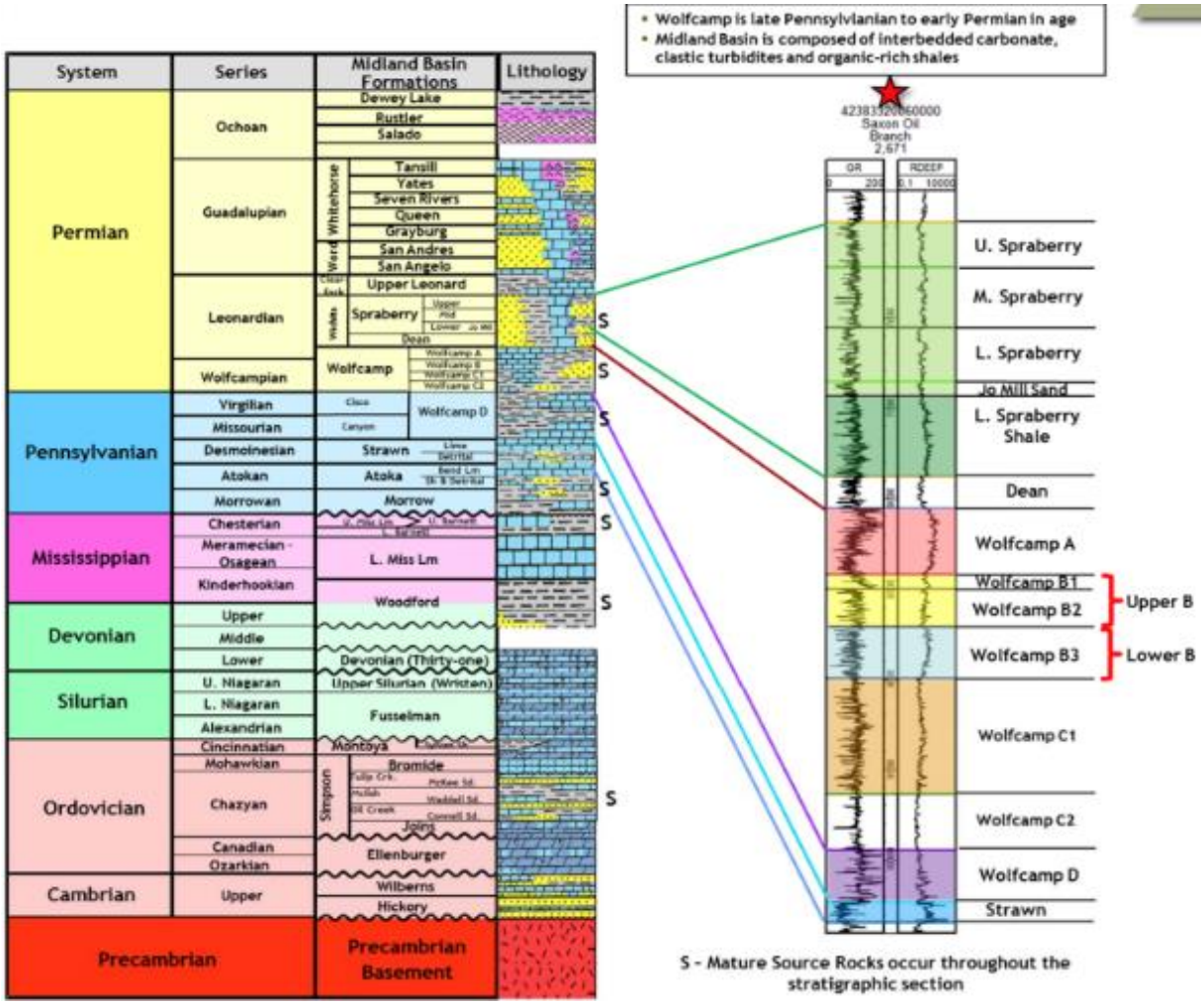

Figure A5: Stratigraphic column for the region showing Spraberry, Dean, and Wolfcamp formations.

Note:

1. From Pioneer Natural Resources (2014) (also, see: Waite, 2019).
2. Wolfcamp is also divided into upper, middle, and lower horizons:
    - Upper Wolfcamp = Wolfcamp A
    - Middle Wolfcamp = Wolfcamp B
    - Lower Wolfcamp = Wolfcamp C and D.
3. See also Smye et al. (2019).

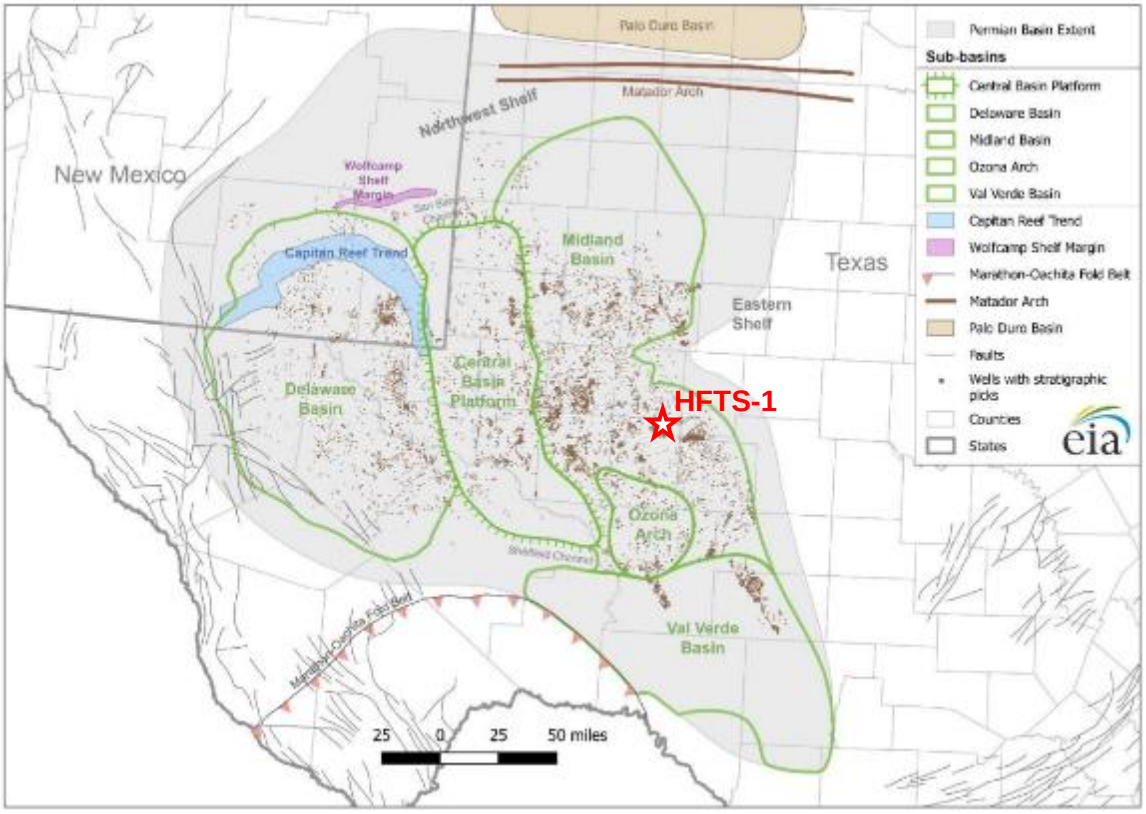

Figure A6: Major structural and tectonic features near HFTS-1 site in the central Midland Basin, Texas.

Note: Modified from EIA (2020).

This page intentionally left blank.

APPENDIX B: RELATED LITERATURE DATA

B.1 LITERATURE

Related literature on engineering aspects of and correlations with the Permian formations from other sites are relatively sparse. Mineralogy results on the Wolfcamp Formation were the most reported and are consistent with site data (see Figure B1 and B2). Dynamic modulus results versus clay mineral content were reported by Schwartz (2018) (Figure B3) and an evaluation of brittleness of the Wolfcamp is shown by Salahshoor et al. (2020) (see Figure B4). The stratification of these formations is also recognized by various authors (e.g., Figure B5).

(a)

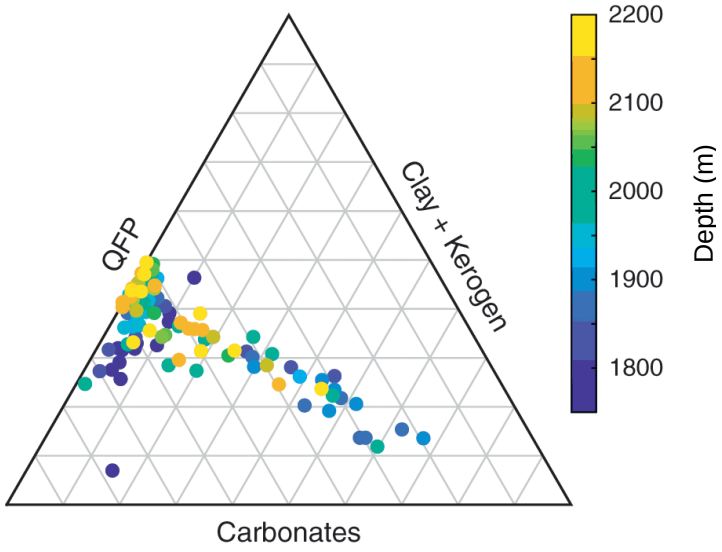

(b)

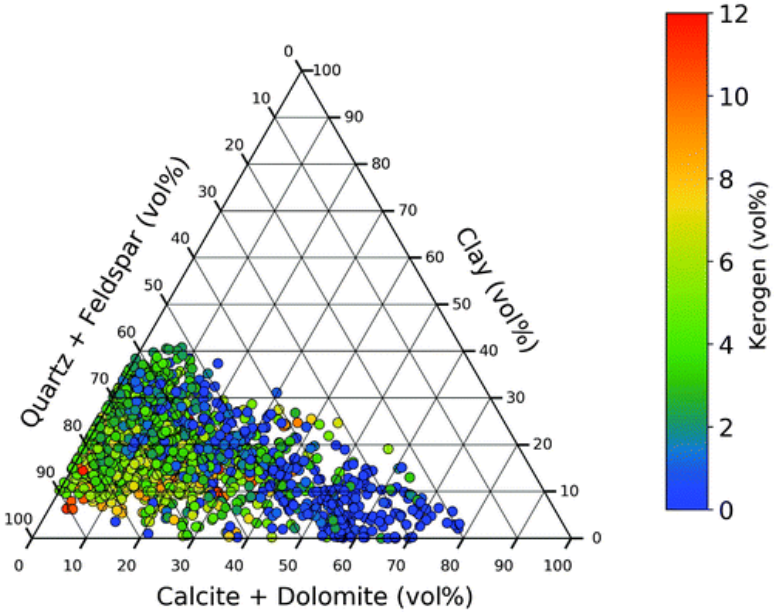

Figure B1: Ternary mineral diagrams of Wolfcamp Formation from the literature.

Note:

1. Figure (a) is from Zoback and Kohli (2019); Figure (b) is from Sayers et al. (2019).
2. The figure from Sayers et al. also suggests a possible trend of increased kerogen content with increased quartz and feldspar content (?).

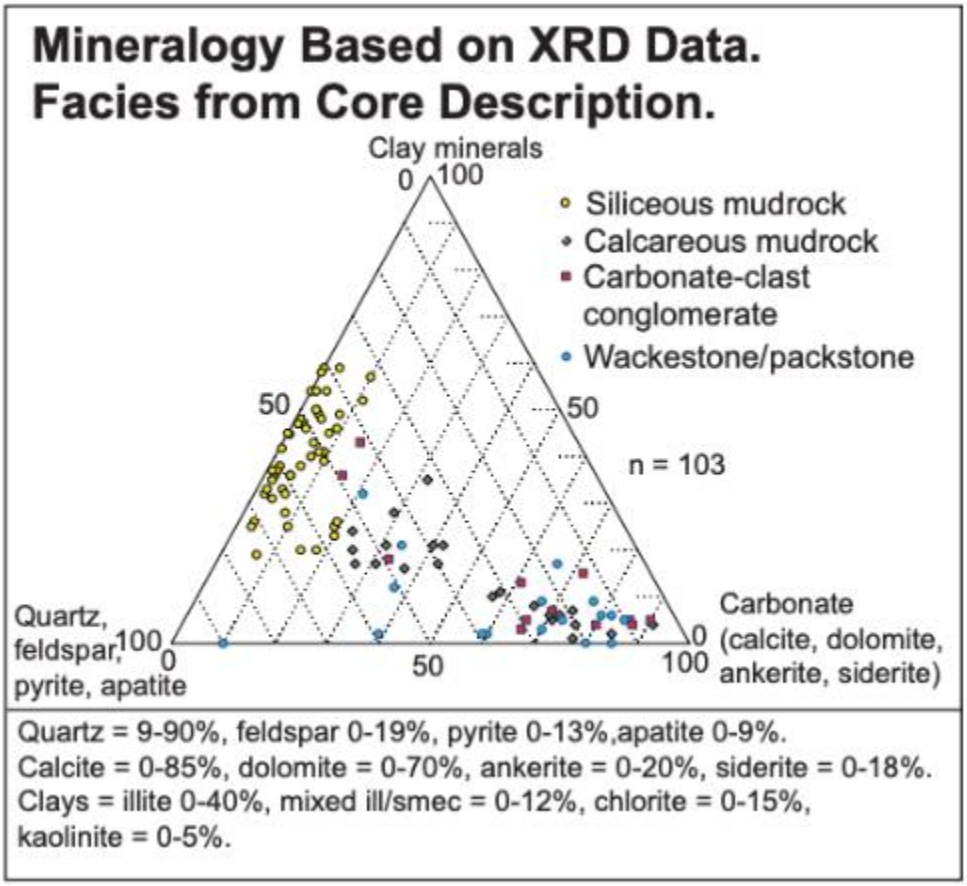

Figure B2: Additional ternary mineral diagram of Wolfcamp Formation from Midland Basin.

Note:

1. From Baumgardner et al. (2014).
2. Samples are from Lower Leonard and Upper Wolfcamp (operational Wolfcamp A and B) strata.
3. Authors indicate that: high gamma ray reading (GR) responses generally correlate with siliceous mudrocks and high total organic carbon (TOC) content. They also indicate that rock strength (unconfined compressive strength) decreases with silicon content because much silicon is in, or associated with, clay minerals and that rock strength increases with carbonate content, like Haynesville shale.

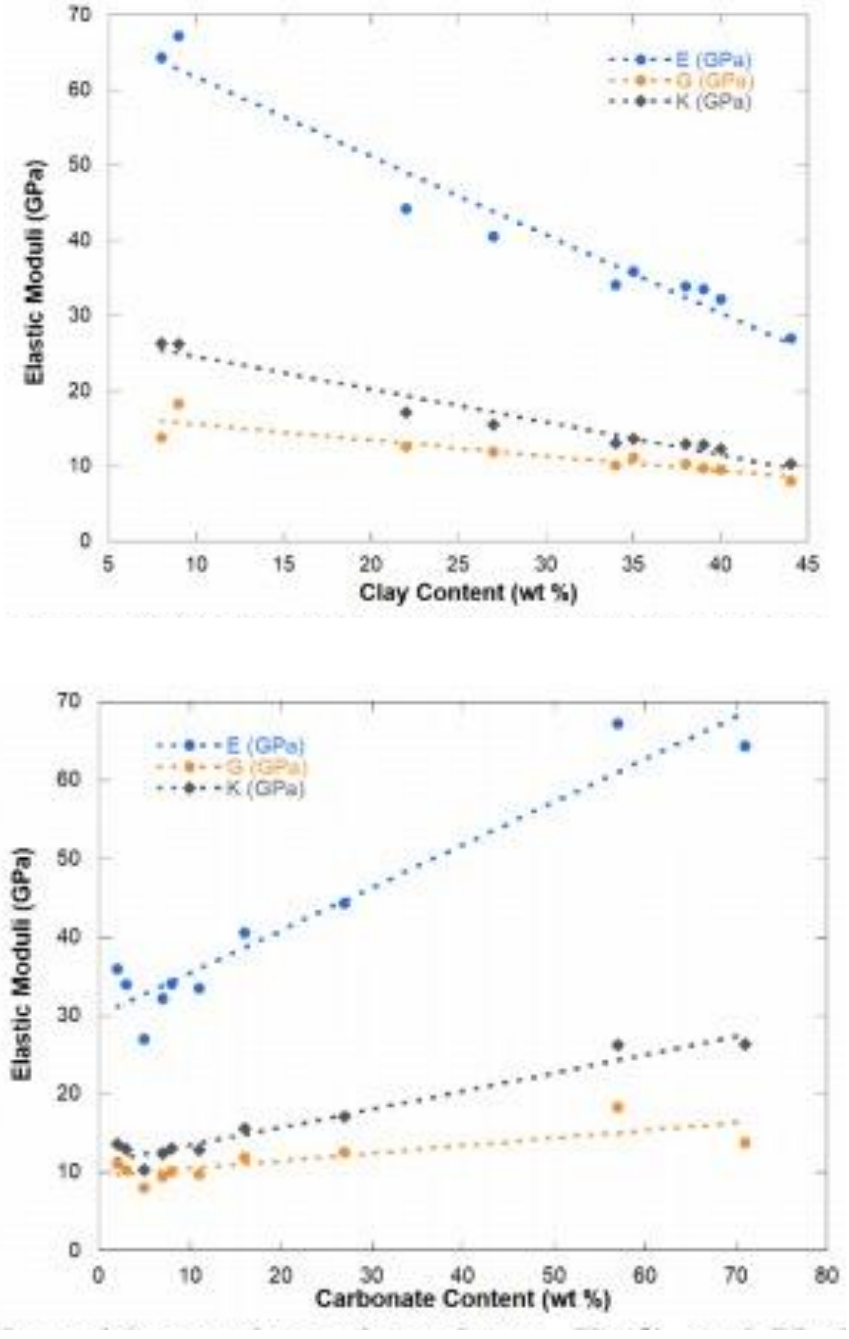

Figure B3: Elastic dynamic moduli with varying clay mineral and carbonate content for the Wolfcamp Formation.

Note:

1. From Schwartz (2018).
2. Legend for figure: E = Young's modulus, G = shear modulus; K = bulk modulus, wt % = percent weight, GPa = gigapascal
3. Results are dynamic moduli based on sonic well logging.

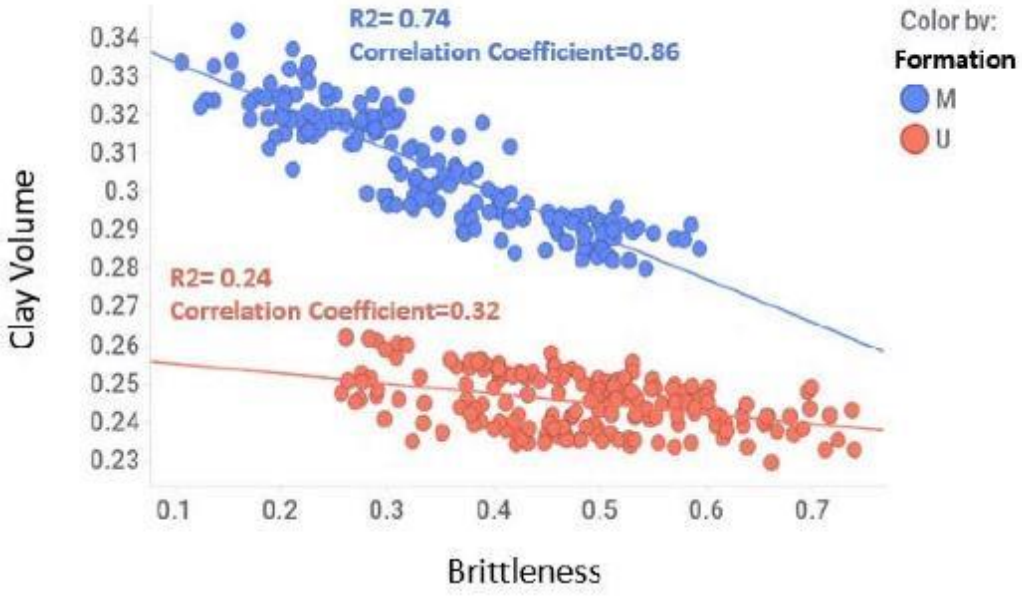

Figure B4: Correlation between clay mineral content and brittleness in Upper and Middle Wolfcamp at HFTS.

Note:

1. From Salahshoor et al. (2020). See Campbell et al. (2018) for other brittleness correlations.
2. U = Upper Wolfcamp; M = Middle Wolfcamp.
3. Note that the maximum clay mineral content shown is less than 35%.
4. It is assumed that Brittleness is as defined by Rickman et al. (2008). The Rickman equations can have the combined general form (Bai, 2016):

$$B_r = \frac{50}{7}(E - 28\nu + 10.2)$$

where B = Brittleness, E = Young's Modulus and ν = Poisson's ratio; E is in units of Mpsi.

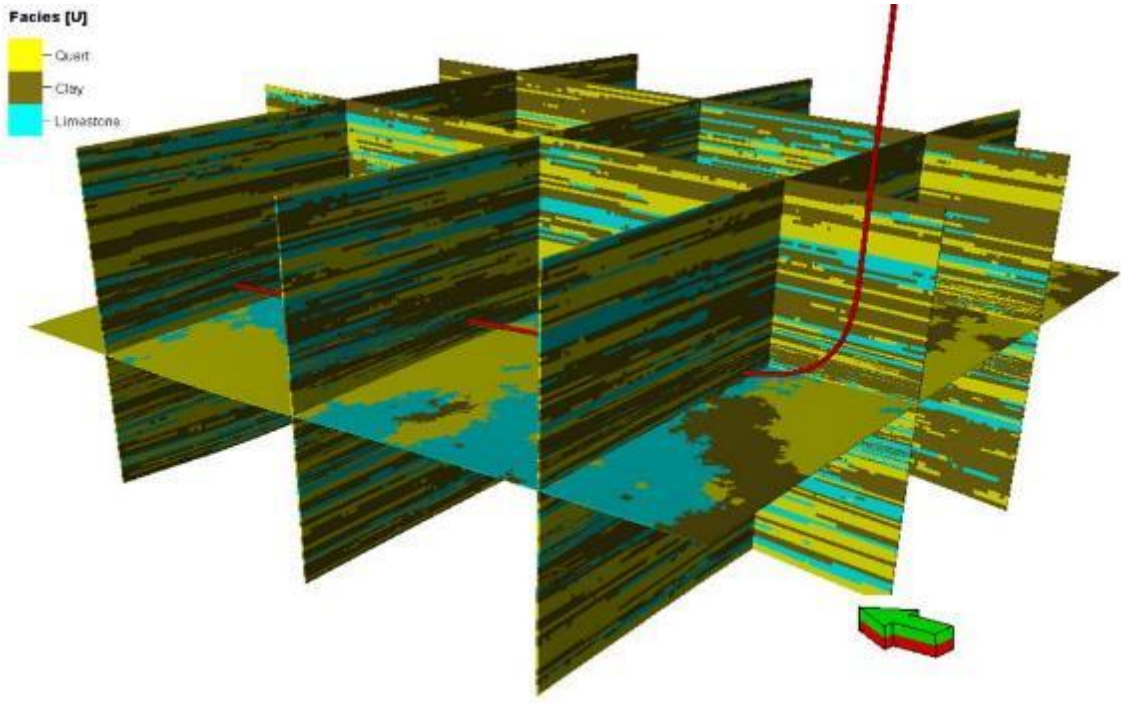

Figure B5: 3D facies model of Upper Wolfcamp (Wolfcamp A) Formation.

Note: From Phan (2019).

APPENDIX C: PILOT WELL LOGS

C.1 PILOT WELL COMPLETION LOGS

Resistivity, GR, and density data from the vertical pilot hole are shown in Figure C1. The general trends in these data differ from "typical" regional results as reported by Waite (2019), which are shown in Figure C2. Aside from the variability, there are only a few mild trends in the HFTS-1 data. One trend is the upper half of Spraberry Formation shows a reduced variability in comparison to other units. In addition, the resistivity in the Dean Formation appears on the average, lower than the adjacent units, while the upper 200 ft of the Upper Wolfcamp shows an increased resistivity. In contrast, there is a significant reduction in calcareous mudstone layering in the Middle Wolfcamp at approximately 7,920 ft to 8,080 ft (based on the petrophysics log for the pilot well), and the various logs in this interval reflect a decreased heterogeneity.

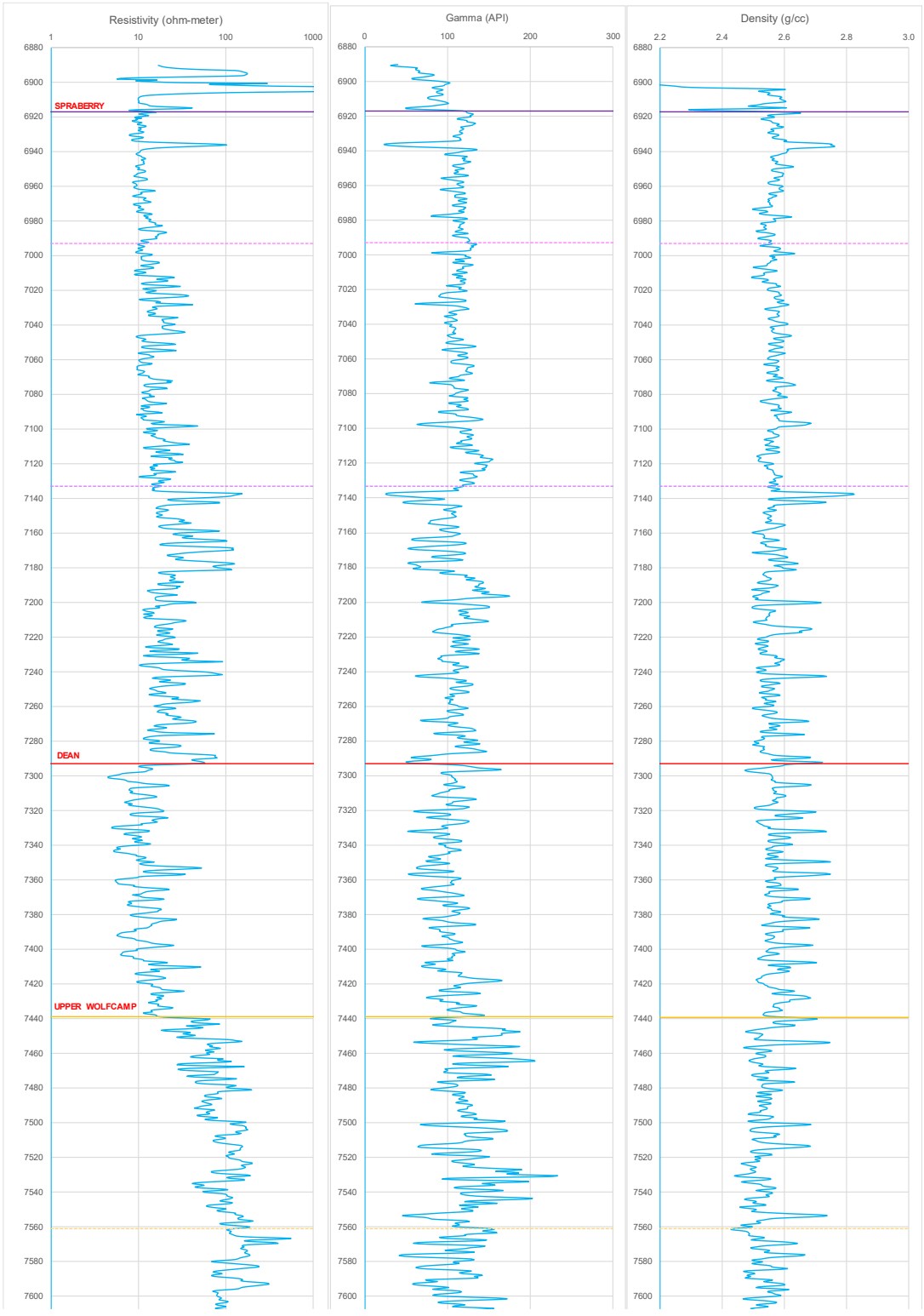

Figure C1: Resistivity, gamma ray and density logs from SUGG-A #171 7SU pilot well (1 of 3).

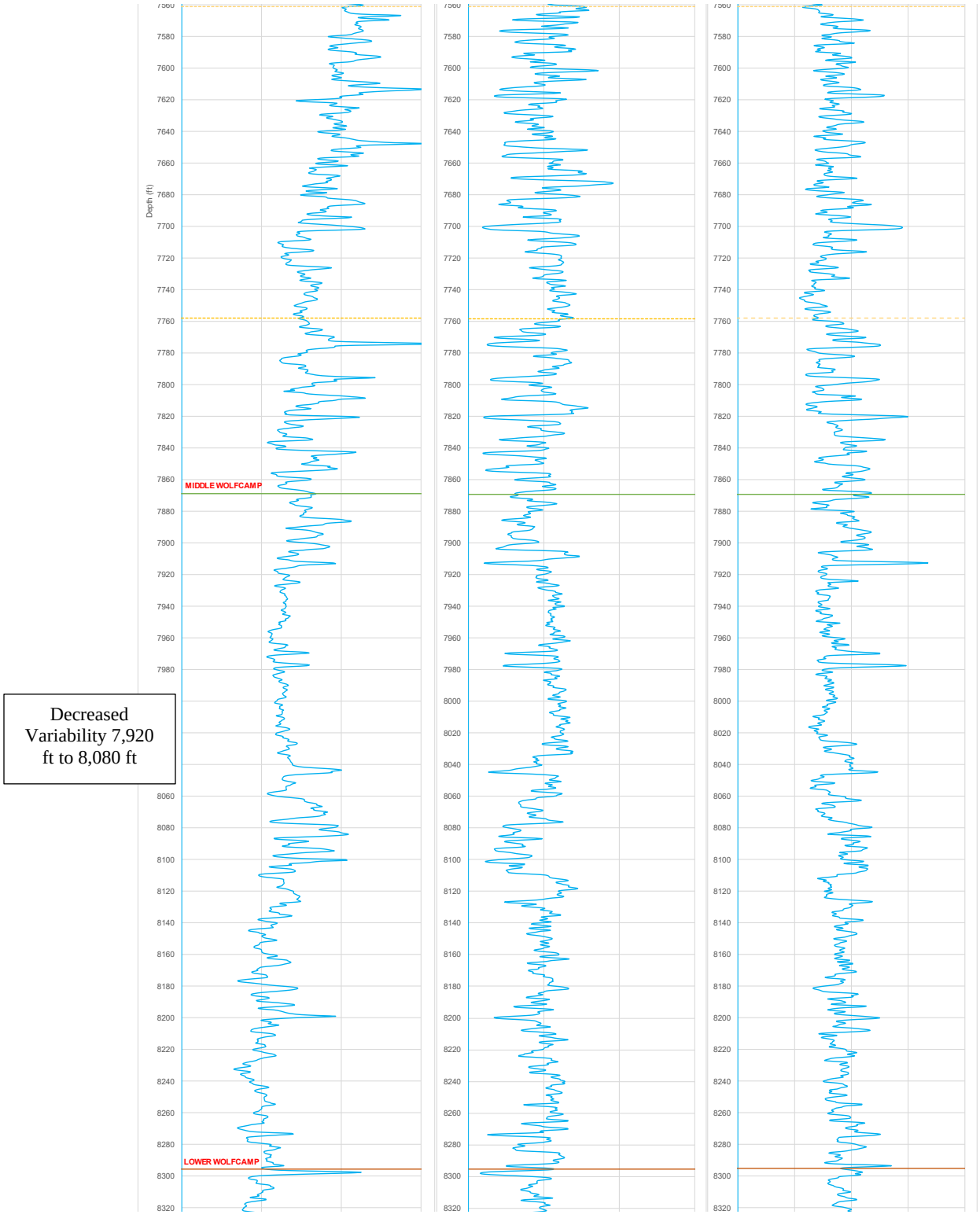

Figure C1 (cont.): Resistivity, gamma ray, and density logs from SUGG-A #171 7SU pilot well (2 of 3).

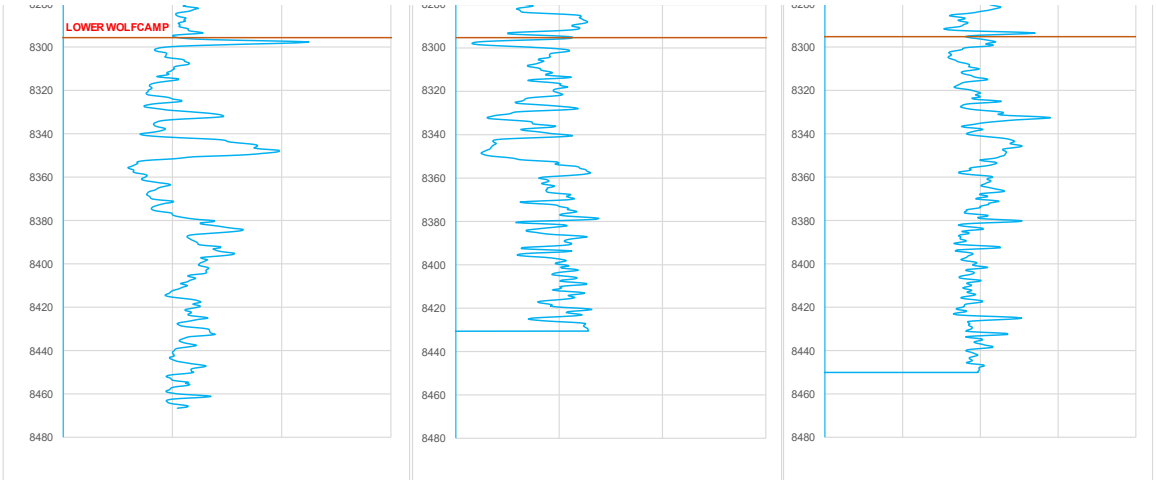

Figure C1 (cont.): Resistivity, gamma, and density logs from SUGG-A #171 7SU pilot well (3 of 3).

Notes:

1. Data from file: LAREDO_PETROLEUM_SUGG_A_171_7SU_TRIPLE_COMBO_LAS.las
2. Directory: /hfts-1-phase-1-individual-well-files/SUGG A 171 7SU Pilot Hole/1_Field Logs/

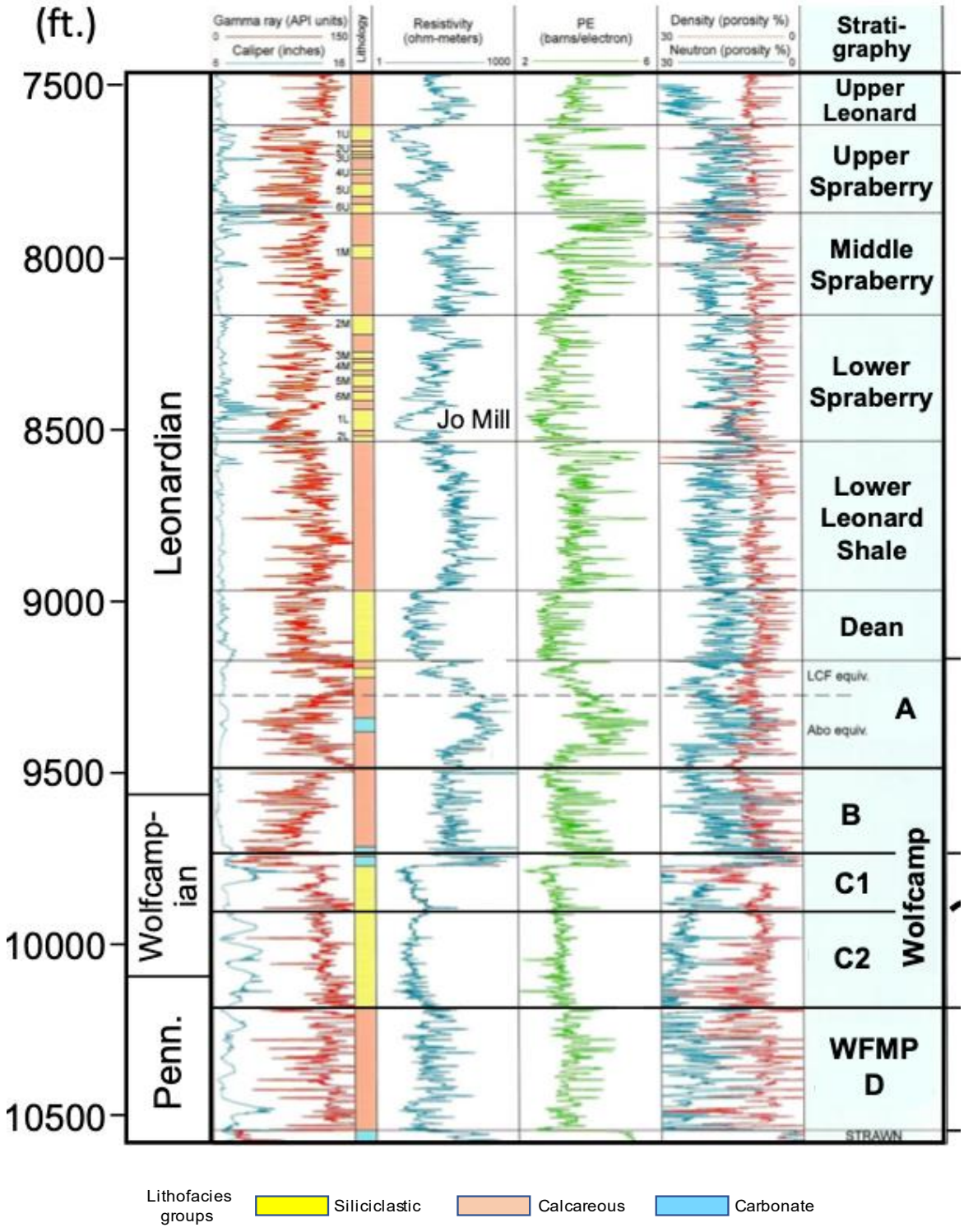

Figure C2: "Typical" Midland Basin stratigraphy and logs.

Notes: From Waite (2019).

This page intentionally left blank.

APPENDIX D: HORIZONTAL GAMMA RAY LOGS

D.1 GAMMA LOGS FROM HORIZONTAL WELLS

Gamma ray logs from horizontal wells in the Upper Wolfcamp are shown in Figure D1. The logs are from wells SUGG-A #171-1SU, -3SU, -5SU, -6SU, and -8SU and SUGG-A #158-1SU.[13] No apparent pattern is evident across the horizon. Each log shows varying degrees of variability across the Upper Wolfcamp. This implies that the horizontal plane is especially heterogenous with varying amounts of calcite and silicate. This is contrary to the common assumption that the horizontal plane in sedimentary formations is generally homogeneous for extended distances.

[13] EDX Directory: /hfts-1-phase-1-individual-well-files.

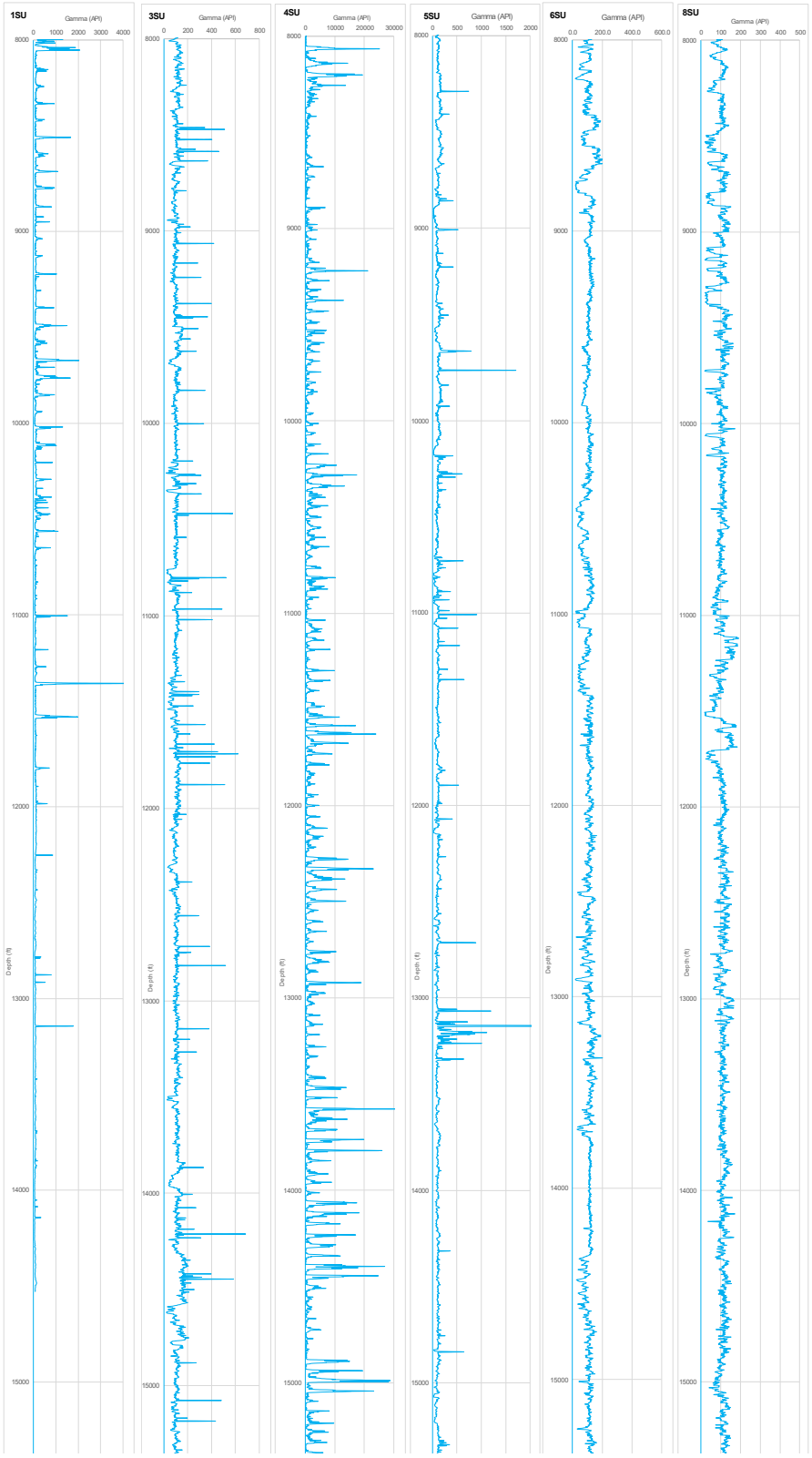

Figure D1: Gamma logs from horizontal wells in the Upper Wolfcamp, Wells SUGG-A #171-1SU, -3SU, -5SU, -6SU, and -8SU and SUGG-A #158-1SU (1 of 2).

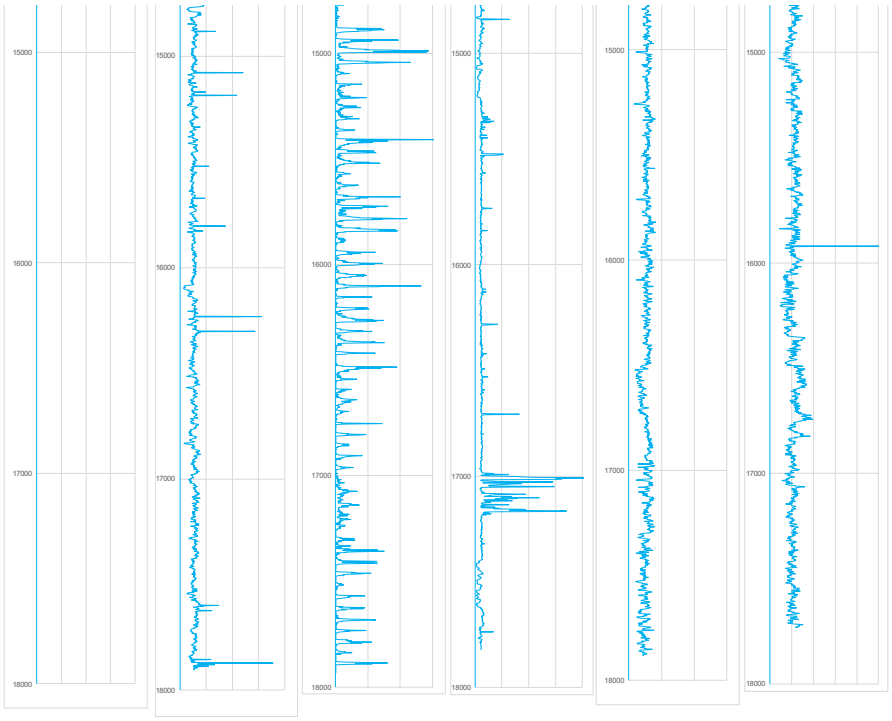

Figure D1 (cont.): Gamma logs from horizontal wells in the Upper Wolfcamp, Wells SUGG-A #171-1SU, -3SU, -5SU, -6SU, and -8SU and SUGG-A #158-1SU (2 of 2).

Notes:

1. X-axis scale adjusted to capture larger values and minimize white space.
2. The "depth" in the horizontal holes is a reference distance along well and is not a vertical depth.
3. The data are from files:
   - Laredo_Sugg_A_171_8SU_SS.las
   - Laredo_Sugg_A171_#6SU_SS.las
   - Laredo_Sugg_A171_#5SU_SS.las
   - Laredo_Sugg_A171_#4SU_SS.las
   - Laredo_Sugg_A171_#3SU_SS.las
   - Laredo_Sugg_A_158_1SU_SS.las.
4. EDX Directory: /hfts-1-phase-1-individual-well-files/[[Well Name]]/Completions/Corelab Spectascan Log.

This page intentionally left blank.

APPENDIX E: COLOR CODE LOG – SLANT WELL

E.1 COLOR-CODED GAMMA LOGS FROM WELL SUGG-A #171 6TW, CORES #1 TO #4

To better understand the variability of the slant well lithology, a combination log was created with photographs of the code exterior and the lithologic proxy log for the first four core runs from the slant well (Figure E1). In addition, a color-based log was developed based on the GR results to indicate areas of increased calcite and clay mineral content.

E.2 DATA

The GR data are taken from Core Laboratories Petroleum Services/Laredo Petroleum Inc. field gamma logs[14]. The proxy log and photographs are from Shell Oil Company[15] for the slant well taken at logged distances of 9,276.0 to 9,717.5 ft. The proxy log is an X-ray fluorescence (XRF) log with lithographic proxies of SiO_2 (for silica content), CaO (for limestone content), and Al_2O_3 (for clay mineral content). The proxy log has the following code:

1. Grey = Al_2O_3 (aluminum oxide)
2. Yellow = SiO_2 (silicon dioxide)
3. Blue = CaO (calcium oxide)

The added color-coded log ("6 Multi-Rule") presumes that low GR results are indicative of increased calcite content and large GR values are indicative clay mineral content, and the two trends are exclusive, i.e., the two trends are independent. In essence, the code is similar to Sadeghvishkaei (2017, Figure 4.7) used to provide a geomechanical profile, but with differing bounds. The log was prepared with Microsoft Excel, using conditional formatting, and the bounds are shown in Table E1.

The 6-level color-code is a simplification of current practice, however itis introduced here to assist in identifying major lithographic conditions for hydraulic fracturing. As noted by several authors (e.g., Petrowiki, 2017; AAPG Wiki, 2019), the gamma ray log character is one of the primary methods used to correlate the stratigraphic section. However, the log response depends on the radiation, tool characteristics, logging parameters, and other factors such as drilling mud can influence results. As provided, the limits for the color code are subjectively correlated with other logs and the comparison is shown in this appendix. For comparison, typical GR values for varying lithologies are shown in Table E2.

[14] From files 1) FieldGamma_C1_Laredo_Sugg_A_171_6TW.xls, 2) FieldGamma_C2_Laredo_Sugg_A_171_6TW.xls, 3) FieldGamma_C3_Laredo_Sugg_A_171_6TW.xls and 4) FieldGamma_C4_Laredo_Sugg_A_171_6TW.xls; EDX directory: ... */ Slant_Well_Data/6TW/*.

[15] From P. Desjardin, 2017, file: *GTI Core 1-4 CT Scans-XRF-Frac - Scale 1-50.pdf*; EDX directory: ... *Data - HFTS-1/Fracture_log_(Slant Core well)*

Table E1: Color-Code for Multi-Rule GR Log

Lithology	Color	GR Values (API units)
Larger Limestone/Dolomite Content	Dark Blue	< 55
Significant Limestone/Dolomite Content	Navy Blue	55 to 70
Moderate Limestone/Dolomite Content	Light Blue	70 to 104
Moderate Clay Mineral Content	Yellow Orange	104 to 145
Significant Clay Mineral Content	Orange	145 to 999
Larger Clay Mineral Content/Radioactive Tracers Present	Red	> 999

Table E2: Typical GR Values for Differing Lithologies

Lithology	Gamma Ray Values (API units)
Sandstone (quartz)	15 to 30 (rarely to 200)
Limestone	10 to 40
Dolomite	15 to 40 (rarely to 200)
Shale	60 to 150
Organic-rich Shale	100 to 250
Anhydrite, Halite	8 to 15
Sylvite	350 to 500
Coal	15 to 150 (any value possible)

Note: From AAPG Wiki (2019).

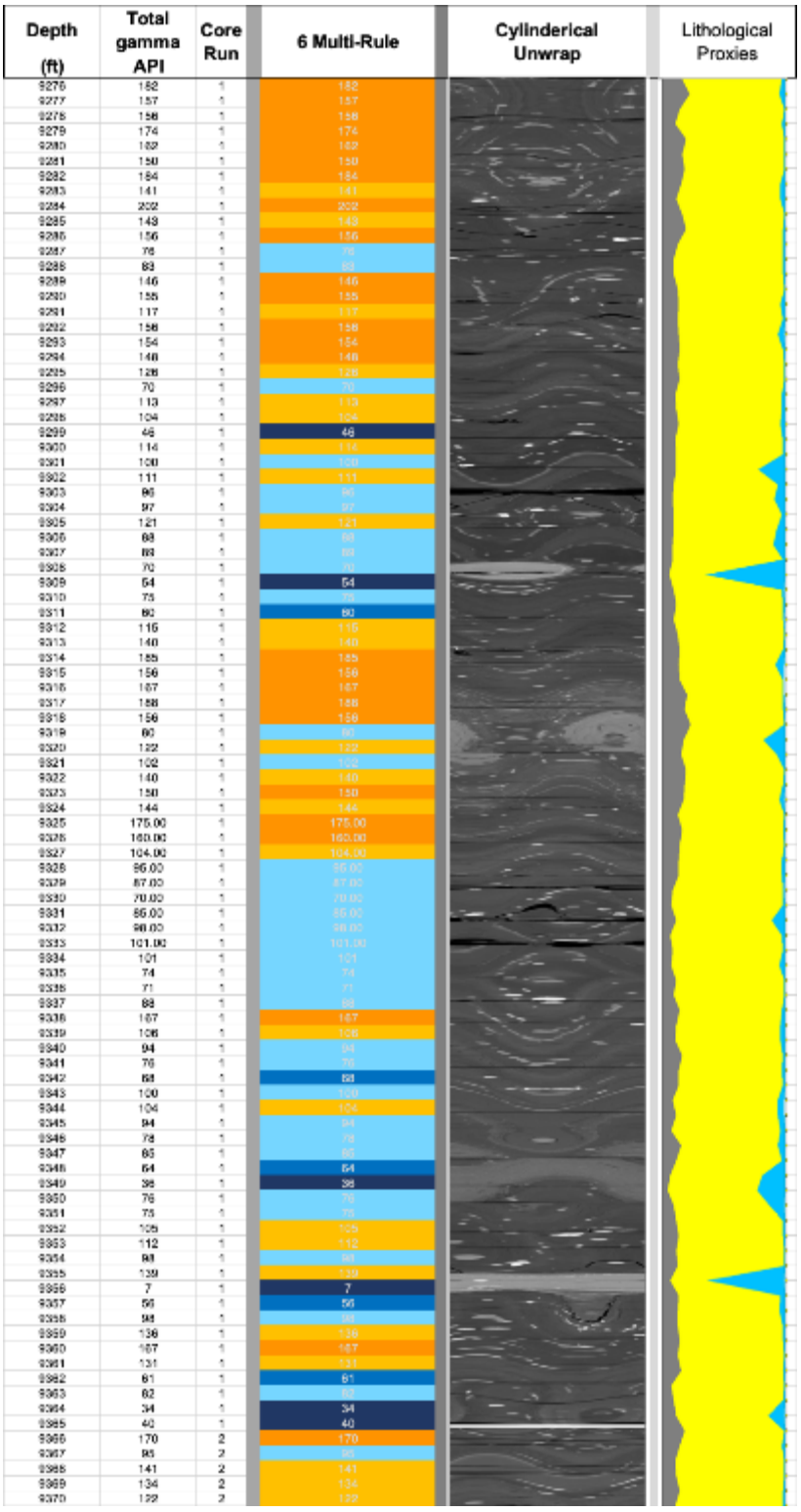

Figure E1: Comparison of color-code log based on gamma results from slant well with log photographs and lithological proxy log (1 of 5).

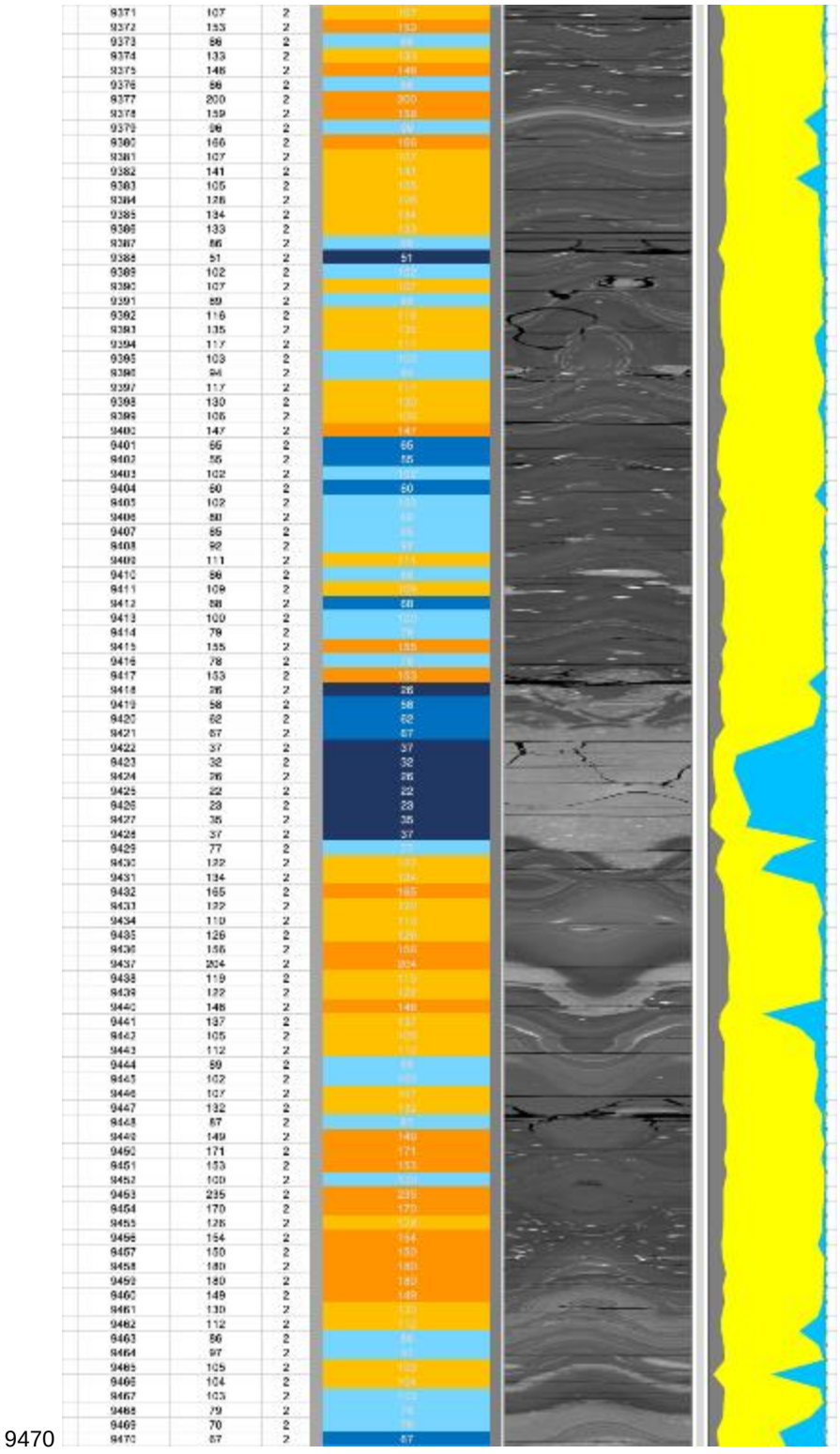

Figure E1 (cont.): Comparison of color-code log based on gamma results from slant well with log photographs and lithological proxy log (2 of 5).

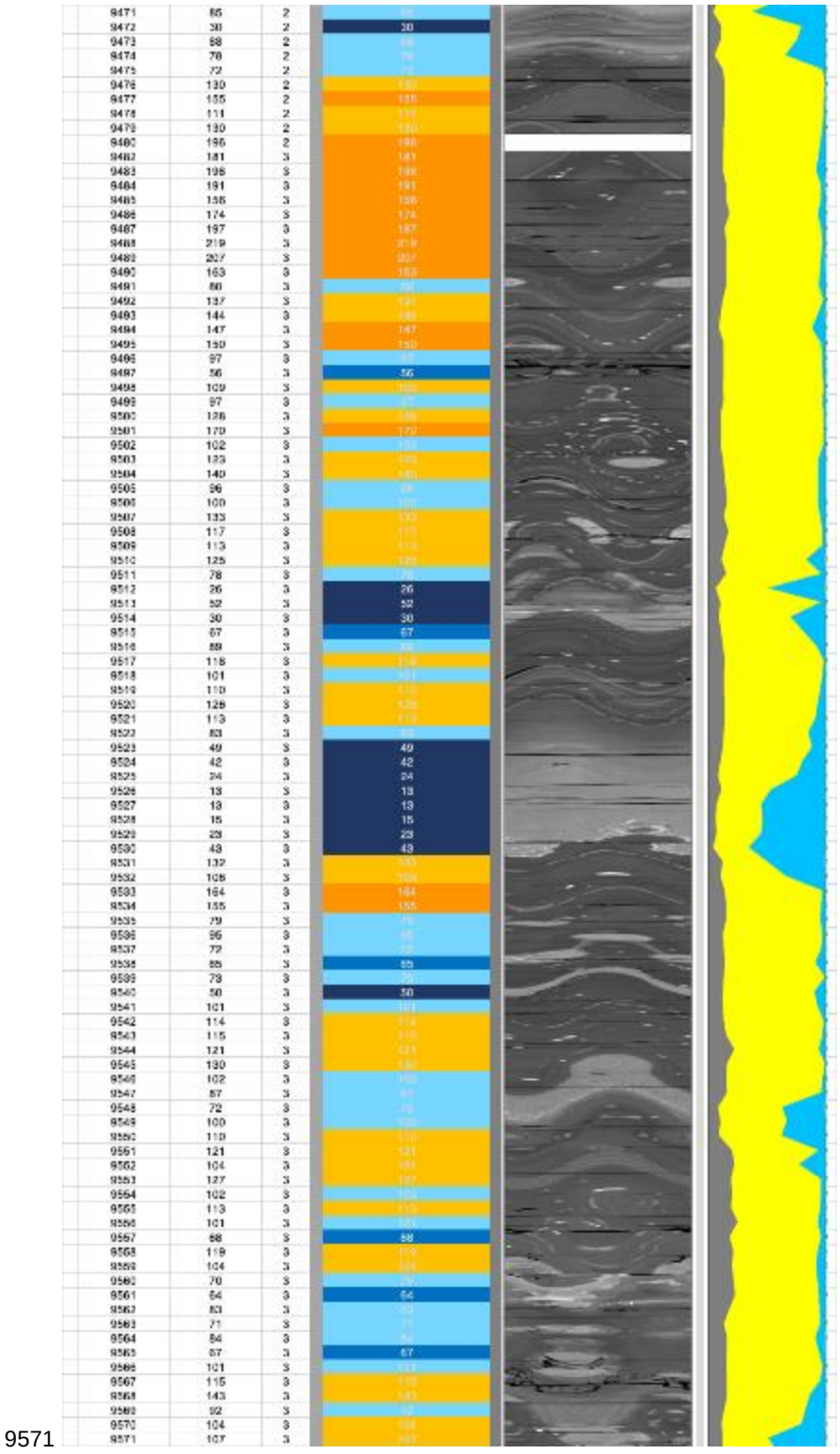

Figure E1 (cont.): Comparison of color-code log based on gamma results from slant well with log photographs and lithological proxy log (3 of 5).

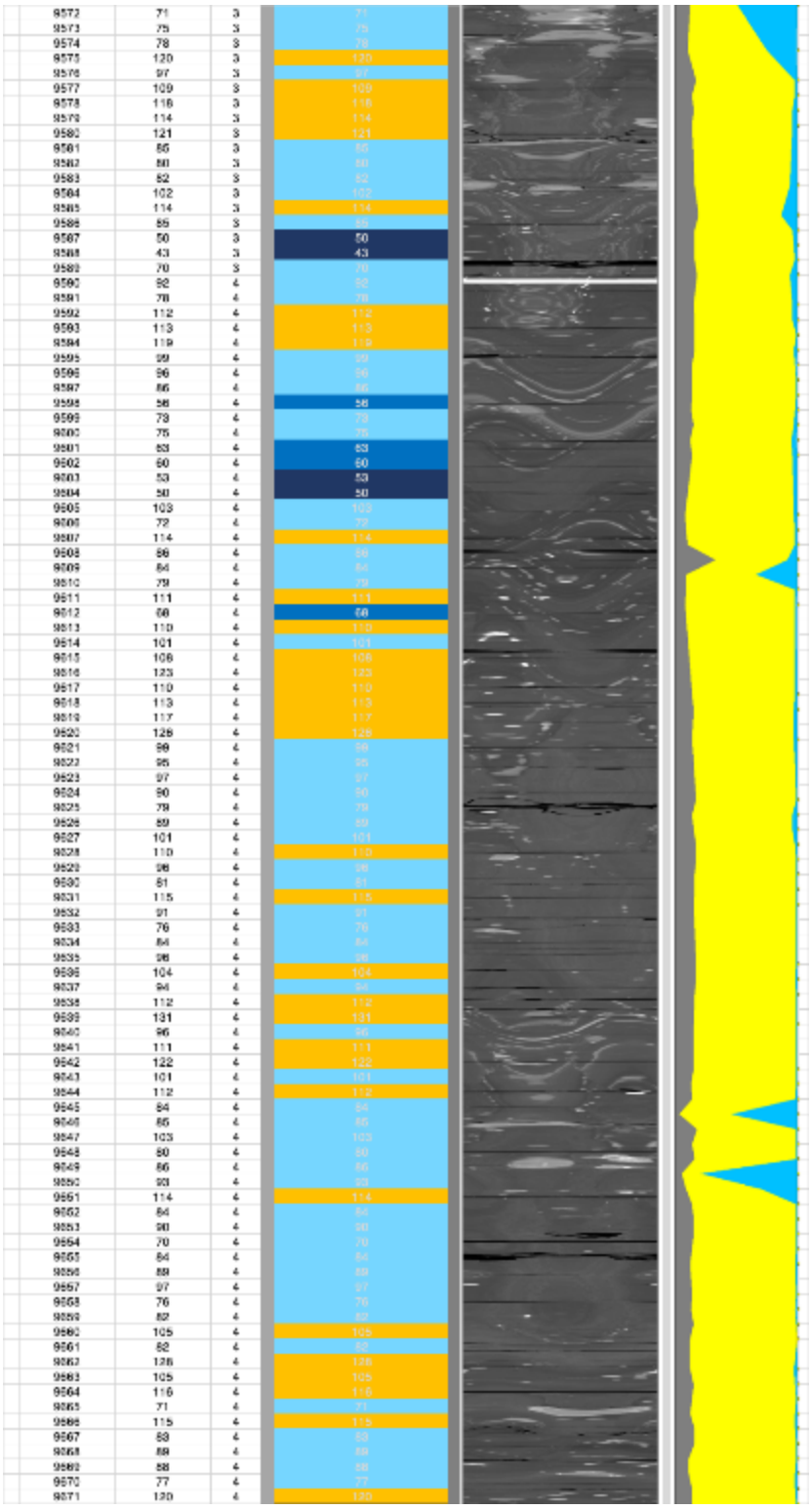

9671

Figure E1 (cont.): Comparison of color-code log based on gamma results from slant well with log photographs and lithological proxy log (4 of 5).

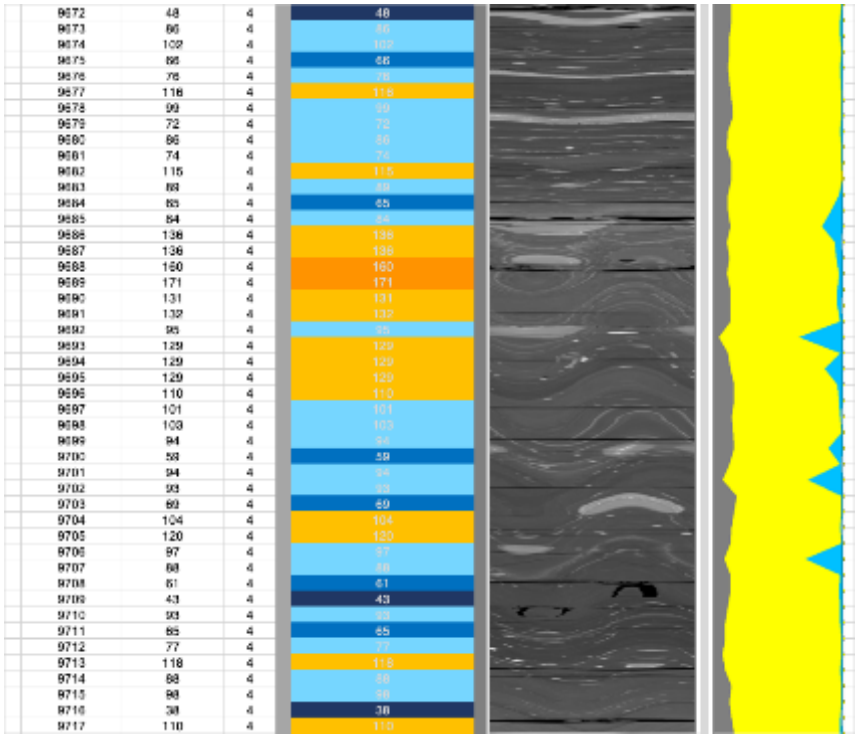

Figure E1 (cont.): Comparison of color-code log based on gamma results from slant well with log photographs and lithological proxy log (5 of 5).

This page intentionally left blank.

APPENDIX F: COLOR CODE LOG –VERTICAL PILOT WELL

F.1 COLOR CODED GAMMA LOGS FROM SUGG-A #171 7SU PILOT WELL

To better understand the variability of the vertical lithology, two color-code log schemes were developed based on the GR results to indicate areas of increased calcite and clay mineral content. The results were compared to the combined petrophysics log for the well prepared for the hydraulic fracture test site #1 (HFTS-1) project. The legend for the combined petrophysics log is shown in Figure F1 and the comparison results are shown in Figure F2.

F.2 DATA

The GR data are from Laredo Petroleum Inc. field gamma logs[16]. and the combined petrophysics log is from the Probabilistic Integrated Petrophysical Evaluation by Laredo Petroleum Inc [17] for the vertical pilot well taken at logged distances of 6,884.0 to 8,481.5 ft.

Two color-code logs were developed using GR data. They both presume that low GR results are indicative of increased calcite content and large GR values are indicative clay mineral content, and the two trends are exclusive, i.e., the two trends are independent.

The first log ("Tri-Zone") was prepared with Microsoft Excel, using conditional formatting. It uses a three zone, graded classification where high GR values are red, low GR values are blue, and intermediate values are white, with varying color intensity within each group (see Table F1).

A second color log ("6 Multi-Rule") also prepared with Excel uses a more-restrictive coloring approach, with no graded shading and is divided into two parts, as described in Table F2.

[16] From file: SUGG-A 171 7SU_GTI.las; EDX directory: /hfts-1-phase-1-individual-well-files/SUGG A 171 7SU Pilot Hole/1_Field Logs.

[17] From file: SUGG A 171 7SU PETROPHYSICS DFIT.tif; EDX directory: ... /hfts-1-phase-1-individual-well-files/SUGG A 171 7SU Pilot Hole/7_Petrophysics.

Table F1: Color-Code for Tri-Zone Log

Lithology	Color	GR Values (API units)
Larger Clay Mineral Content	Red	> 999
In-Between Values	White	
Limestone/Dolomite Content	Dark Blue	< 55

Table F2: Color-Code for 6 Multi-Rule log (2-Column System)

Lithology	Color	GR Values (API units)
Column # 1		
Moderate Clay Mineral Content	Yellow Orange	104 to 145
Significant Clay Mineral Content	Orange	145 to 999
Larger Clay Mineral Content/Radioactive Tracers Present	Red	> 999
Column # 2		
Larger Limestone/Dolomite Content	Dark Blue	< 55
Significant Limestone/Dolomite Content	Navy Blue	55 to 70
Moderate Limestone/Dolomite Content	Light Blue	70 to 104

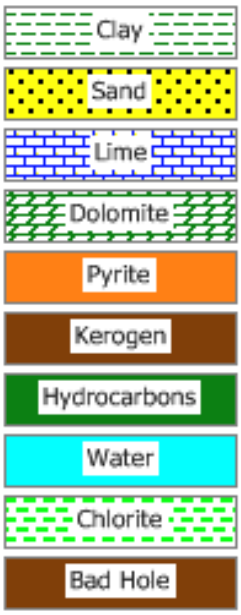

Figure F1: Legend for the combined petrophysics log.

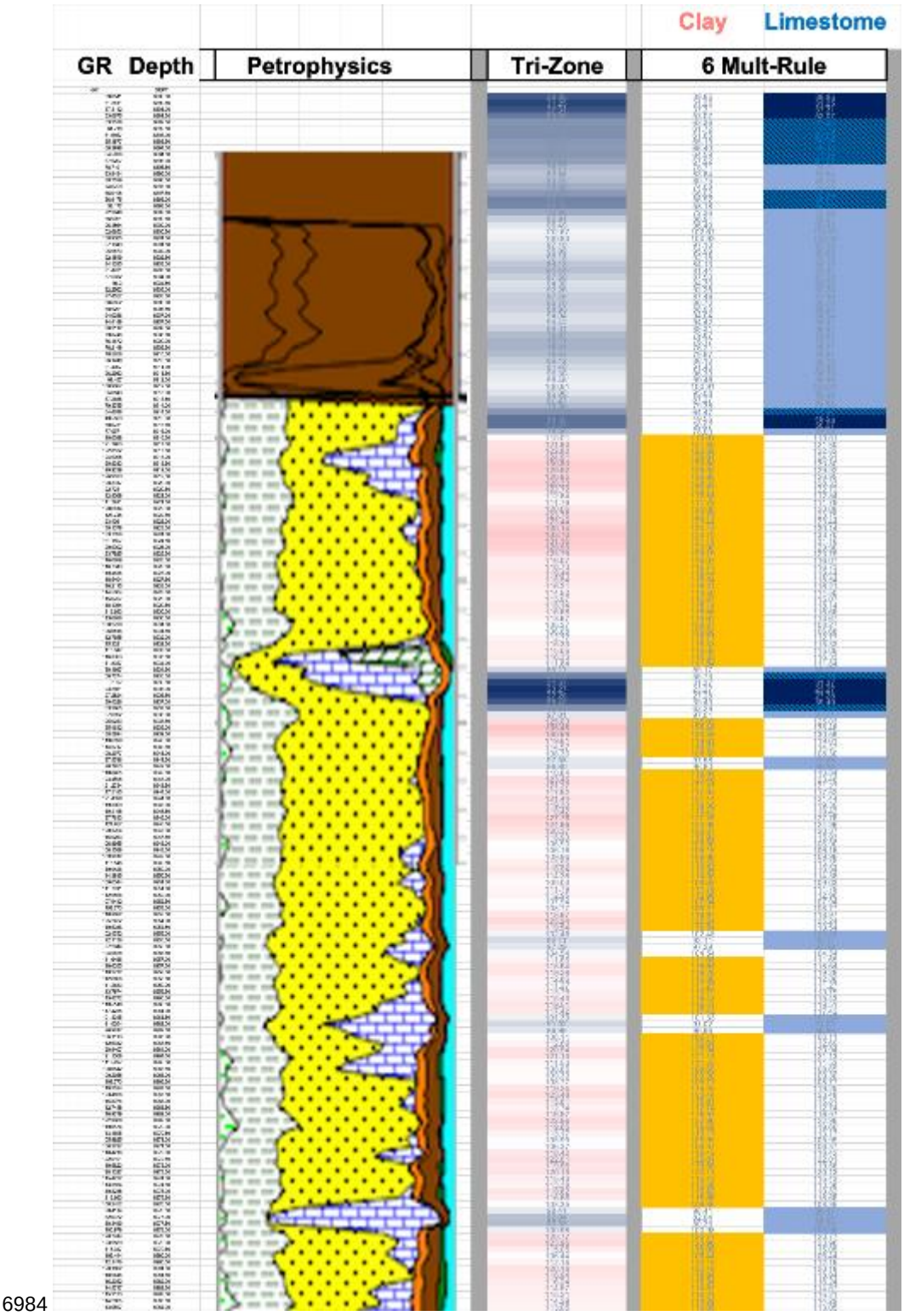

Figure F2: Comparison of color-code logs with lithological log from pilot well (1 of 16).

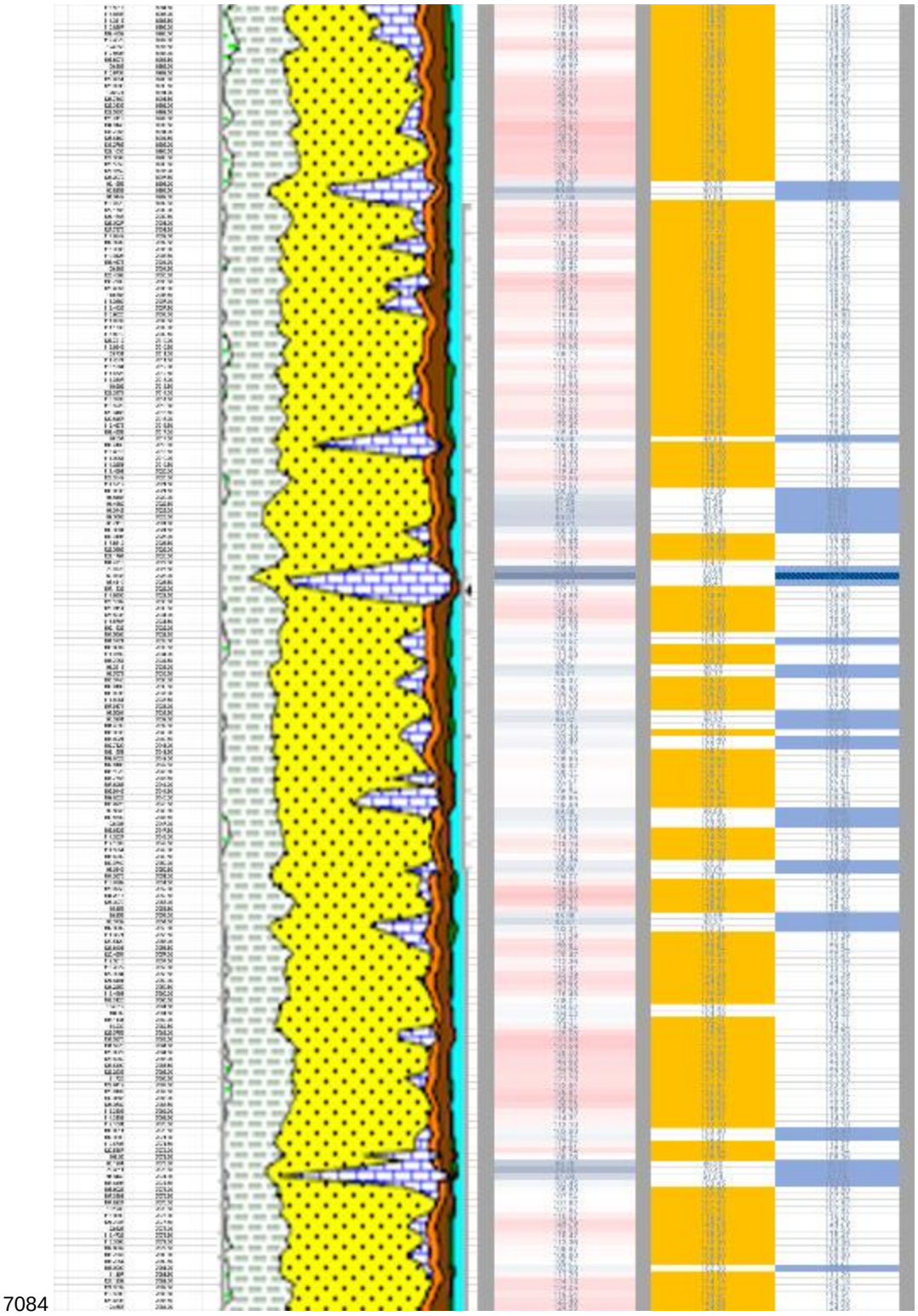

Figure F2 (cont.): Comparison of color-code logs with lithological log from pilot well (2 of 16).

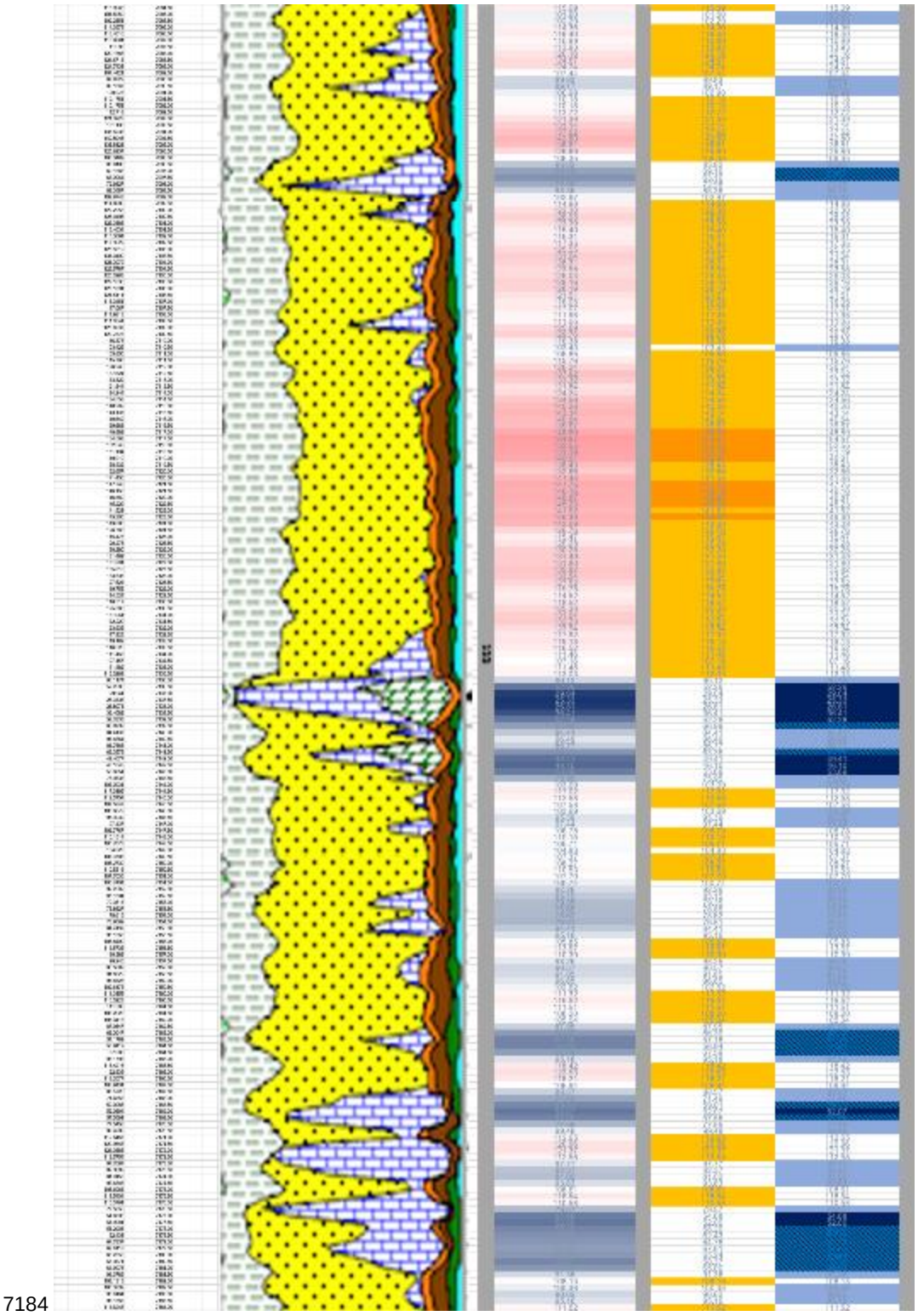

Figure F2 (cont.): Comparison of color-code logs with lithological log from pilot well (3 of 16).

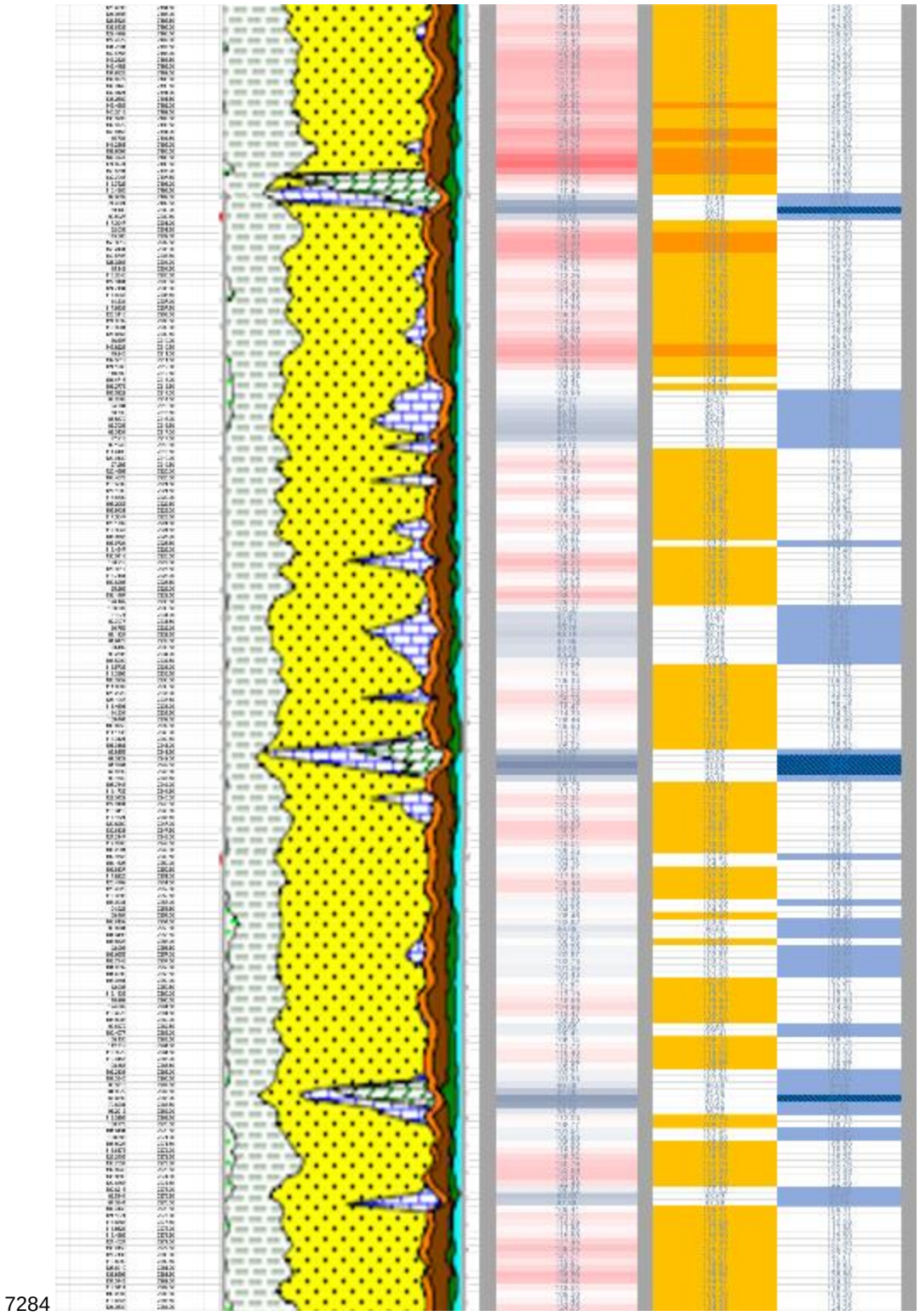

Figure F2 (cont.): Comparison of color-code logs with lithological log from pilot well (4 of 16).

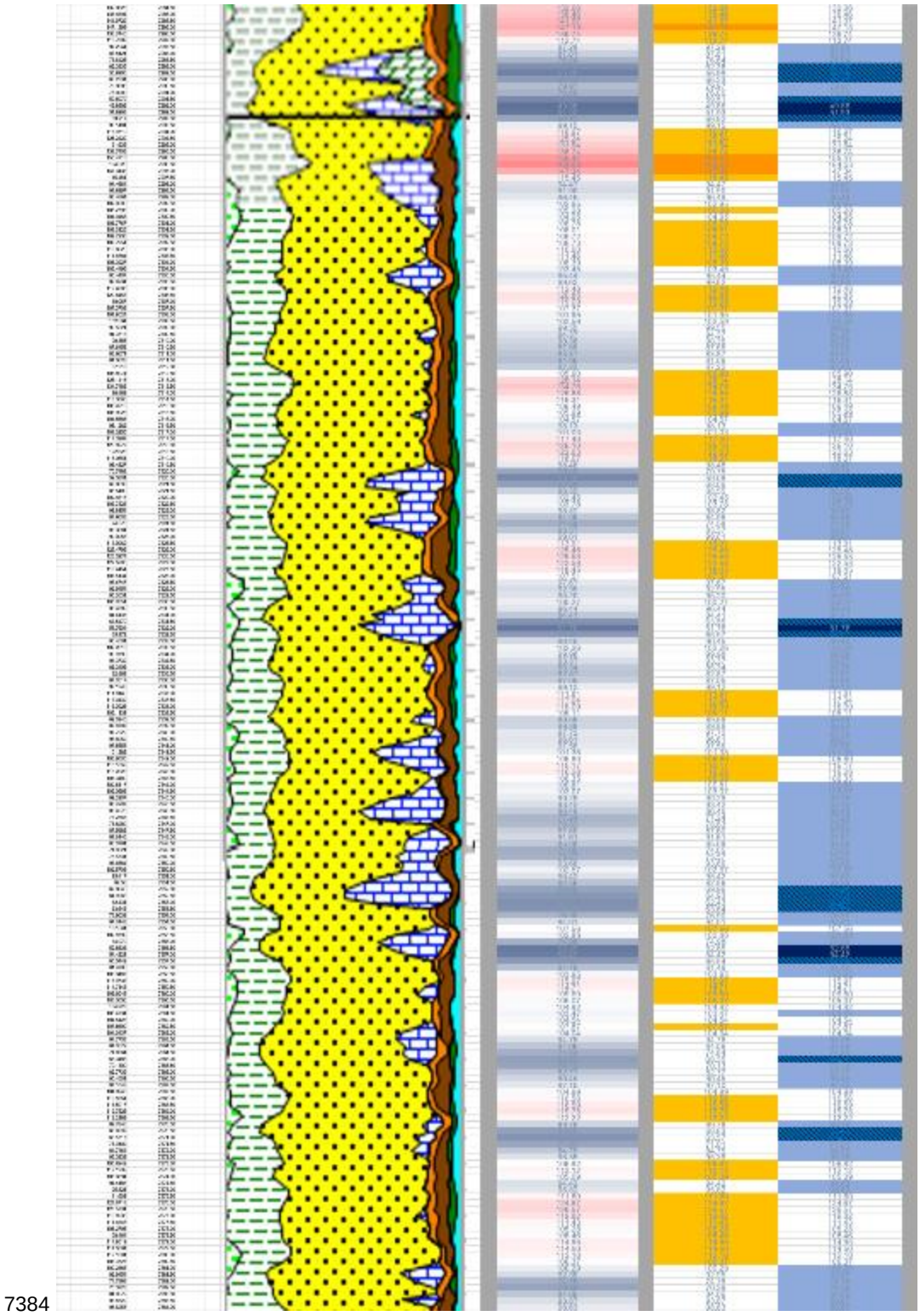

Figure F2 (cont.): Comparison of color-code logs with lithological log from pilot well (5 of 16).

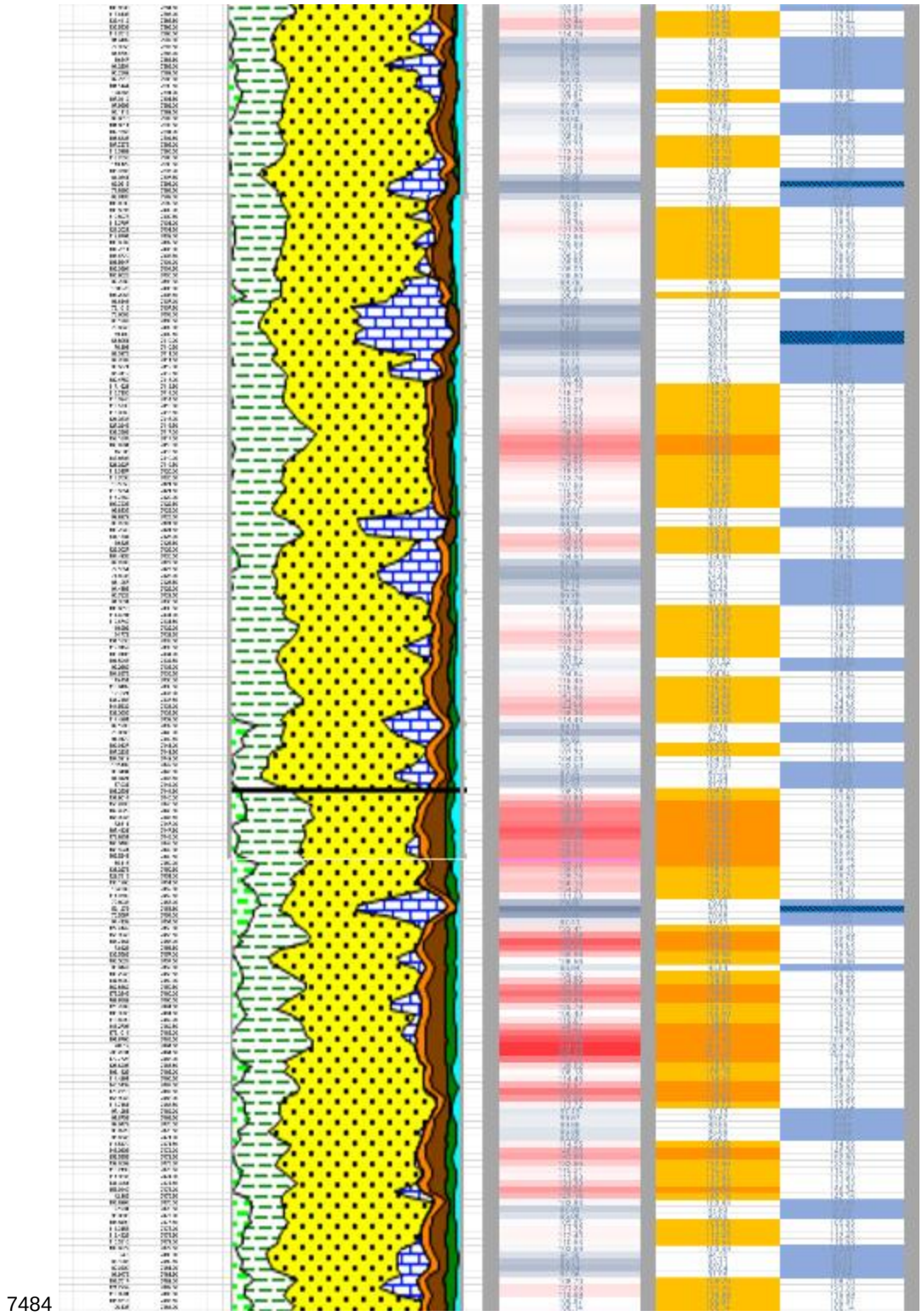

Figure F2 (cont.): Comparison of color-code logs with lithological log from pilot well (6 of 16).

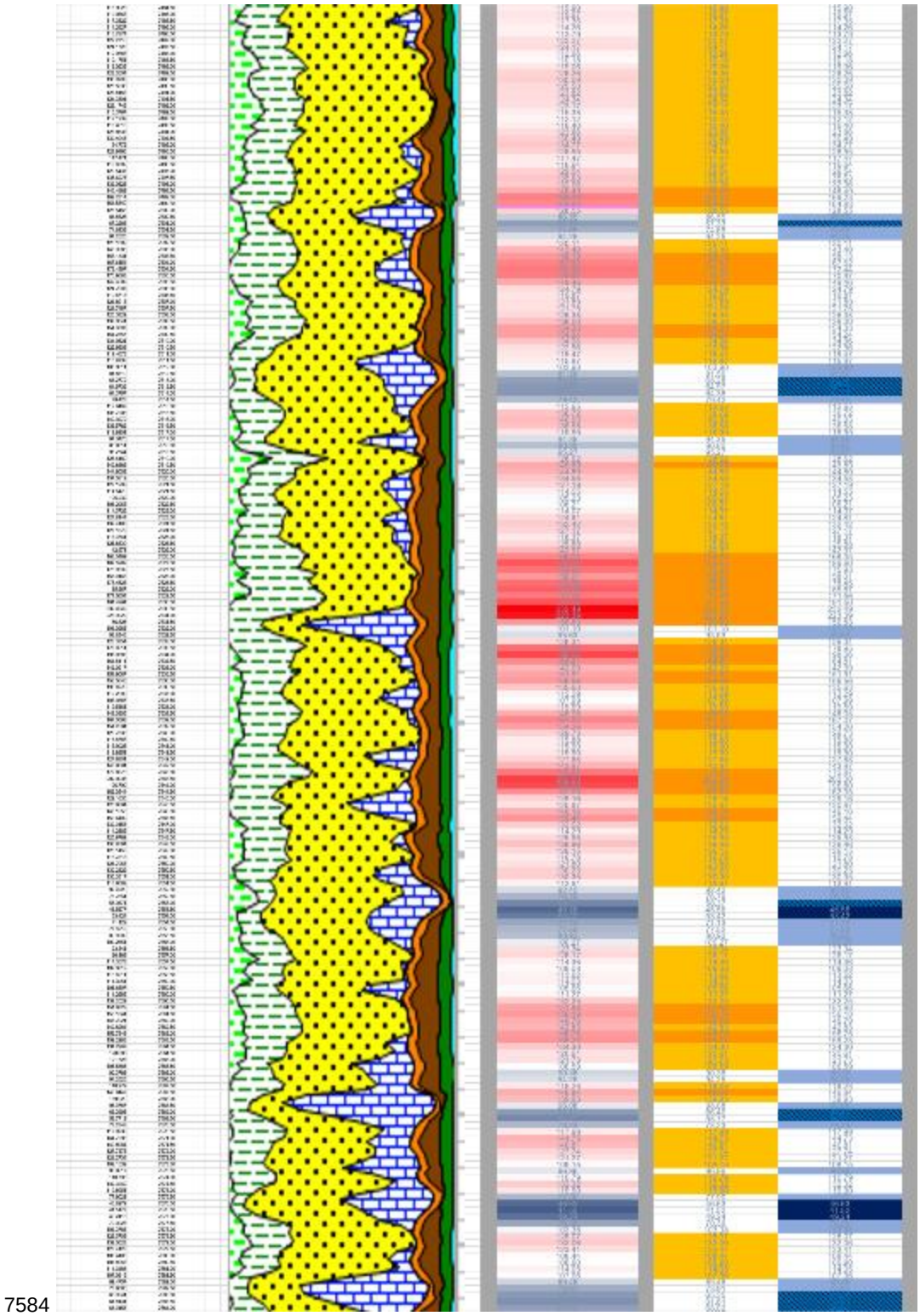

Figure F2 (cont.): Comparison of color-code logs with lithological log from pilot well (7 of 16).

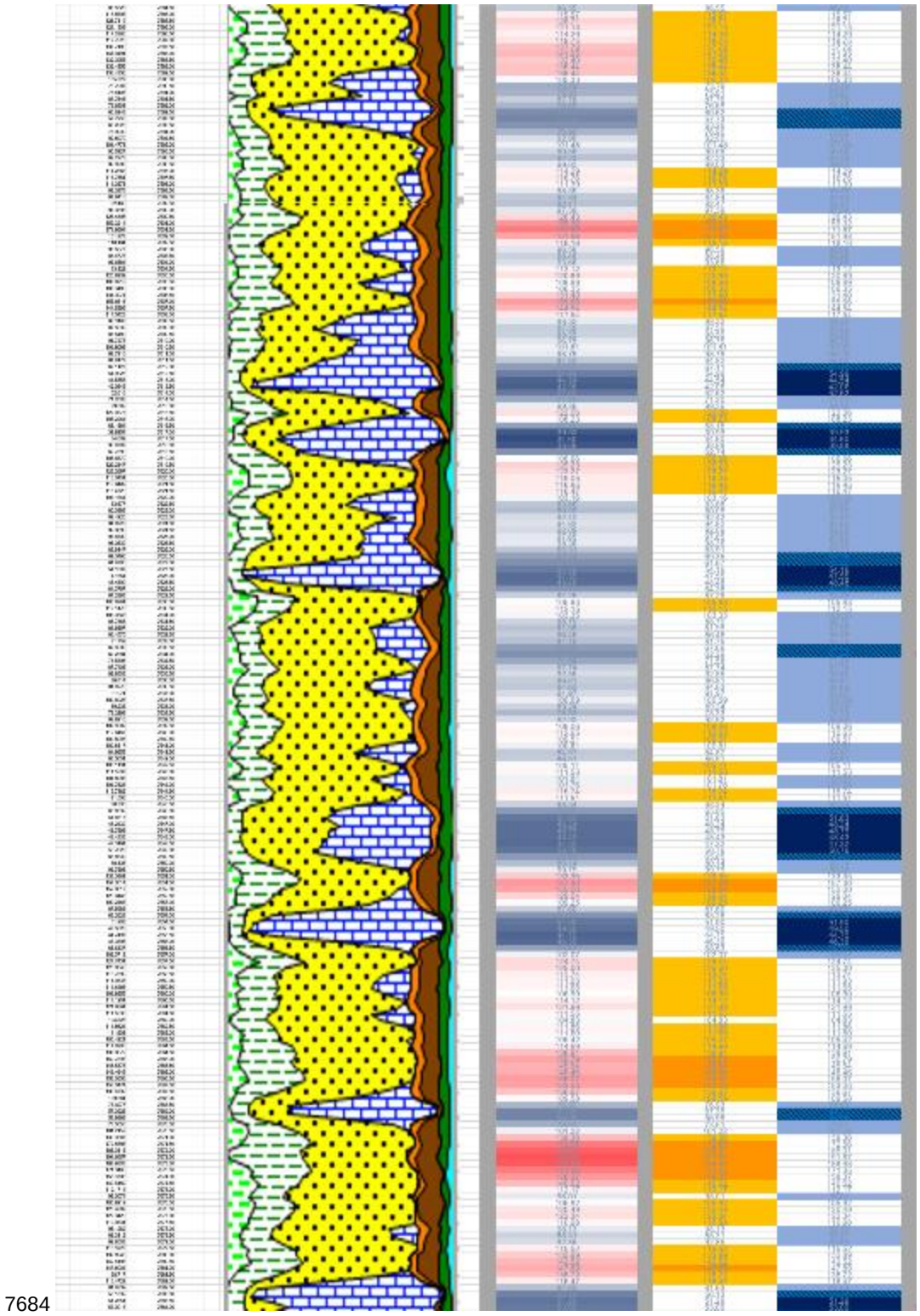

Figure F2 (cont.): Comparison of color-code logs with lithological log from pilot well (8 of 16).

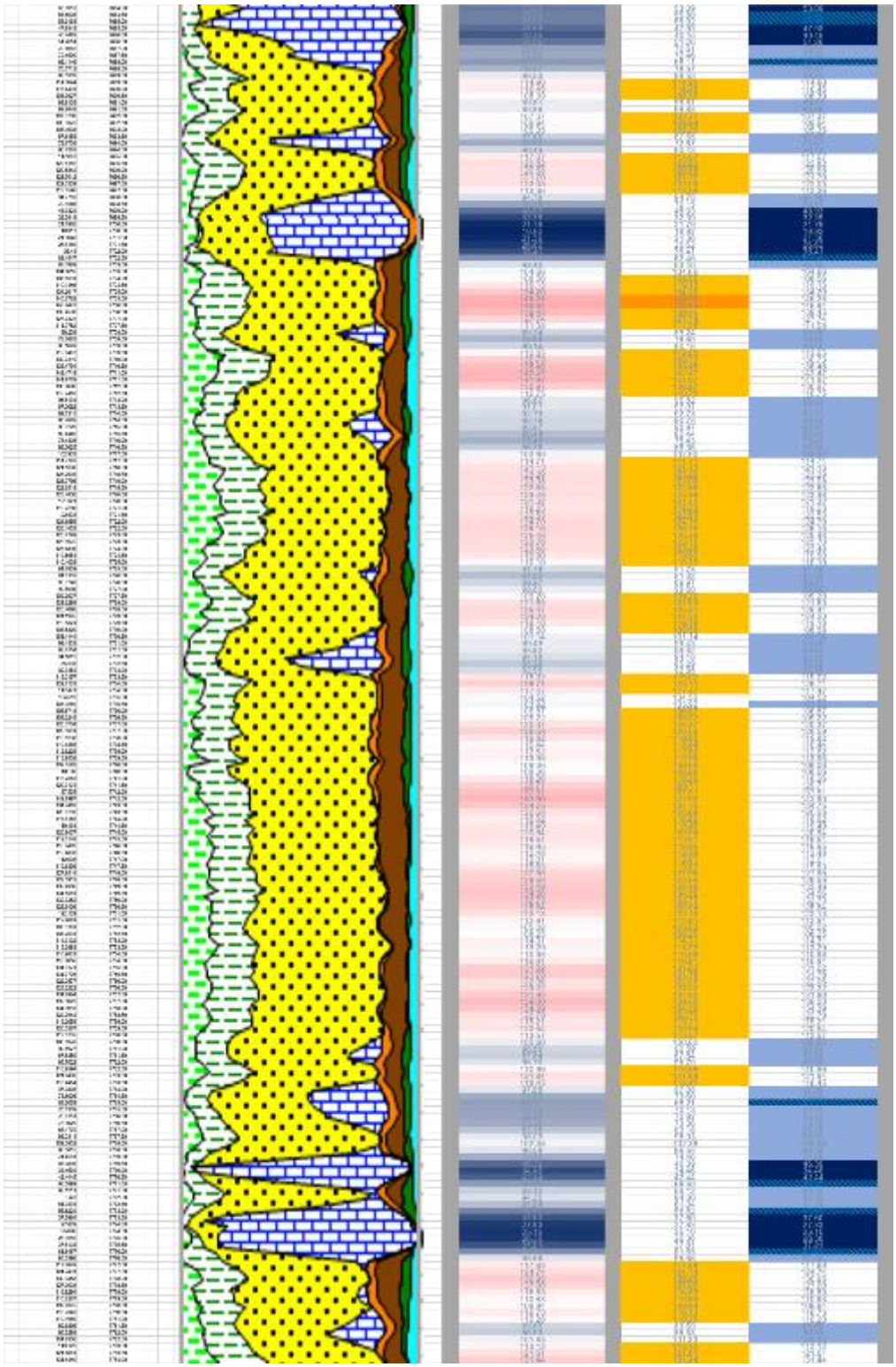

Figure F2 (cont.): Comparison of color-code logs with lithological log from pilot well (9 of 16).

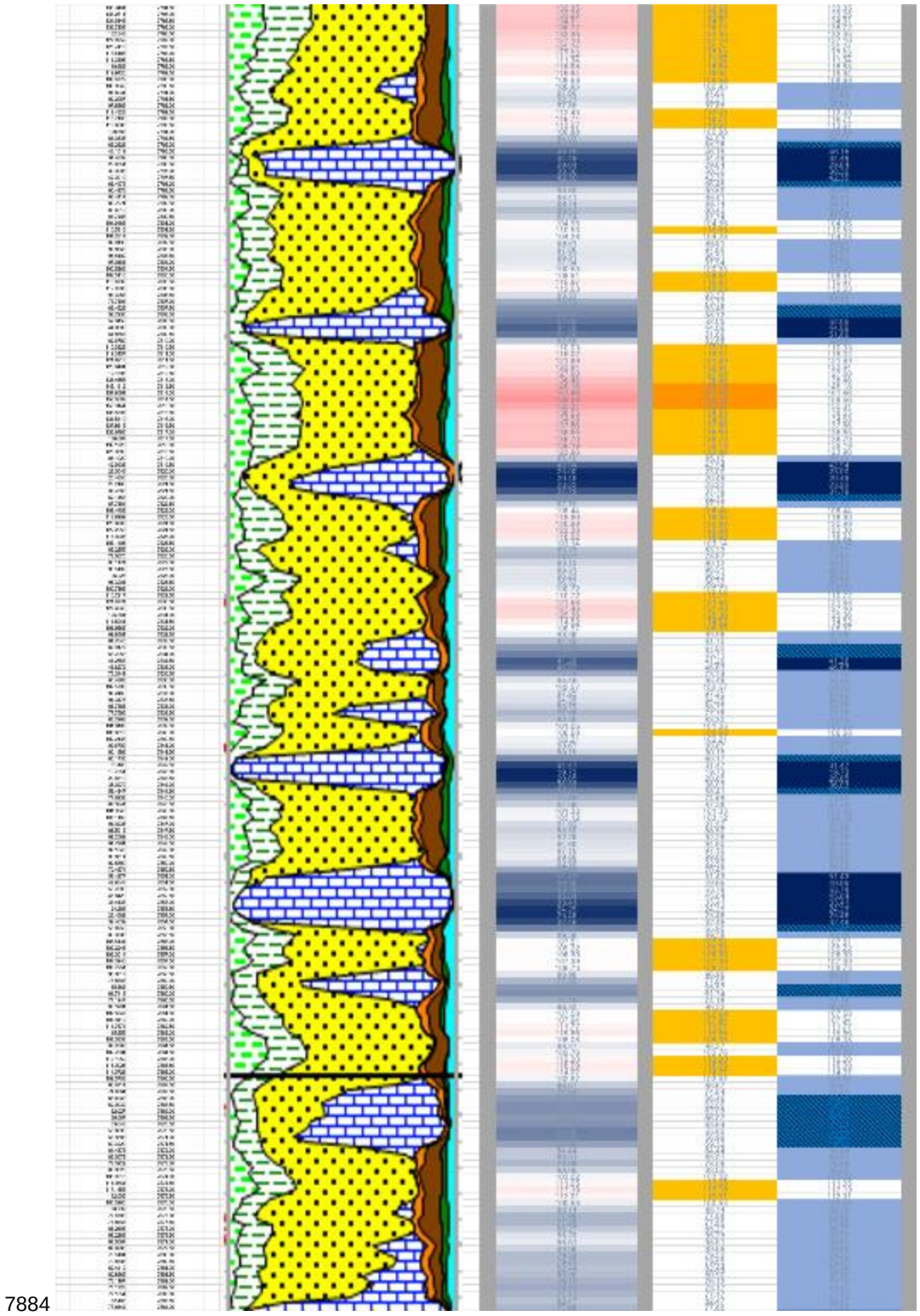

Figure F2 (cont.): Comparison of color-code logs with lithological log from pilot well (10 of 16).

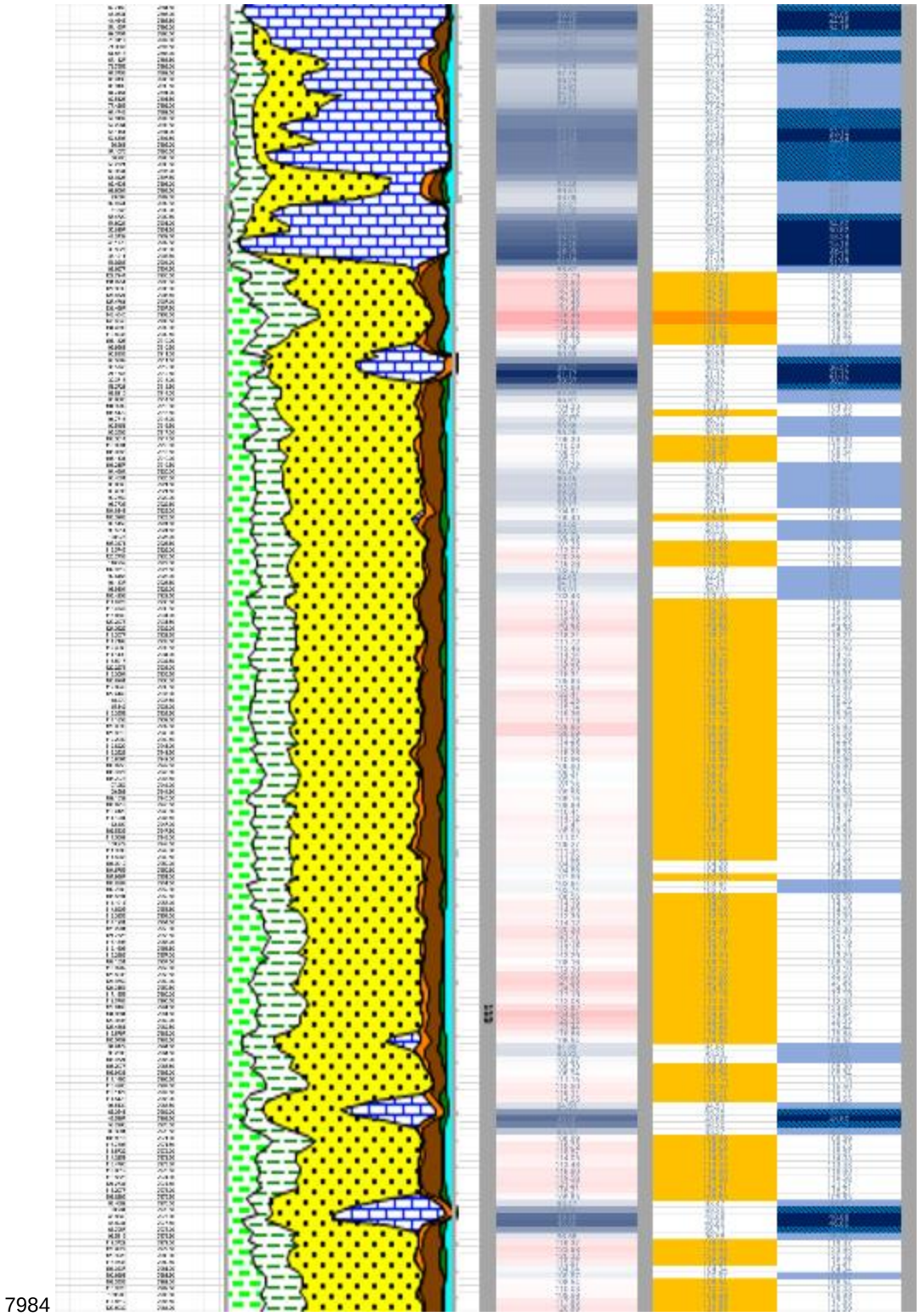

Figure F2 (cont.): Comparison of color-code logs with lithological log from pilot well (11 of 16).

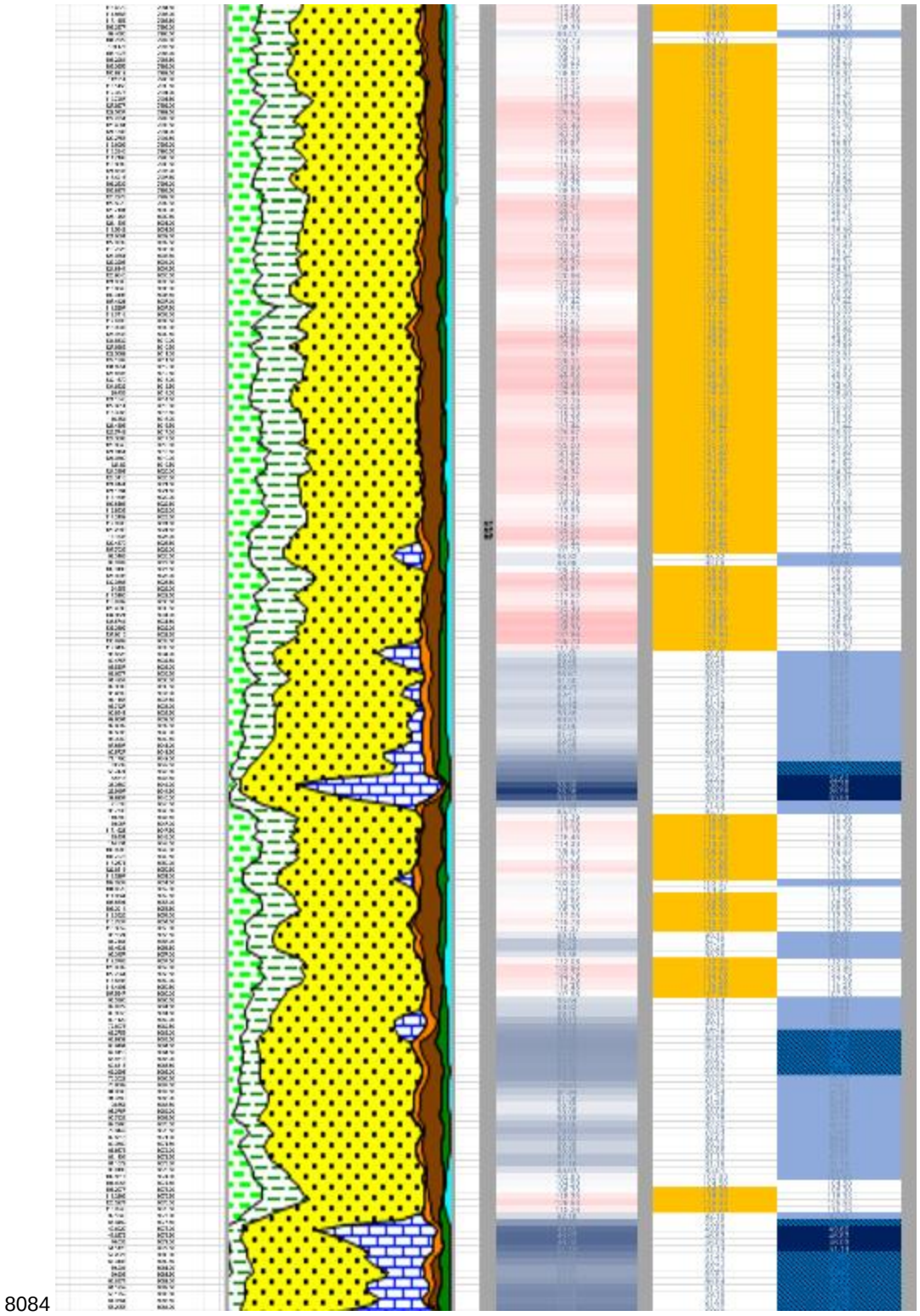

Figure F2 (cont.): Comparison of color-code logs with lithological log from pilot well (12 of 16).

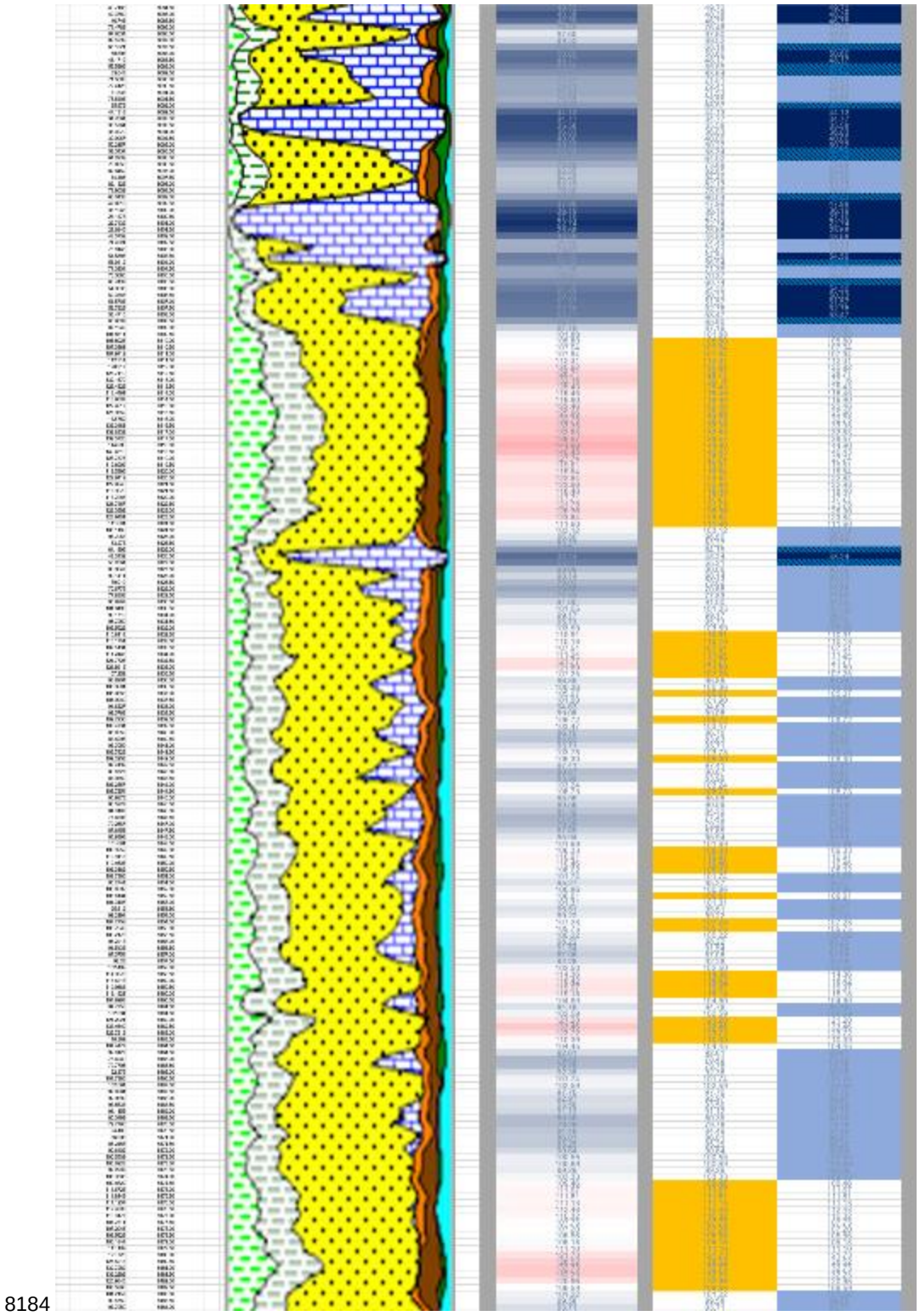

Figure F2 (cont.): Comparison of color-code logs with lithological log from pilot well (13 of 16).

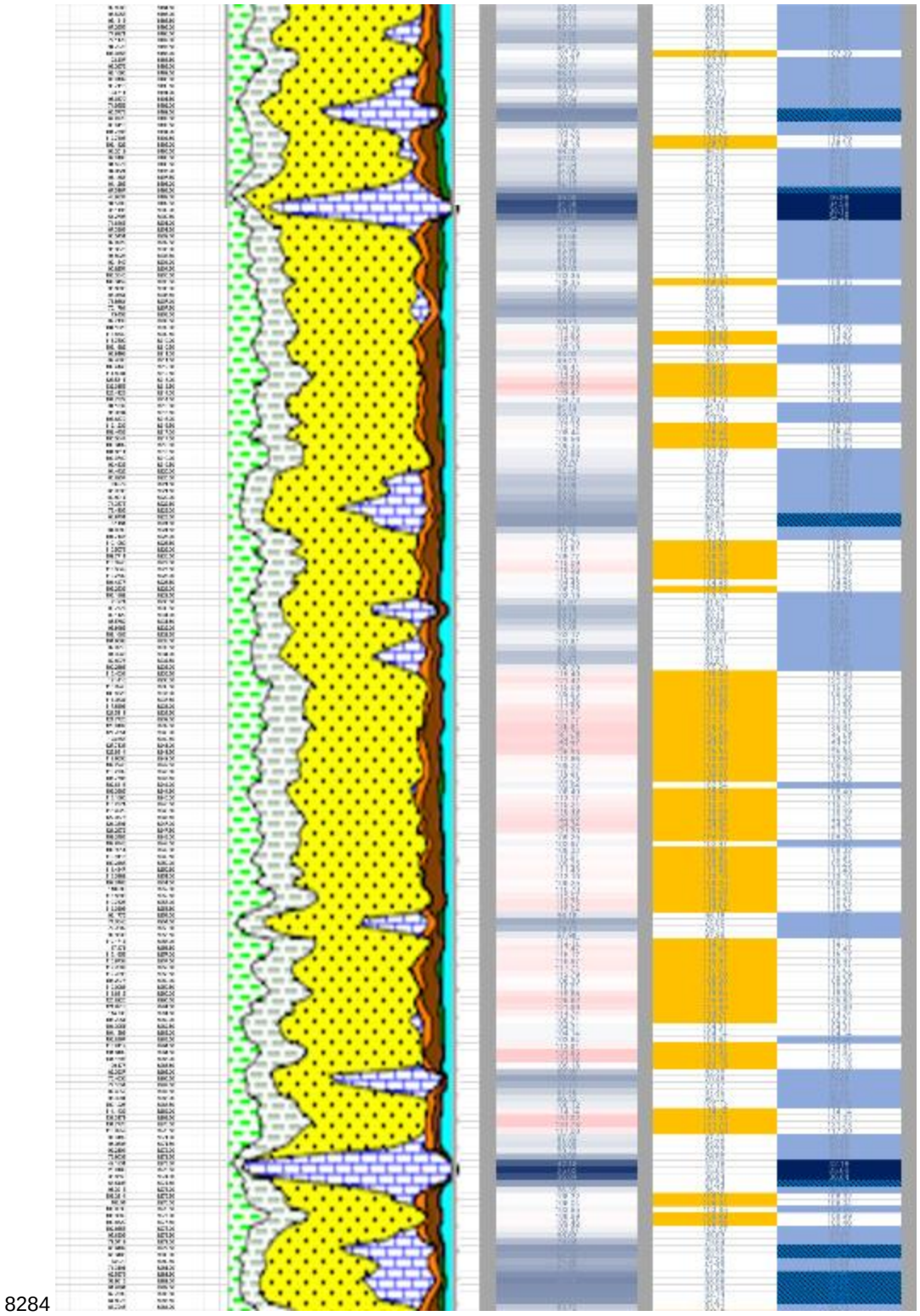

Figure F2 (cont.): Comparison of color-code logs with lithological log from pilot well (14 of 16).

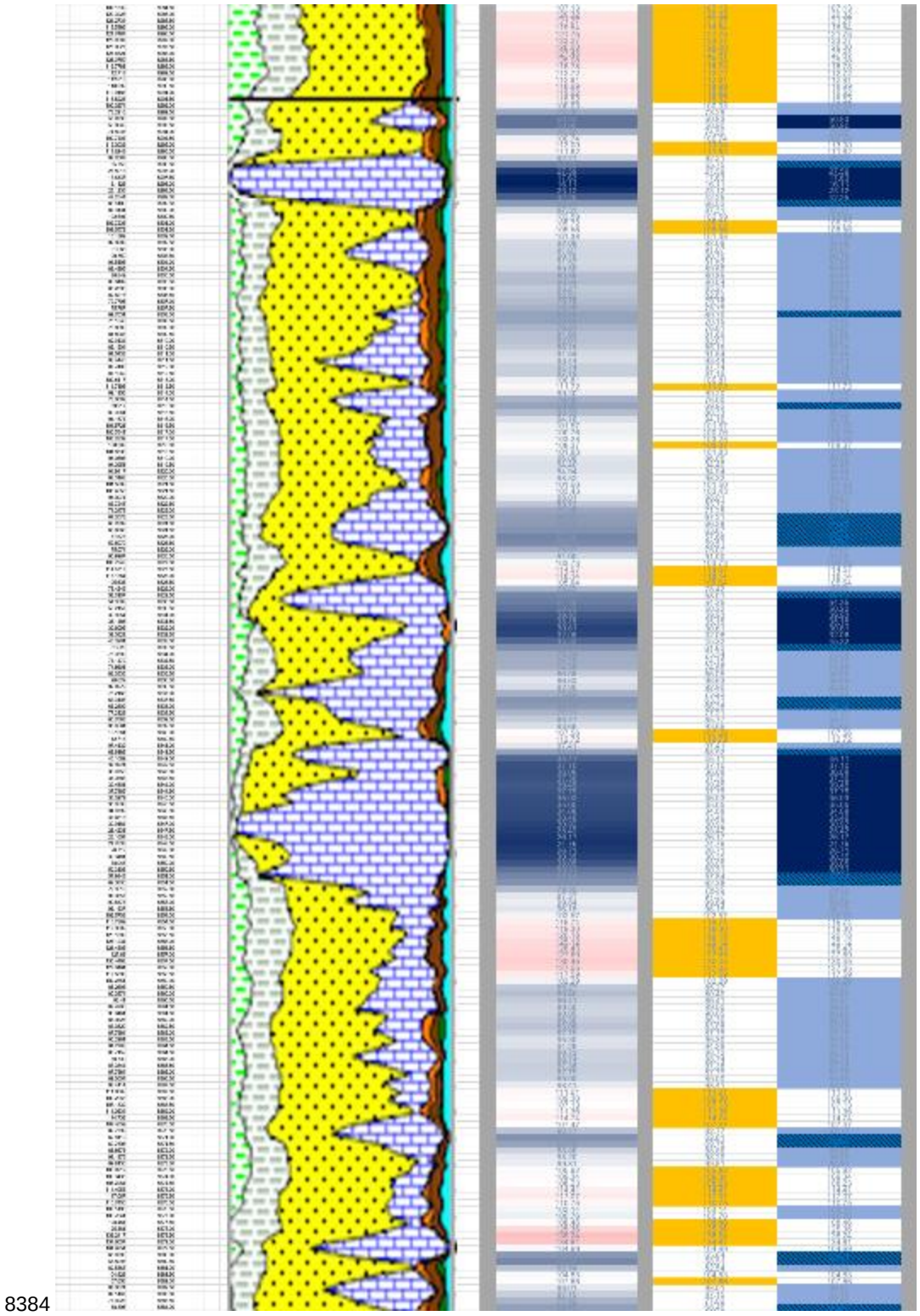

Figure F2 (cont.): Comparison of color-code logs with lithological log from pilot well (15 of 16).

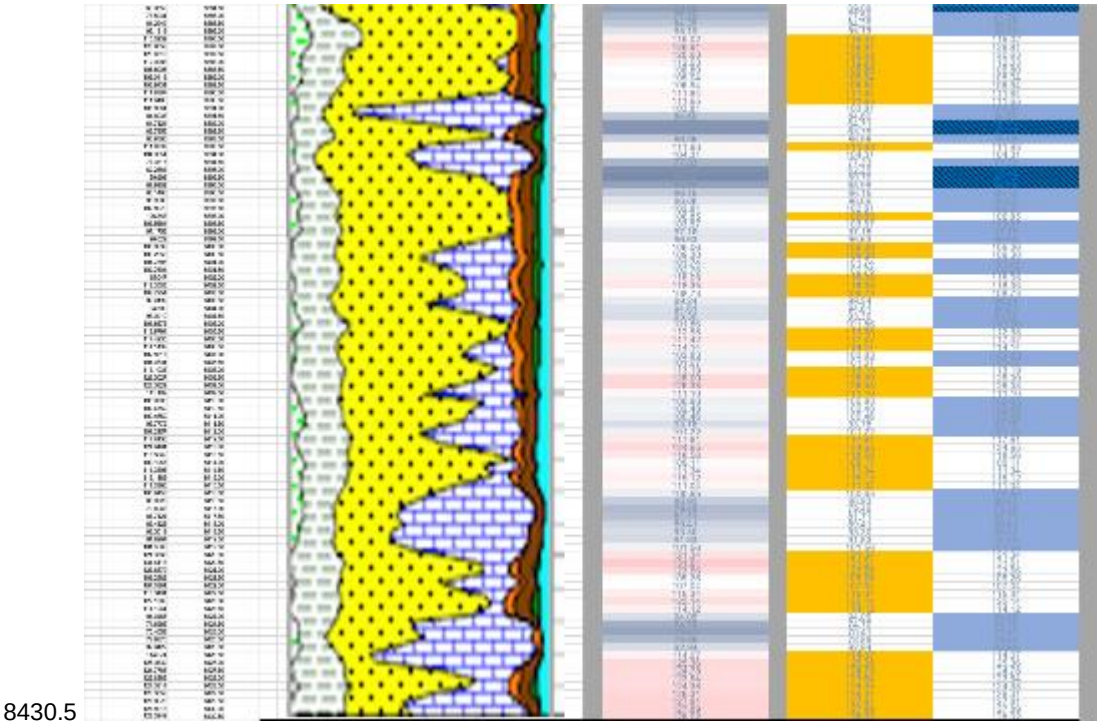

Figure F2 (cont.): Comparison of color-code logs with lithological log from pilot well (16 of 16).

This page intentionally left blank.

APPENDIX G: COLOR CODE LOG –HORIZONTAL WELLS

G.1 COLOR-CODED GAMMA LOGS FROM HORIZONTAL WELLS

To better understand the variability of the horizontal lithology, a color-code log scheme was developed based on the GR results to indicate areas of potential increased calcite and clay mineral content. The color code was applied to the GR results of selected horizontal wells in the Upper Wolfcamp Formation (i.e., labeled "SU"). No other logs (density, modulus, etc.) were available for these wells.

The resulting diagram (Figure G1) shows no discernable pattern although adjacent borings can show occasional similarities. The variation is to some degree cyclical and can be the result of cyclical patterns of deposition on a periodic basis.

In well SUGG-A #171-4SU, at depths of roughly 500 ft[18] and greater, very large GR values (greater than 1,000 API) are evident in the completion log, as indicated by large patches of red. This also occurs in the raw data of SUGG-A #171-6SU (i.e., in the completion log). The cause of these large values is undetermined, but in all likelihood, is due to the presence of radioactive tracers. Log 6SU has apparently been corrected; corrected GR data for well 4SU appears in graphic form but not in numerical data.[19]

G.2 DATA

The color-coded logs use a multi-color presentation ("6 Multi-Rule") which presumes that low GR results are indicative of increased calcite content and large GR values are indicative of clay mineral content, and the two trends are exclusive, i.e., the two trends are independent. The log was prepared with Microsoft Excel, using conditional formatting. The bounds used in the 6-level conditional format are shown in Table G1.

The logs[20] are presented in 100 ft sections with the relative bottom depth of each section shown on the bottom left. Only the first 1,000 ft of each horizontal well is shown in this appendix (with 10 sheets).

[18] The "depth" in the horizontal holes is a reference distance along well and not a vertical depth.

[19] A line of data, labeled as "GR OH" (open hole?) appears in file, Laredo_Sugg_A171_#4SU_SS.pdf, but is not shown in the accompanying *.las file, Laredo_Sugg_A171_#4SU_SS.las.

[20] The data for the logs are from files:
- Laredo_Sugg_A_171_8SU_SS.las
- LAREDO PETROLEUM_SUGG A #1716SU_2609_128306104_RUN 1_MAIN PASS_LAS.las
- Laredo_Sugg_A171_#5SU_SS.las
- Laredo_Sugg_A171_#4SU_SS.las
- Laredo_Sugg_A171_#3SU_SS.las
- Laredo_Sugg_A_158_1SU_SS.las.

Table G1: Color-Code for 6 Multi-Rule GR Log

Lithology	Color	GR Values (API units)
Larger Limestone/Dolomite Content	Dark Blue	< 55
Significant Limestone/Dolomite Content	Navy Blue	55 to 70
Moderate Limestone/Dolomite Content	Light Blue	70 to 104
Moderate Clay Mineral Content	Yellow Orange	104 to 145
Significant Clay Mineral Content	Orange	145 to 999
Large Clay Mineral Content/Radioactive Tracers Present	Red	> 999

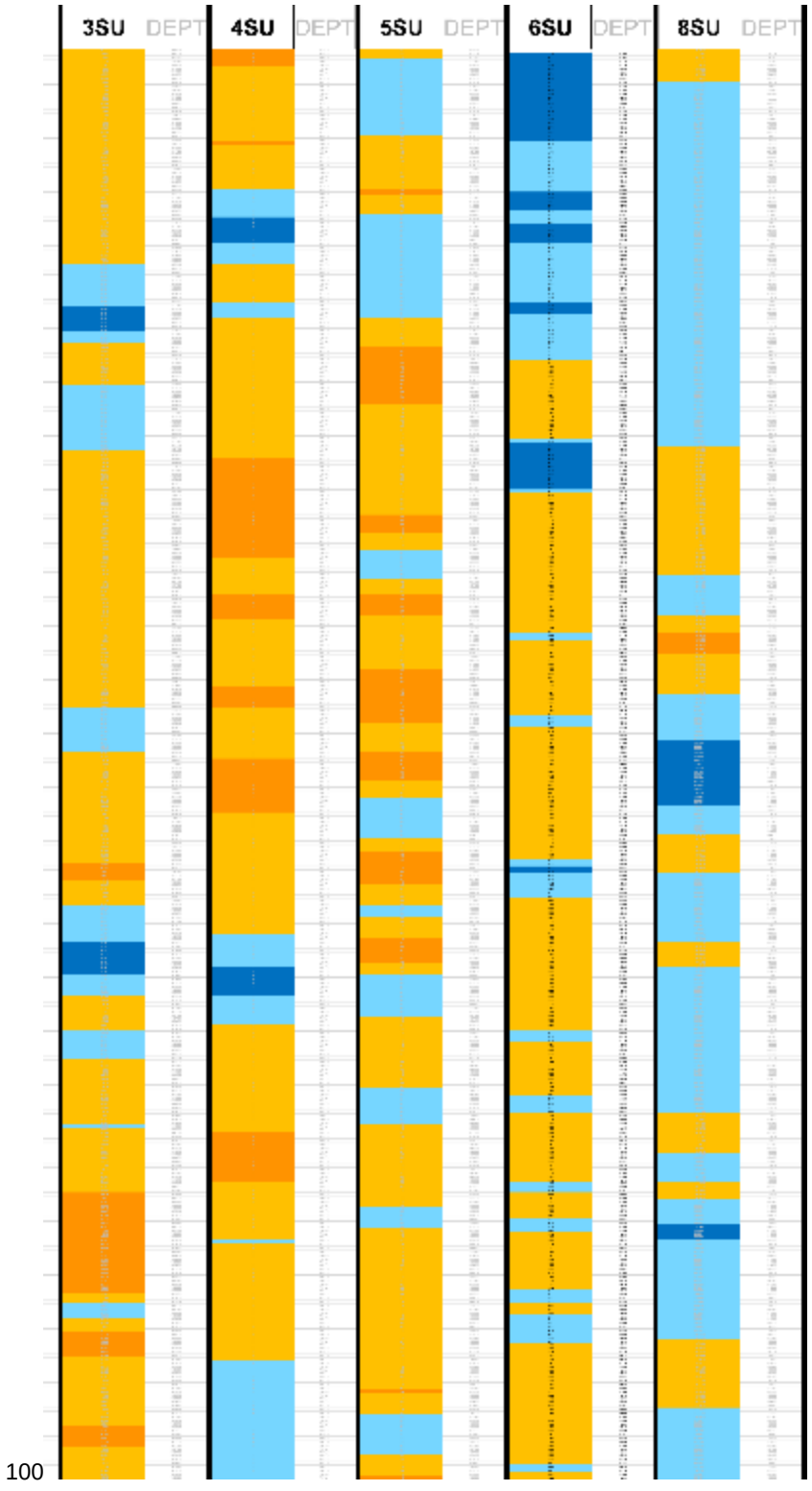

Figure G1: Color-code of GR values for horizontal logs (1 of 10).

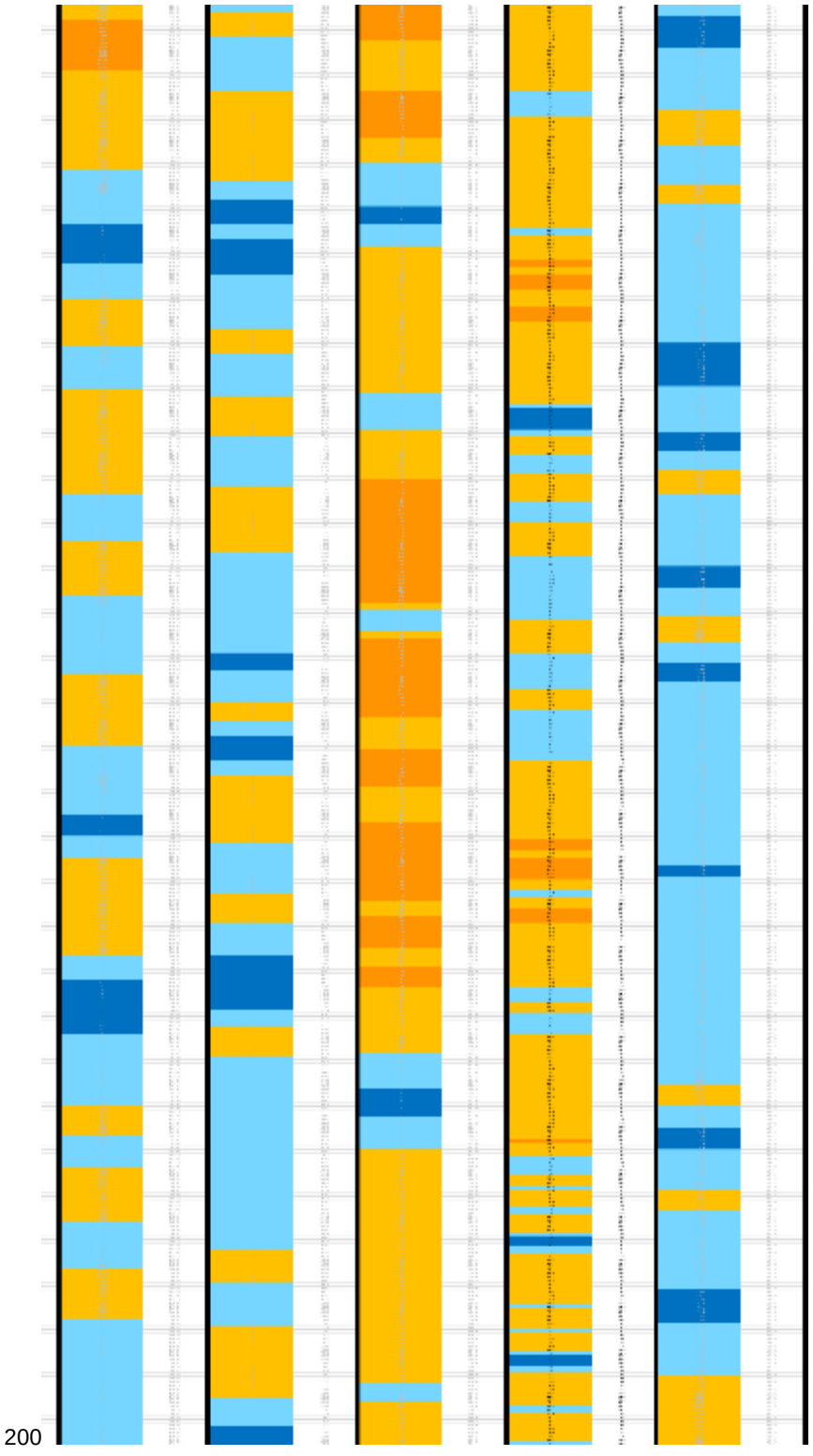

Figure G1 (cont.): Color-code of GR values for horizontal logs (2 of 10).

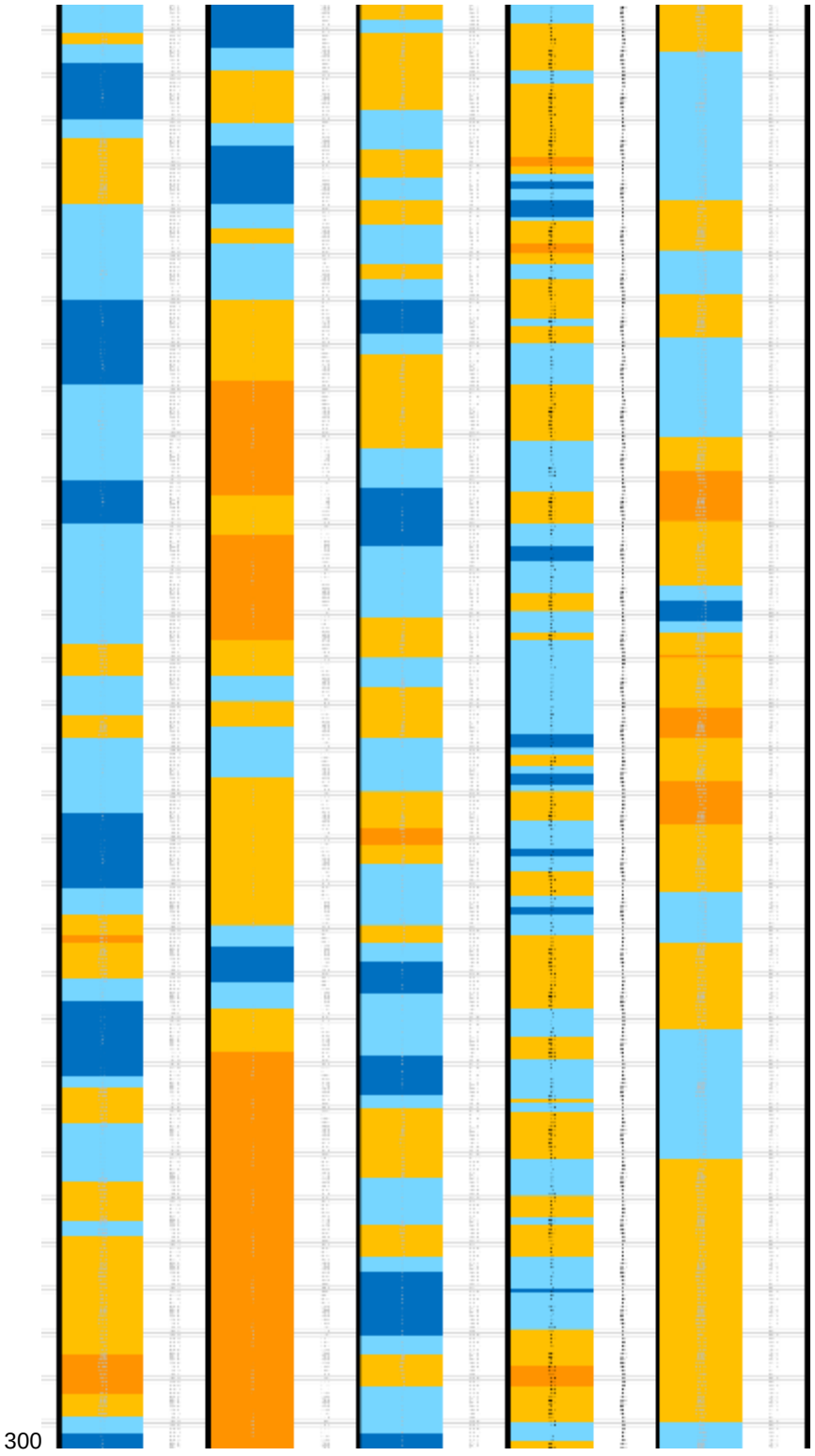

Figure G1 (cont.): Color-code of GR values for horizontal logs (3 of 10).

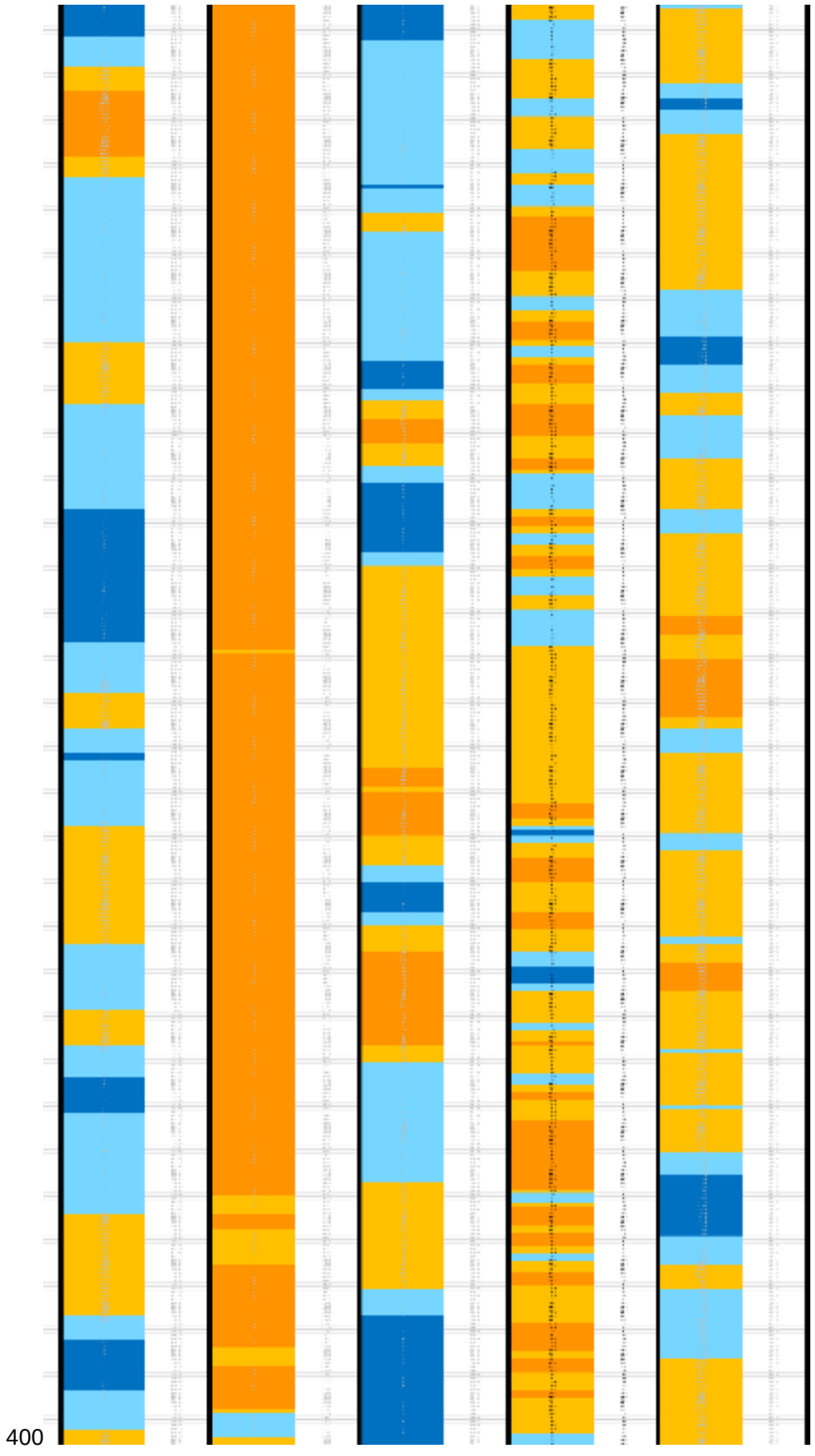

Figure G1 (cont.): Color-code of GR values for horizontal logs (4 of 10).

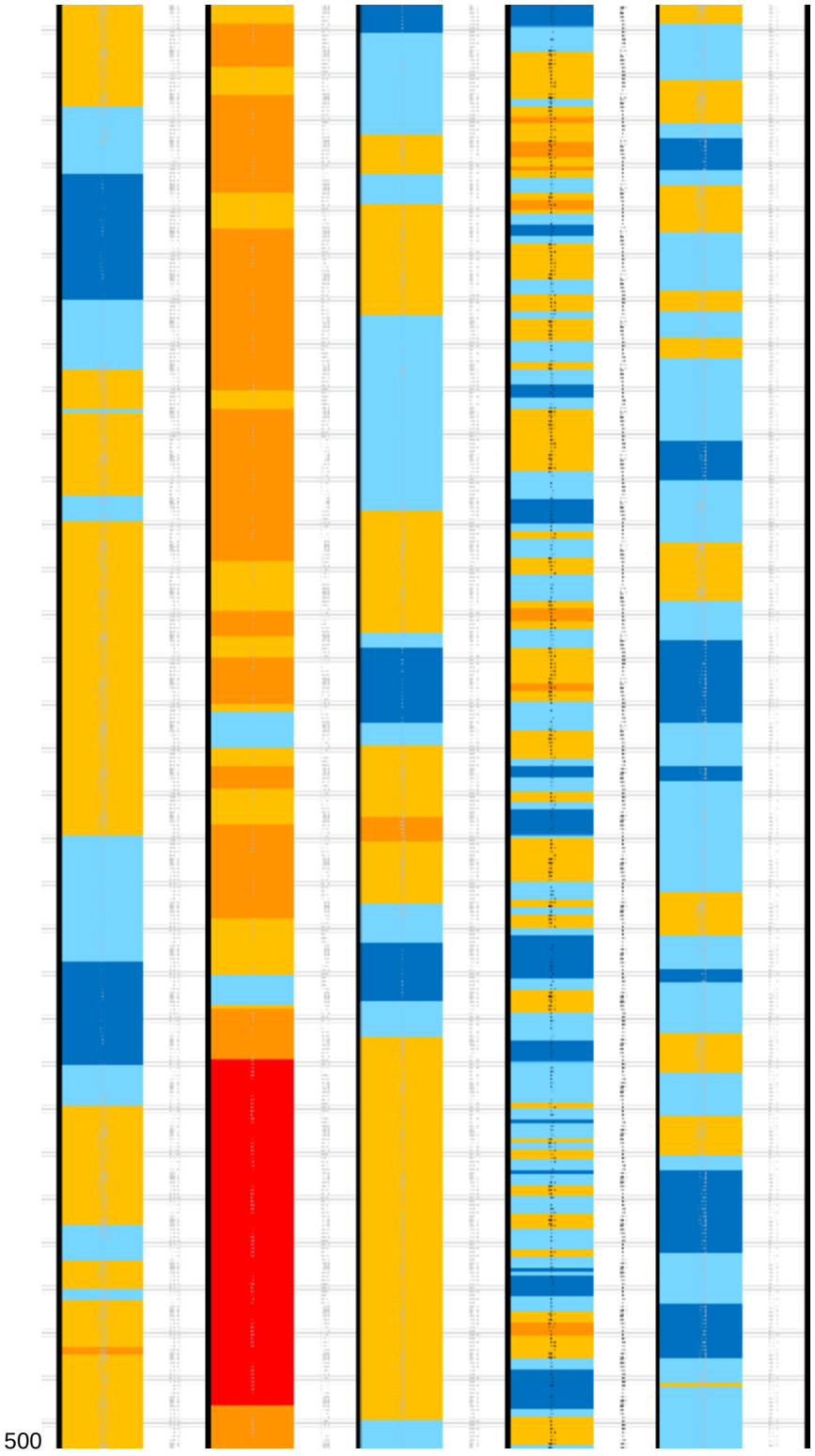

Figure G1 (cont.): Color-code of GR values for horizontal logs (5 of 10).

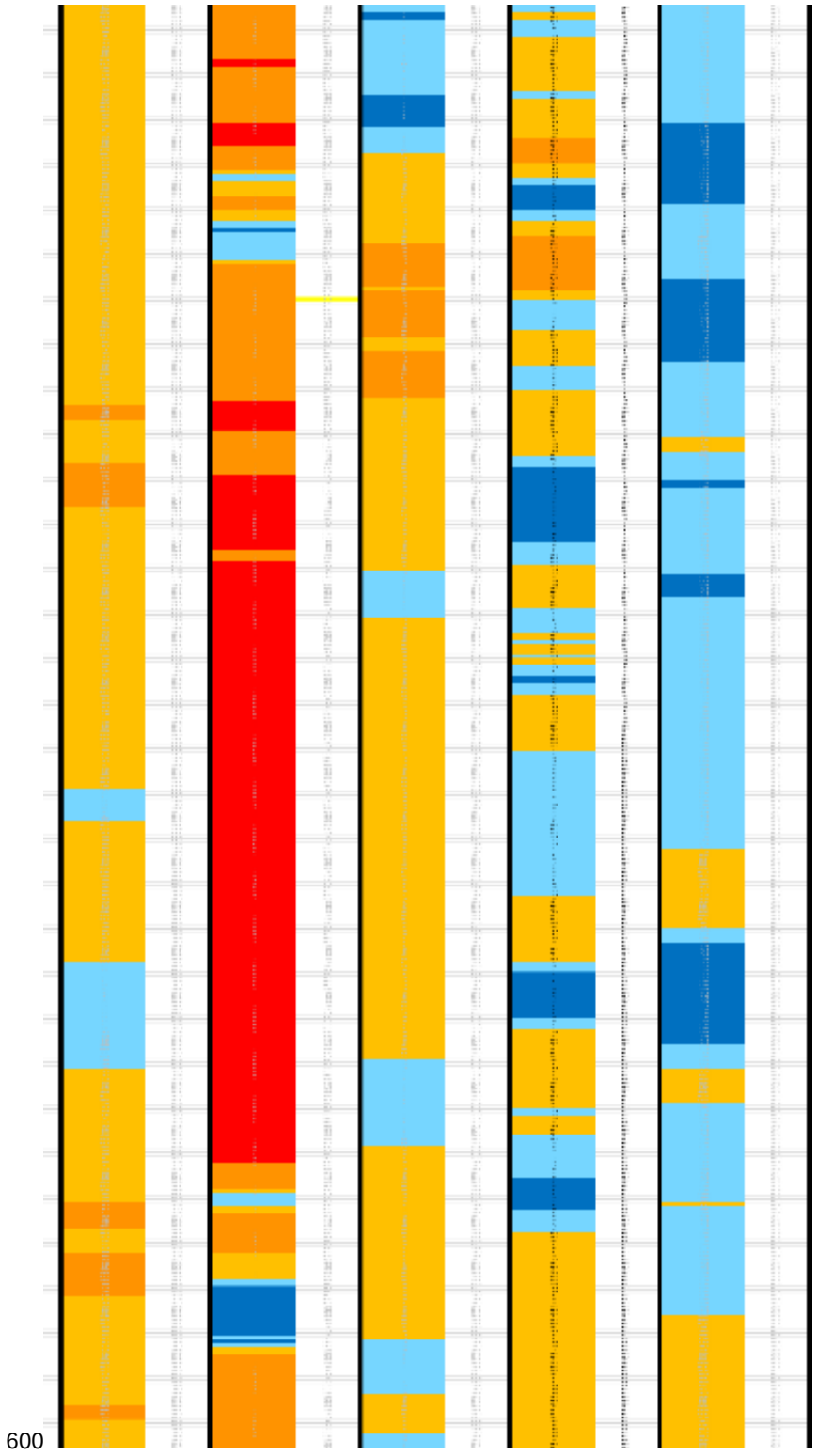

Figure G1 (cont.): Color-code of GR values for horizontal logs (6 of 10).

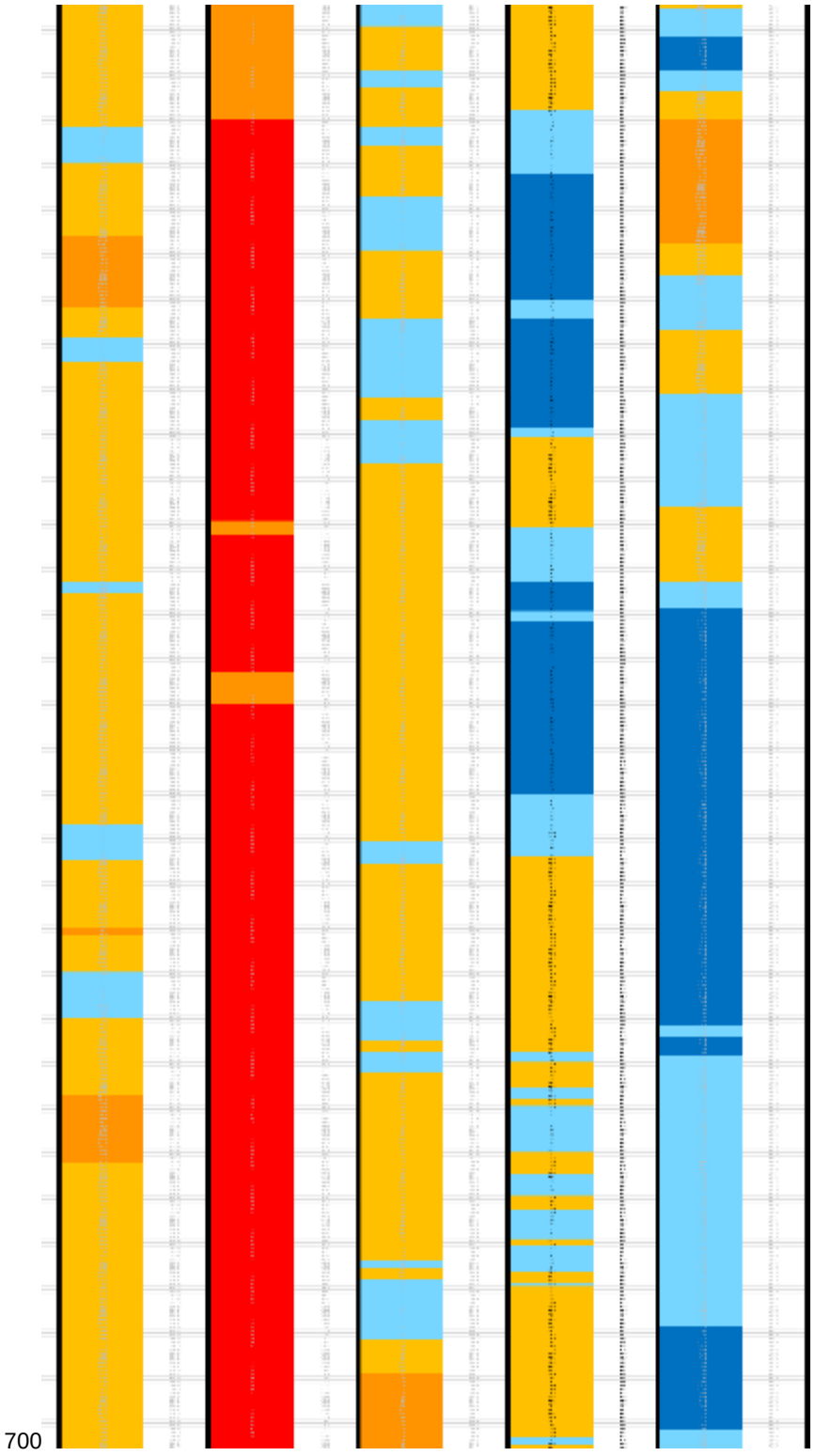

Figure G1 (cont.): Color-code of GR values for horizontal logs (7 of 10).

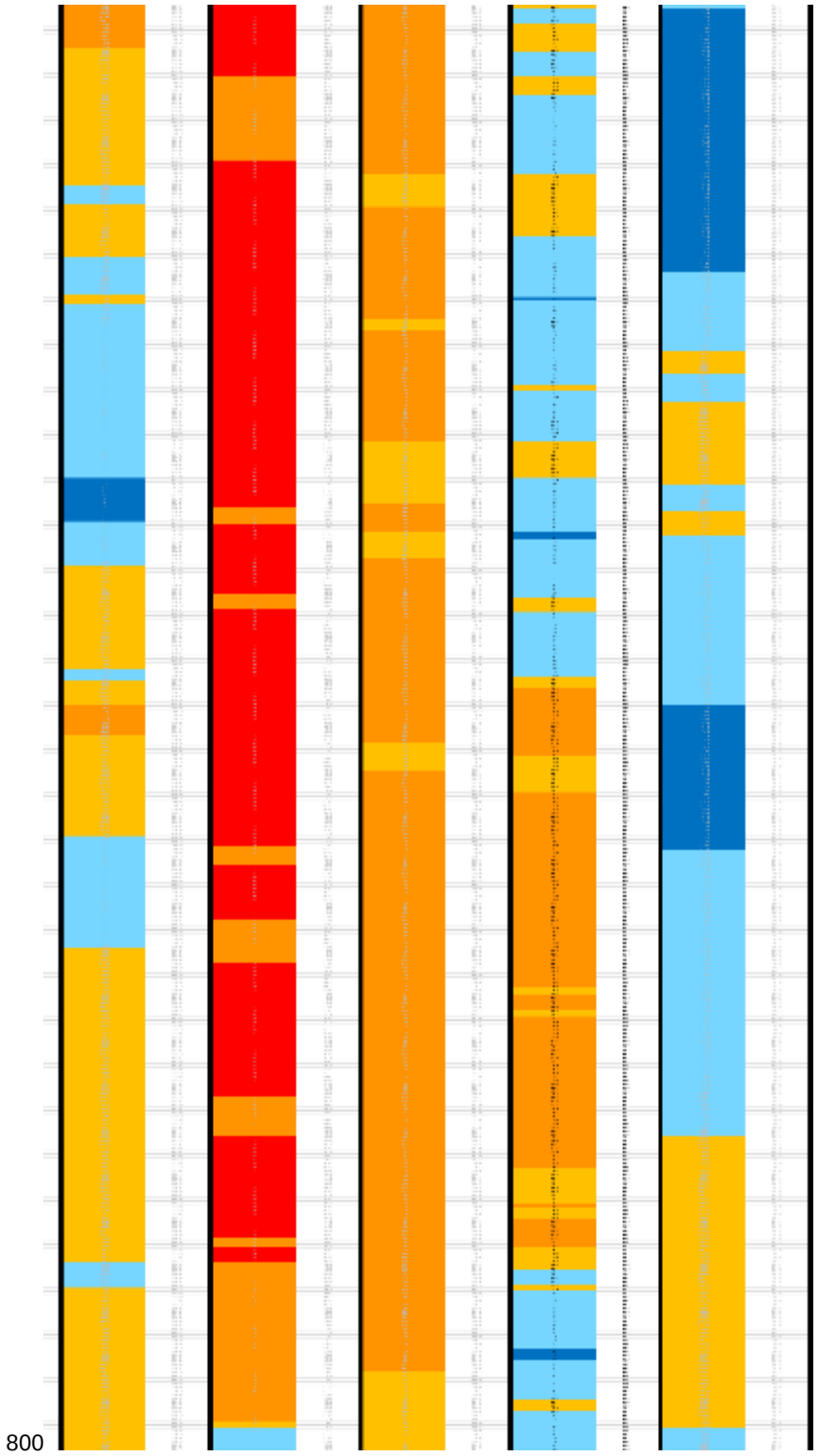

Figure G1 (cont.): Color-code of GR values for horizontal logs (8 of 10).

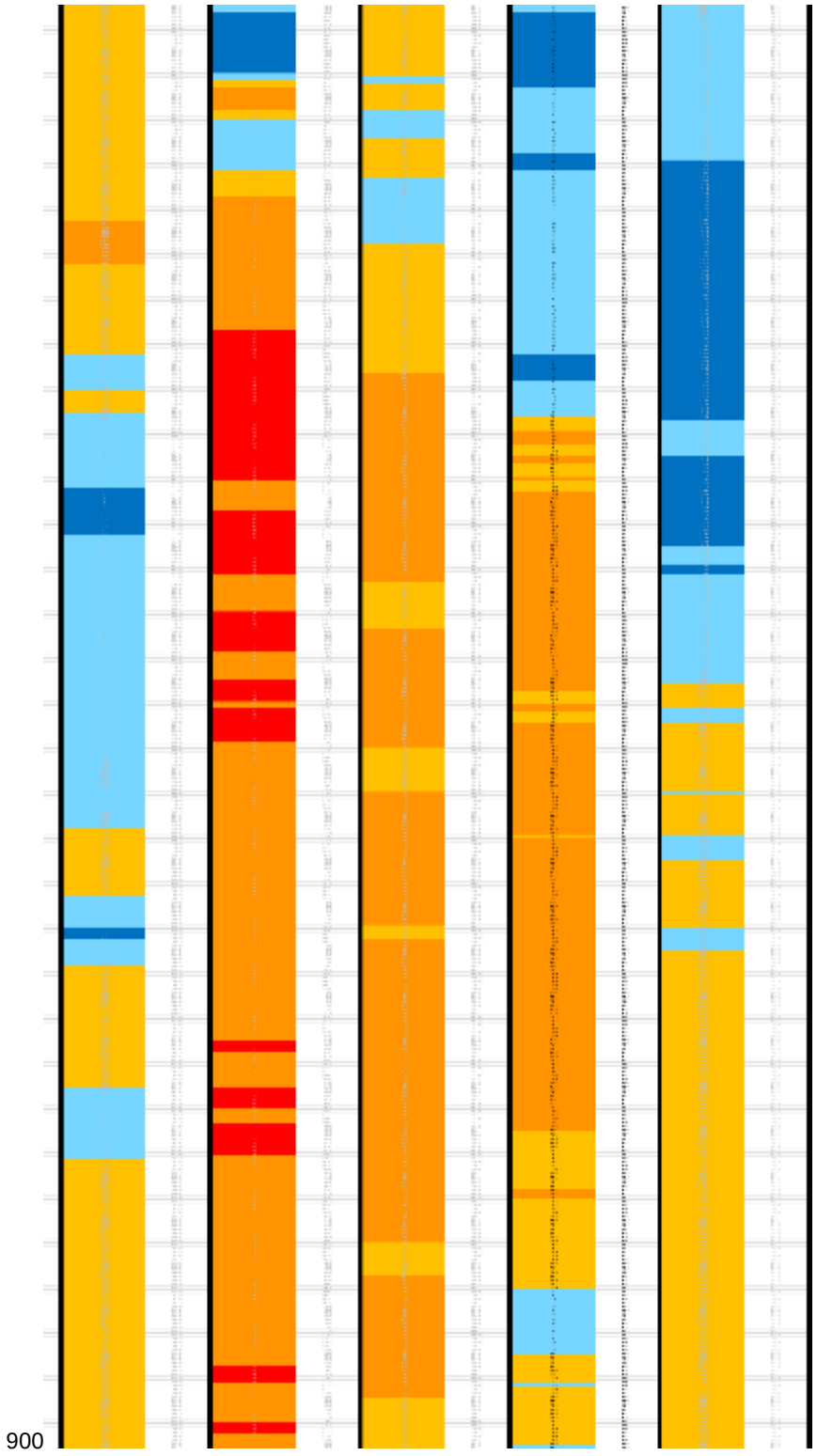

Figure G1 (cont.): Color-code of GR values for horizontal logs (9 of 10).

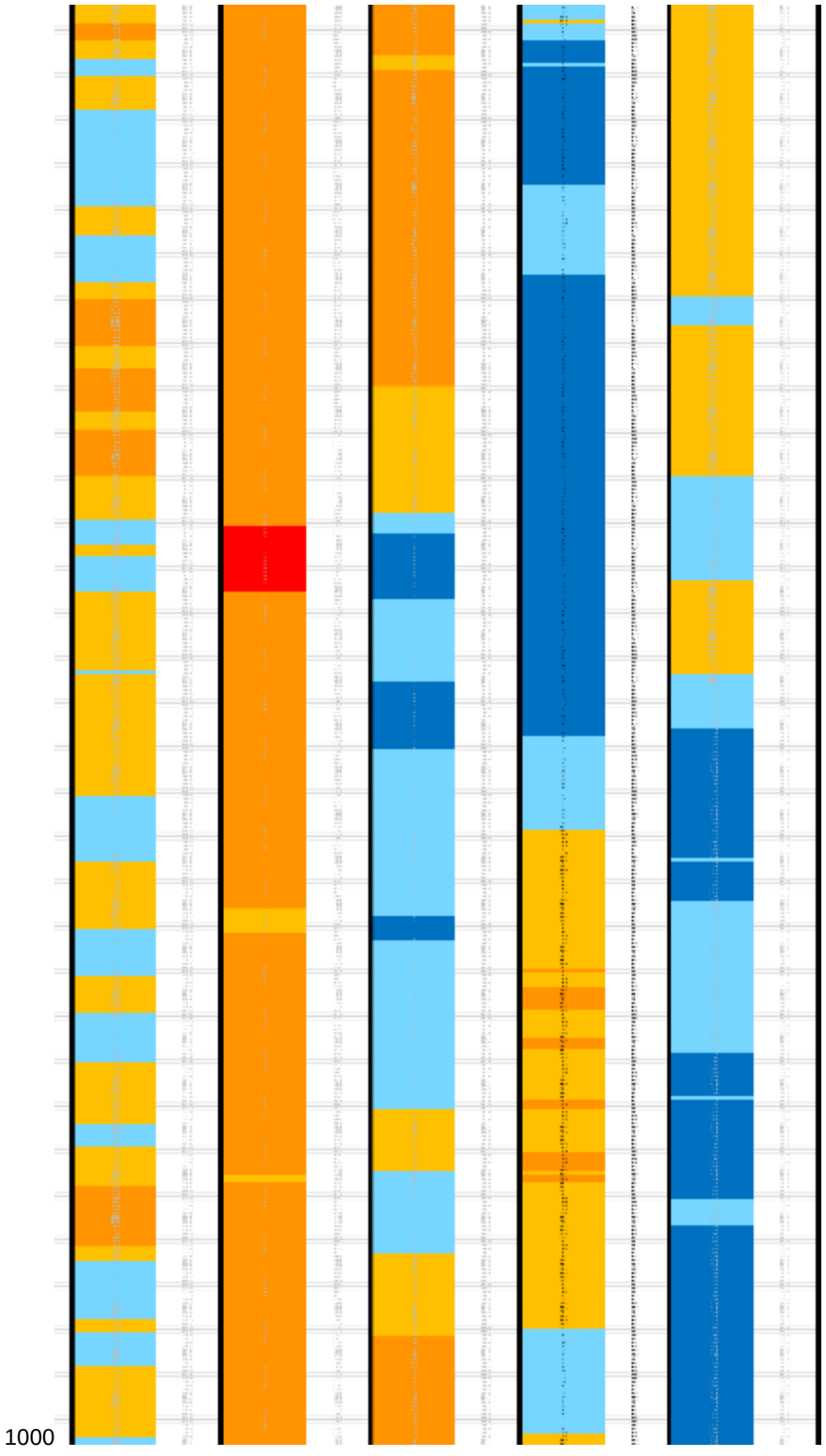

Figure G1 (cont.): Color-code of GR values for horizontal logs (10 of 10).

APPENDIX H: FRACTURE STATISTICS IN HORIZONTAL WELLS

H.1 NATURAL FRACTURE STATISTICS FOR WELLS 6SU AND 6SM PER STAGE

To better understand the variability of the natural fractures in relation to hydraulic fracture stages employed at the site, two horizontal wells at the center of the site, SUGG-A #171 6SU and SUGG-A #171 6SM, were analyzed. These wells are the only two horizontal wells having the natural fracture data to permit this analysis.

Fracture types were defined as provided in Table H1. Tables H2 and H3 show the analysis results for 6SU and 6SM for the Upper and Middle Wolfcamp wells, respectively, for each fracture stage[21]. In review, the average number of natural fractures per stage is relatively low for both wells, with a general average of approximately 18 fractures per stage in well 6SU, and 19 fractures per stage in well 6SU[22]. These values result in average fracture spacings of 15.7 ft and 20.4 ft in 6SU and 6SM per stage, respectively. The overall range in the number of fractures per stage differs somewhat between the two wells, with a range of 0 to 35 fractures per stage in well 6SU and 1 to 45 fractures per stage in well 6SM.

In both wells, the dip of natural fractures is mostly near-vertical (averaging about 82^{o}), but with other sets (with differing dips) appearing intermittently in the data. The general average azimuth of all fractures again is similar for both wells at approximately 207^{o} and 205^{o}[23], for a general direction of SSW. Eight faults were noted in the tabulated data of well 6SU, but no faults were included in the 6SM data.

H.2 DATA IN STAGES

The fracture data from the underlying source files were subdivided based on the stage distances of each sequence. For well SU6, the data was extracted from the log ASCII standard file for well data (*.las), while 6SM data were taken from a comma-separated values (*.csv) file.[24] The analysis includes all natural fractures and faults within the boundaries of each stage. Most fractures are designated as "partial fractures." The results shown in the table are simple averages of the raw data and the data were not processed or subdivided into fracture sets. The pumping data was provided by A. Kumar from his analysis of other data.

[21] The stage length varies with each well. The length of stage is taken from the distance from the top perforations to the bottom perforations.

[22] Note that each stage is approximately 181 ft to 184 ft in length between perforations except for stage #37 in well 6SU, with a length of 219 ft.

[23] A simple average of the azimuths was computed, and they were not modified to a range of 0^{o} to 180^{o}.

[24] Files: *2609-128306104_Laredo_Sugg_A-171-6SU_COI_Final_DipData.las* and *8201-129725767_Laredo_Sugg A 171_6SM_COI_Fractures_DIP_CSV for import to IP.csv.*

Table H1: Key for Numeric Types of Discontinuities shown in Tables H2 and H3

Type No.	Discontinuity
1	Bedding
2	Conductive Fracture
3	Resistive Fracture
4	Partial Fracture
5	Conductive Fault
6	Resistive Fault
7	Partial Fault

Table H2: Analysis of Natural Fracture Statistics in Well SUGG-A #171 6SU

Well 6SU

Natural Fracture Description												Pumping Data		
Stage	Top Perforation (ft)	Bottom Perforation (ft)	Section Length (ft)	Number of Natural Fractures in Stage	Fracture Types in Stage (see Key)				Fracture Intensity (Frac./length)	Average Azimuth (°)	Average Dip (°)	Treatment Pressure (psi)	Slurry Rate (bpm)	Proppant Concentration (lb/gal)
					#2	#3	#4	Faults						
1	17,696.50	17,916.00	219.50	2	0	0	2	0	0.0091	176.2	70.6	6829.1	88.89	0.5980
2	17,427.50	17,609.00	181.50	13	0	0	13	0	0.0716	233.4	83.7	6000.5	81.90	0.5946
3	17,158.50	17,340.00	181.50	11	0	0	11	0	0.0606	200.6	82.6	6292.7	83.38	0.7098
4	16,889.50	17,071.00	181.50	13	0	0	13	0	0.0716	292.9	83.3	5917.4	81.03	0.7109
5	16,620.50	16,802.00	181.50	16	0	0	16	0	0.0882	217.9	84.5	5823.7	80.62	0.6698
6	16,351.50	16,533.00	181.50	26	0	0	26	0	0.1433	201.1	83.8	6083.4	83.57	0.7406
7	16,082.50	16,264.00	181.50	34	0	2	32	0	0.1873	196.5	81.2	6003.9	80.41	0.6790
8	15,813.50	15,995.00	181.50	32	0	1	31	0	0.1763	176.0	82.0	5997.6	79.96	0.6568
9	15,544.50	15,726.00	181.50	30	0	2	28	0	0.1653	196.8	81.4	5588.0	74.32	0.5885
10	15,275.50	15,457.00	181.50	6	0	0	6	0	0.0331	294.1	84.1	5331.6	71.92	0.5763
11	15,006.50	15,188.00	181.50	35	0	0	34	1	0.1928	202.9	82.9	5781.6	82.07	0.6152
12	14,737.50	14,919.00	181.50	19	0	0	19	0	0.1047	199.2	82.1	5821.3	80.84	0.6717
13	14,468.50	14,650.00	181.50	8	1	0	7	0	0.0441	242.3	78.6	5785.1	81.50	0.6706
14	14,199.50	14,381.00	181.50	25	0	1	23	1	0.1377	250.3	81.3	5572.9	80.37	0.7053
15	13,930.50	14,112.00	181.50	34	0	1	32	1	0.1873	199.5	80.2	5816.1	81.72	0.6340
16	13,661.50	13,843.00	181.50	24	0	1	23	0	0.1322	208.7	77.2	5763.4	80.74	0.6523
17	13,392.50	13,574.00	181.50	18	0	0	16	2	0.0992	168.9	77.4	5667.6	82.19	0.3954
18	13,123.50	13,305.00	181.50	8	0	0	8	0	0.0441	199.7	81.7	5463.5	80.49	0.7007
19	12,854.50	13,036.00	181.50	18	0	0	18	0	0.0992	196.9	81.7	5408.5	81.19	0.7059
20	12,585.50	12,767.00	181.50	20	0	0	20	0	0.1102	149.0	76.7	5240.1	78.32	0.6441
21	12,316.50	12,498.00	181.50	23	0	0	23	0	0.1267	162.5	79.3	5658.5	82.36	0.6710
22	12,047.50	12,229.00	181.50	27	0	0	27	0	0.1488	184.0	79.9	5269.1	81.68	0.6953
23	11,778.50	11,960.00	181.50	26	0	0	26	0	0.1433	200.1	84.2	5373.4	82.59	0.6736
24	11,509.50	11,691.00	181.50	35	0	0	35	0	0.1928	174.4	81.6	5343.6	81.92	0.7290
25	11,240.50	11,422.00	181.50	8	0	0	8	0	0.0441	260.9	83.2	5367.3	81.00	0.6759
26	10,971.50	11,153.00	181.50	22	0	0	22	0	0.1212	197.2	79.4	5243.9	82.82	0.7293
27	10,702.50	10,884.00	181.50	11	0	1	10	0	0.0606	215.5	83.8	5549.3	83.12	0.6849
28	10,433.50	10,615.00	181.50	17	0	0	17	0	0.0937	193.9	81.7	5309.6	81.39	0.7395
29	10,164.50	10,346.00	181.50	7	0	0	6	1	0.0386	221.1	78.5	5487.2	81.75	0.7108
30	9,895.50	10,077.00	181.50	22	0	1	19	2	0.1212	189.7	80.4	5478.5	78.97	0.6838
31	9,626.50	9,808.00	181.50	16	0	0	16	0	0.0882	197.9	79.9	5167.5	82.81	0.7238
32	9,357.50	9,539.00	181.50	16	0	0	16	0	0.0882	198.7	82.6	5415.6	83.04	0.7316
33	9,088.50	9,270.00	181.50	11	0	0	11	0	0.0606	196.3	80.3	5580.6	83.42	0.6751
34	8,819.50	9,001.00	181.50	12	0	0	12	0	0.0661	213.0	82.1	5150.5	85.47	0.7369
35	8,550.50	8,732.00	181.50	5	0	0	5	0	0.0275	226.5	79.7	4979.6	81.17	0.6821
36	8,281.50	8,463.00	181.50	7	0	0	7	0	0.0386	206.8	83.7	5027.7	84.86	0.7161
37	8,012.50	8,194.00	181.50	0	0	0	0	0	---	---	---	5181.6	85.26	0.7505
			Average =	18					0.1005	207	81	5588.4	81.6	0.674
			Maximum =	35					0.1928	294	85	6829.1	88.9	0.750
			Minimum =	0					0.0091	149	71	4979.6	71.9	0.395
				Sum =	1	10	638	8						

Notes:

1. The data are from files: 2609-128306104_Laredo_Sugg_A-171-6SU_COI_Final_DipData.las and Sugg A 171 #6SU & #6SM Proppant Sequence. Stage 1 data excluded from orientation averages.
2. National Energy Technology Laboratory's Energy Data eXchange (EDX) Directory: … /hfts-1-phase-1-individual-well-files/SUGG A 171 6SU Horizontal/2_Processed Image Log.
3. The length of stage is taken from the top perforation to the bottom perforation in data files.
4. Numeric key for fracture types (shown in Table H1) differ from source.
5. Bedding observations are not included in fracture data.

Table H3: Analysis of Natural Fracture Statistics in Well SUGG-A #171 6SM

Well 6SM

Natural Fracture Description												Pumping Data		
Stage	Top Perforation (ft)	Bottom Perforation (ft)	Section Length (ft)	Number of Natural Fractures in Stage	Fracture Types in Stage (see Key)				Fracture Intensity (Frac./length)	Average Azimuth (°)	Average Dip (°)	Treatment Pressure (psi)	Slurry Rate (bpm)	Proppant Concentration (lb/gal)
					#2	#3	#4	Faults						
1	18,055.50	18,239.00	183.50	9	0	0	9	0	0.0490	260.7	85.0	6395.4	87.5185	0.5854
2	17,784.00	17,967.50	183.50	28	0	0	28	0	0.1526	232.3	84.2	6146.8	80.2548	0.6746
3	17,512.50	17,696.00	183.50	42	0	0	42	0	0.2289	230.0	86.2	4885.3	59.7362	0.3921
4	17,241.00	17,424.50	183.50	37	0	0	37	0	0.2016	226.9	83.5	5678.1	73.4643	0.6212
5	16,969.50	17,153.00	183.50	45	0	0	45	0	0.2452	184.7	81.1	5625.7	75.2267	0.6643
6	16,698.00	16,881.50	183.50	31	0	0	31	0	0.1689	193.6	82.1	5836.3	79.9627	0.6284
7	16,426.50	16,610.00	183.50	13	0	0	13	0	0.0708	144.0	86.5	6099.4	79.3133	0.6998
8	16,155.00	16,338.50	183.50	8	0	0	8	0	0.0436	251.4	84.2	6157.1	80.4603	0.6489
9	15,883.50	16,067.00	183.50	12	0	0	12	0	0.0654	177.4	83.7	5892.8	79.9630	0.7010
10	15,612.00	15,795.50	183.50	7	0	0	7	0	0.0381	140.2	75.8	5867.7	78.7910	0.6428
11	15,340.50	15,524.00	183.50	16	0	0	16	0	0.0872	190.3	79.7	5735.0	79.3113	0.6851
12	15,069.00	15,252.50	183.50	25	0	0	25	0	0.1362	189.4	75.9	5753.1	80.5561	0.6612
13	14,797.50	14,981.00	183.50	3	0	0	3	0	0.0163	218.2	78.0	5845.6	80.5984	0.6642
14	14,526.00	14,709.50	183.50	15	0	0	15	0	0.0817	203.2	83.6	5730.4	80.8442	0.6087
15	14,254.50	14,438.00	183.50	23	0	0	23	0	0.1253	201.5	80.4	4908.9	63.0874	0.5548
16	13,983.00	14,166.50	183.50	11	0	0	11	0	0.0599	186.2	81.4	5445.5	79.3986	0.6607
17	13,711.50	13,895.00	183.50	31	0	0	31	0	0.1689	238.0	82.6	5568.1	80.9670	0.7095
18	13,440.00	13,623.50	183.50	28	0	1	27	0	0.1526	191.0	79.1	5448.7	82.7768	0.6586
19	13,168.50	13,352.00	183.50	22	0	0	22	0	0.1199	181.0	79.1	5517.6	79.7508	0.7077
20	12,897.00	13,080.50	183.50	1	0	0	1	0	0.0054	156.2	87.7	5536.2	76.9341	0.6225
21	12,625.50	12,809.00	183.50	8	0	0	8	0	0.0436	177.7	80.1	5697.0	82.6150	0.6976
22	12,354.00	12,537.50	183.50	22	0	1	21	0	0.1199	243.3	83.6	5233.0	81.0011	0.6948
23	12,082.50	12,266.00	183.50	32	0	0	32	0	0.1744	202.5	79.4	5500.0	82.1968	0.6410
24	11,811.00	11,994.50	183.50	24	0	0	24	0	0.1308	202.9	78.2	5249.3	80.9719	0.6942
25	11,539.50	11,723.00	183.50	21	0	0	21	0	0.1144	209.3	79.6	5351.8	79.2176	0.6634
26	11,268.00	11,451.50	183.50	37	0	0	37	0	0.2016	200.0	84.9	5107.9	81.9764	0.7111
27	10,996.50	11,180.00	183.50	19	0	0	19	0	0.1035	192.6	84.3	5178.8	84.5132	0.7294
28	10,725.00	10,908.50	183.50	8	0	0	8	0	0.0436	234.4	84.4	5195.8	82.0301	0.6988
29	10,453.50	10,637.00	183.50	13	0	0	13	0	0.0708	190.6	79.5	5409.1	83.2537	0.7163
30	10,182.00	10,365.50	183.50	5	0	0	5	0	0.0272	207.1	79.0	5230.9	80.6071	0.7006
31	9,910.50	10,094.00	183.50	4	0	0	4	0	0.0218	202.9	80.4	5386.7	83.6350	0.7092
32	9,639.00	9,822.50	183.50	13	0	0	13	0	0.0708	249.0	84.5	5316.5	85.4007	0.7679
33	9,367.50	9,551.00	183.50	20	0	0	20	0	0.1090	242.9	83.4	4957.3	82.5579	0.7301
34	9,096.00	9,279.50	183.50	25	0	0	25	0	0.1362	216.2	82.1	4949.5	81.5504	0.8049
35	8,824.50	9,008.00	183.50	14	0	0	14	0	0.0763	221.1	81.3	5038.5	81.7786	0.7342
36	8,553.00	8,736.50	183.50	8	0	0	8	0	0.0436	175.3	81.7	5035.0	84.5823	0.7726
37	8,281.50	8,465.00	183.50	4	0	0	4	0	0.0218	155.9	81.0	4722.8	84.8531	0.8434
			Average =	18					0.1007	203.2	82	5476.6	80.0	0.7
			Maximum =	45					0.2452	260.7	88	6395.390	87.5	0.8
			Minimum =	1					0.0054	140.2	76	4722.800	59.7	0.4
				Sum =	0	2	682	0						

Notes:

1. The data are from files: 8201-129725767_Laredo_Sugg A 171_6SM_COI_Fractures_DIP_CSV for import to IP.csv and Sugg A 171 #6SU & #6SM Proppant Sequence.
2. EDX Directory: /hfts-1-phase-1-individual-well-files/SUGG A 171 6SM Horizontal/2_Processed Image Log.
3. The length of stage is taken from the top perforation to the bottom perforation.
4. Numeric key for fracture types (shown in Table H1) differs from source.
5. Bedding observations are not included in fracture data.

Brian Anderson
Director
National Energy Technology Laboratory
U.S. Department of Energy

Sean Plasynski
Deputy Director & Chief Technology Officer
Technology Development Center
National Energy Technology Laboratory
U.S. Department of Energy

Maria Vargas
Associate Director
Natural Gas & Oil
Technology Development Center

Bryan Morreale
Associate Laboratory Director for Research & Innovation
National Energy Technology Laboratory
U.S. Department of Energy

Grant Bromhal
Technical Director, Smart Initiative
Geological and Environmental Systems
National Energy Technology Laboratory
U.S. Department of Energy

Jennifer Wilcox
Principal Deputy Assistant Secretary
Office of the Assistant Secretary
Fossil Energy and Carbon Management
U.S. Department of Energy

NETL Technical Report Series